Precipitation and Fracture in a Ferritic Stainless Steel

A thesis submitted to the Faculty of Engineering and the Built Environment of the University of Cape Town in fulfilment of the requirements for the degree of Master of Science in Applied Science

By

Adam James Lidstone Scott

Centre for Materials Engineering

April 2000

Acknowledgements

My supervisor, Associate Professor Rob Knutsen, for his guidance and encouragement

Research and Development at Columbus Stainless, for their financial and practical support, including a very warm thank you to Lucien Matthews and Bruce Muller, who were always there to put me on the right track

Adriaan Loedolff, for his enthusiastic wide-ranging practical expertise from metallography to photography and automotive engines

Glen Newins, without whose technical wizardry in the workshop this project would have been impossible

The Electron Microscope Unit's Miranda Waldron, for whom nothing ever seemed to be too much trouble and Dane Gerneke, for his ardent professionalism

Mira Topic, for her assistance with metallography

Janet Basson, who in her indefatigable, good humoured pursuit of her PhD and general readiness to assist sets a very fine example

Julie-Ann Henry, for her unstinting administrative work

J.J. 'Koos' Terblans at the Department of Physics at the University of the Orange Free State, for his time and generous assistance with the Scanning Auger Microscope

Dr Candy Lang, for her very professional approach to presentation preparation

All Materials Engineering staff, postgraduate and undergraduate students who have together made the last few years so memorable and educational

My friends and housemates, for a superb all-round University experience

And to my parents, for their boundless love and support

Synopsis

A dual stabilised ferritic stainless steel with titanium and niobium additions had been experiencing failures during production. Following hot rolling and cooling while coiled and prior to annealing, the steel had been prone to shattering across its width during uncoiling. This project was initiated by the manufacturers, Columbus Stainless, so that the present understanding of this stainless steel could be expanded, with the ultimate aim of avoiding production losses.

This stainless steel is designed for high temperature use in automotive exhaust systems. This requires a good blend of hot strength, creep and corrosion resistance. The composition (notably the niobium addition) and manufacturing processes (where the precipitation and grain size are major concerns) are intended to provide these properties. This thesis puts the steel into the broader context of the ferritic stainless steels and discusses its high temperature use and its dual stabilisation. The literature on precipitation in stabilised stainless steel is reviewed. Probable consequences of its dual stabilisation are explored, such as for the interstitial content of the matrix and the makeup of the grain boundaries.

The failures are investigated, with an examination of the fracture surface and the shattered steel's microstructure using electron and optical microscopy. Tensile tests of the shattered steel show embrittlement, with cracks forming before failure. Taken together, this provides insight into the probable causes of the embrittlement. A possible combination of mechanically deleterious factors is proposed as the reasons for the failures. The initiation of cracks at grain boundaries is favoured by intragranular precipitation and unusually low cohesivity between the matrix and the grain boundary. These are particular to the embrittled steel, with the generally poor fracture toughness of ferritic stainless steels an additional culprit. The interplay of these factors is discussed, from the origin of the cracks to final failure.

The composition of a fracture surface is studied using Auger Electron Spectroscopy. The degree of precipitation is then explored for different times and temperatures using optical and electron microscopy, as a guide to precipitation during cooling after hot rolling. A comparison is then made with precipitation at service temperatures over a far longer period of 100 hours. The experimental results are then compared with both the hypothesis outlined above and previous knowledge of this steel and conclusions are drawn.

Table of Contents

Chapter 1 Introduction

1.1 Project Background

Columbus Stainless of Middelburg, Mpumalanga, is a manufacturer of rolled stainless steel products. One product is a dual stabilised ferritic stainless steel, conforming to the specification of DIN 1.4509. With a basic composition of 17% chromium and extra-low carbon and nitrogen levels, it has stabilising additions of titanium and niobium. Exhibiting superior corrosion and creep resistance, it is intended for use in automotive exhaust systems. The Columbus designation for this steel is 44101 and this name will be used hereafter.

Columbus Stainless had experienced some production problems with this stainless steel, leading to losses in product and production time. Following hot rolling of the cast slabs, the 5mm thick sheets are coiled. The stainless steel sheets cool to ambient temperature while coiled and are then unrolled prior to annealing and pickling. During unrolling of these coils, occasional brittle failure would occur across the width of the coil. This meant that the sheet could not be processed further and with production interrupted and material lost, it was an expensive problem.

The composition of this ferritic stainless steel has been specially formulated for high temperature use, yet little information was available regarding the consequences of this dual stabilisation during the production process. In this particular situation it was speculated that undesirable levels of precipitation during cooling in the coil had a role in the production failures. Information on the temperature and times required for precipitation would allow the producer to know what cooling rate would be required to avoid deleterious precipitation.

It was decided that research should be undertaken into this stainless steel, in order to increase understanding of its particular characteristics. The core issue was uncertainty about the nature and extent of the precipitation found in this stainless steel. Any influence of precipitation on the creep resistance of the stainless steel during service was also a matter of concern.

1.2 Project Aims

The composition of this ferritic stainless steel, 44101, was intentionally formulated for high temperature use in highly corrosive environments. It possesses greater ratios of titanium and niobium than are necessary for stabilisation. In order to gain a fuller knowledge of this steel, we must first clarify the reasoning behind its design. With this as a basis, we also aim to expand the knowledge of the precipitation within this ferritic stainless steel and to explore possible consequences of its stabilised nature.

With an understanding of the relationship between composition, microstructure and properties, its production can be managed effectively and its properties maximised. If further failures following hot rolling could be avoided, the savings in time, material and cost would be substantial. An increased overall understanding of this steel could also help the producer to better the service properties of its steel, especially with regard to its creep resistance.

This ferritic stainless steel is metallurgically interesting in itself, with its dual stabilised nature producing a variety of precipitates. There has been little research on over stabilised ferritic stainless steels of this type and experimental work is justified due to its relative novelty.

The broad aims can therefore be summarised as follows:

1) to investigate the failures following hot rolling and to suggest possible solutions.

2) to acquire qualitative data of the degree of precipitation, over a range of times and temperatures, likely to be experienced during cooling after hot rolling.

3) to investigate this precipitation, specifically with regard to the grain boundaries, and again after long term treatment at service temperatures.

Chapter 2 Literature Review

2.1 Ferritic Stainless Steels

2.1.1 General Introduction

The addition of chromium to a steel is the fundamental requirement for the steel to be 'stainless.' The 17% chromium ferritic stainless steels are the simplest in composition and most economical to manufacture of the stainless steels. With no expensive nickel required, they are approximately a quarter of the cost of austenitic stainless steels and comprise about 20% of world-wide stainless steel production. Modern stainless steel producers, with the latest expertise in controlling the levels of minor elements, can manufacture ferritic stainless steels that can supersede their austenitic stainless steel counterparts in many applications [1,2,3,4]. The equilibrium diagram below depicts the phase fields of the iron-chromium binary alloy system. Note the innate 'gamma loop' on the left hand side, which allows for the manufacture of martensitic and ferritic/ martensitic stainless steels without nickel additions. (see section 2.1.4)

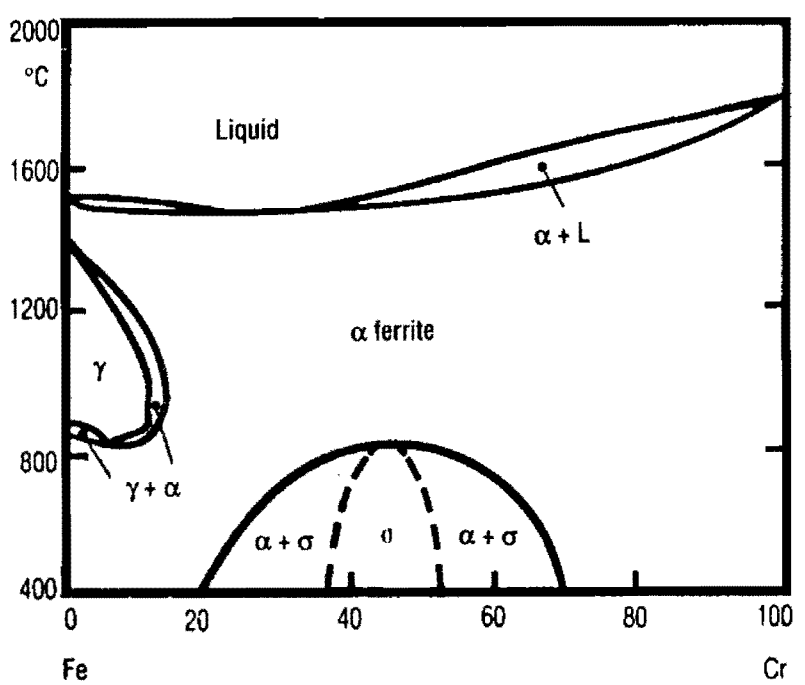

Figure 2.1 The Fe-Cr-C phase equilibrium diagram, from Stainless Steels[2]

2.1.2 Characteristics

Ferritic stainless steels have good resistance to atmospheric corrosion and oxidation, yet possess generally lower corrosion resistance, lower formability and lower toughness than austenitic stainless steels. They do have several performance advantages over their austenitic rivals. Chief among these is their virtual immunity to transgranular stress corrosion cracking, as long as nickel and copper additions are low, and their resistance to chloride stress corrosion cracking [1,2,3,4].

The yield strength of ferritic stainless steels is greater than that of austenitics, ranging between 280 MPa to 460 MPa, compared to approximately 230 MPa. Yet with their face-centred cubic crystal structure, austenitic stainless steels can be work hardened far more than ferritic stainless steels. As a consequence ferritic stainless steels have better drawability, with only a small increase in strength as the steel is plastically deformed [3,4]. Ferritic stainless steels are formed at room temperature for most applications. They must have shallower draws and more generous radii than austenitic steels. Ferritic stainless steels have an expansion co-efficient close to that of plain carbon or low-alloy steels, facilitating the use of mixed structures [1,2].

Historically ferritic stainless steels did not have the impact properties necessary for high strength applications. Technical progress has made lower carbon levels commonplace, increasing ferritics' impact toughness substantially[3]. Grain refinement is another avenue for improvements in toughness. This does not change the strength, which in high-chromium ferritics is dependent on subgrain size, but it does increase the energy absorbed in impact. Improvements in impact toughness were instrumental in the increased use of ferritic stainless steels [3,4].

2.1.3 Classification

A convenient way of describing the ferritic stainless steels is by placing them into one of the following four groups:[2]

1) A 17%Cr grade, AISI 430, is the most common ferritic stainless steel and is widely used in a large number of everyday applications, such as automotive trim and cooking utensils. Numerous variants exist, differing mostly in their carbon contents [1,2].

2) The 11%Cr to 12%Cr corrosion resistant steels are useful in a large number of applications and are the most economical. The careful choice of further alloying elements and the development of new production methods has greatly expanded the potential applications of these grades, with their fair corrosion and oxidation resistance and good fabricability at low cost. Columbus Stainless Steels' 3CR12 is an example of these steels[5]. The most prominent is AISI 409, which is used in automotive exhaust systems[1].

3) The high chromium ferritic grades, with between 24%Cr and 28%Cr, are used when very high levels of corrosion and oxidation resistance are required[2].

4) The stabilised 17%Cr grades contain additions, such as titanium and niobium, with strong affinities for carbon. Stabilised 17%Cr grades replace AISI 430 whenever resistance to intergranular corrosion in welded zones is essential[2]. The ferritic stainless steel 44101, DIN 1.4509, is in this category. (see section 2.3)

Alloying elements such as molybdenum and small amounts of nickel are used to modify compositions in all the above grades, particularly in adaptations for severely corrosive environments [1,2].

2.1.4 Austenite versus Ferrite

Chromium is a ferrite stabiliser and pure binary 17% chromium-iron alloys would be ferritic to the melting temperature. Note that the interstitial elements, carbon and nitrogen, which are always present to some degree in steels, are both strong austenite stabilisers. They widen the 'gamma loop' of the equilibrium diagram, as shown in Fig. 2.2 below. The term 'ferritic' when in reference to these steels is technically correct only when in the annealed condition. Only then is their body-centred cubic crystal structure necessarily the same as iron at ambient temperature. Ferritic stainless steels such as AISI 430 have a dual austenite/ferrite structure at high temperatures[1,2,3,4].

AISI 430 has a specified upper carbon limit of 0.08%, but is now more often between 0.02%C and 0.03%C, so as to enhance ductility [1,3]. Lower interstitial levels mean that the gamma loop on the equilibrium diagram goes to the left and less austenite forms at higher temperatures. The final ratio between carbide, martensite and ferrite phases depends on the thermomechanical processing route, especially final cooling rates. Rapid cooling encourages the formation of martensite, while slower cooling allows for decomposition of the austenite into ferrite and carbides[2].

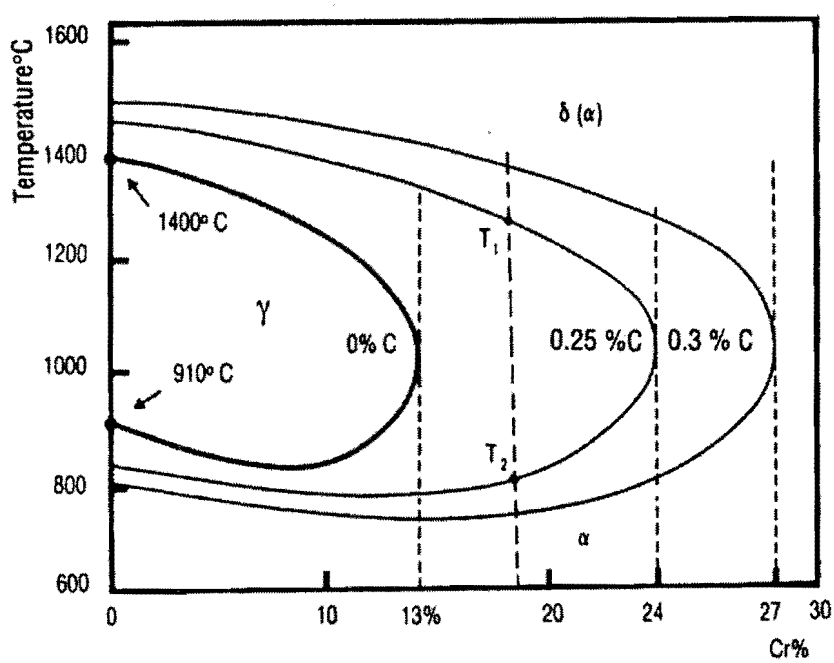

Figure 2.2 A projection of sections of the Fe-Cr-C diagram with increasing carbon content on the temperature - %Cr plane, from Stainless Steels[2]

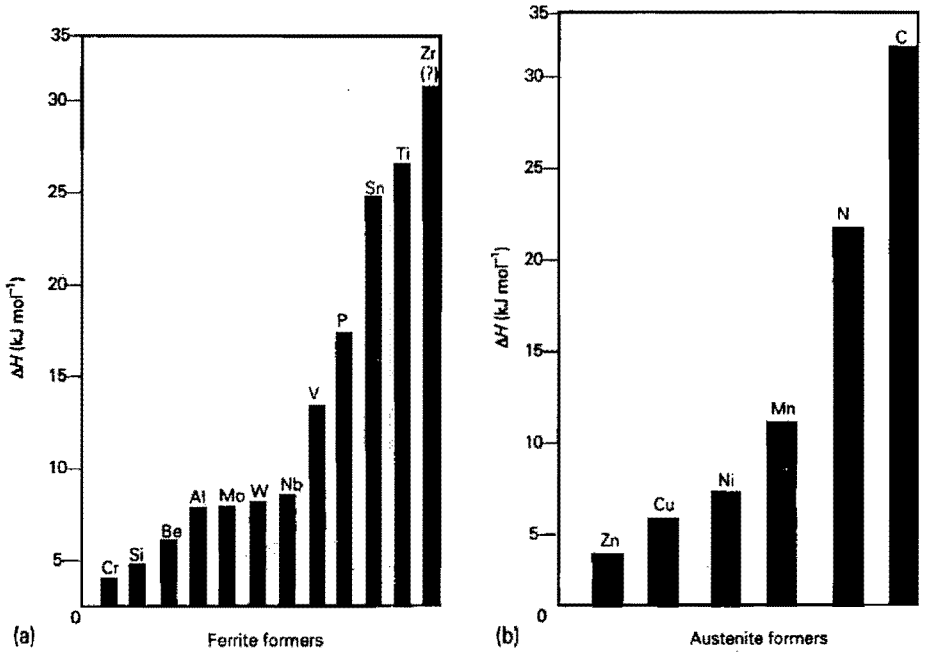

Figure 2.3 The relative strength of alloying elements as (a) ferrite formers; (b) austenite formers by Andrews[6]

Fig. 2.3 shows to what degree alloying elements other than carbon and nitrogen also encourage austenite or ferrite formation[6]. This is especially relevant for 44101 because it is a stabilised stainless steel (see section 2.3) with titanium and niobium additions. By combining with most of the carbon, the level of free interstitials decreases and the gamma loop on the Fe-Cr-C phase diagram is shifted to the left [2,7,8]. Titanium and niobium are strong ferrite formers in themselves and 0.5%Nb could be expected to be effective in preventing austenite formation [2,3].

The simpler 12%Cr grades, deep within the gamma loop of Fig. 2.2, are fully austenitic at high temperatures. The phraseology, whether the steel is termed ferritic or martensitic, relies not on composition but on the processing, which, either annealed or quenched and tempered, will produce ferritic or martensitic steels respectively [2,3].

The high chromium grades have fully ferritic structures at all temperatures, because the additional chromium places them far to the right of the gamma loop in Fig. 2.2.

Similarly for a ferritic stainless steel to be described as stabilised, it too must remain fully ferritic at all temperatures[2]. This is owing directly to the presence of strong

ferrite stabilisers, such as zirconium, titanium or niobium. Stabilisers also lessen the free carbon and nitrogen in the matrix and so promote ferrite indirectly [2,4].

2.1.5 Hot Rolling

The hot rolling of non-stabilised ferritic stainless steels is governed by the appearance of the two-phase region at high temperatures. Controlled rolling in this region can avoid undesirable grain growth. Coarser grains imply a lower impact toughness and ductile to brittle transition temperature (DBTT[4]). However fully stabilised ferritic stainless steels, being body-centred-cubic (bcc) at all temperatures, are non-transformable. The titanium nitrides or niobium carbonitrides retard grain growth, raise the coarsening temperature and retard recrystallisation [2,4].

If a stainless steel is processed above 870°C, austenite reforms in regions locally enriched in carbon by the dissolution of carbides. If held at high temperature for only a short period, that carbon rich austenite may form martensite at room temperature. This can cause production failures due to embrittling martensite on hot rolled coils. Rodrigues and co-workers[9] studied this phenomenon and concluded that this can be avoided if rolling parameters are adjusted correctly to obtain a fine grain size and a recrystallised and homogeneous structure.

2.1.6 Interstitial Content

The lowering of carbon and nitrogen levels in ferritic stainless steels through improved production methods has benefited corrosion resistance, weldability and toughness. However less carbon and nitrogen means substantially less interstitial strengthening and less grain pinning, allowing for grain growth and lower impact toughness [1,2]. If interstitial levels are very low, then there may be insufficient carbonitrides to pin grain boundaries. Careful rolling methods may offset this to some extent[4]. Carbides and nitrides increase the strength and decrease the toughness and ductility. This is a valid while free carbon and nitrogen levels remain above a critical level (≈ 500 ppm) and the matrix possesses meaningful interstitial strengthening. If precipitation depletes the matrix of interstitials much below that, then the ductility of the matrix increases [3,4].

2.2 The High Temperature Use of Stainless Steels

2.2.1 Introduction

Stainless steels have many advantages for high temperature use. They have excellent high temperature oxidation resistance, aqueous corrosion resistance, superior thermal fatigue resistance, creep resistance, superior surface quality and good formability and weldability [1,2]. Predominantly austenitic stainless steels are used, with success up to 1150°C. Cheaper martensitic corrosion resistant steels can never be used above 550°C as they would transform[3]. Stainless steels intended for high temperature use, such as 44101, must be designed and manufactured with the key principles for improving creep resistance in mind[2]. (see sections 2.2.8-11)

2.2.2 Ferritic Stainless Steels

Ferritic stainless steels have less hot strength than austenitic stainless steels, and mark easily during hot working. Their creep resistance is lessened by the greater atomic mobility in body-centred-cubic (bcc) than face-centred-cubic (fcc) metals. This greater atomic mobility also allows for grain growth at 600°C, far lower than austenitic steels which experience no grain growth below 900°C [1,2]. Grain growth is beneficial for creep resistance, but lowers impact toughness at room temperature. Ferritic stainless steels should not be used if room temperature impact toughness is a major concern, as they can suffer long term 475°C or σ embrittlement[3]. (See sections 2.2.3-4 below)

Ferritic stainless steels have longer thermal fatigue lives than austenitics due to their lower coefficients of expansion. Having similar expansion coefficients to carbon and low-alloy steels, there is also less thermally induced strain in multiple assemblies[1].

The most common ferritic stainless steel, AISI 430, exhibits a marked decrease in creep strength above 700°C and even at extremely low stresses can not be used above 850°C. Above that it oxidises badly due to the formation of austenite, which leads to stresses at the metal/oxides interface. Spalling can occur, because of the loss of scale through local cracking[2].

2.2.3 475°C Embrittlement

After prolonged exposure to temperatures at or around 475°C, ferritic stainless steels suffer from a specific form of embrittlement. Once the steel is returned to ambient temperatures there is a marked increase in hardness and simultaneous loss of toughness and corrosion resistance. A miscibility gap in the iron-chromium system (see Fig. 2.1) is responsible, leading to decomposition of the ferrite into a chromium-rich, iron-poor phase α' alongside iron-rich, chromium-poor ferrite [1,2,3,4].

Chromium carbides and chromium nitrides readily form at around the same temperatures and embrittlement from this relatively rapid precipitation has often been confused with the slower formation of α'. It has proven difficult to lessen 475°C embrittlement by alloying, as almost all additions have been shown to hasten α' formation[4]. Grain-size refinement caused by niobium and titanium additions improve the ductility of α' embrittled steel, even allowing for the hastening of embrittlement caused by increased alloying[2].

475°C embrittled steel does not exhibit microcracks, instead the embrittlement is as a result of the increased flow stress associated with α' precipitation. Given that α' precipitation takes about 10 to 100 hours near 475°C before it becomes apparent, it is not normally encountered during production processes. It can be a problem in actual practice if there are repeated heating and cooling cycles through the danger region[3].

2.2.4 σ (Sigma) Embrittlement

The other well-known form of ferritic stainless steel embrittlement results from the formation of σ phase. Though theoretically possible anywhere between 600°C and 900°C, in actual practice σ phase never occurs below 750°C for steels containing less than 20% chromium, unless stabilised by a significant amount of molybdenum[2]. Small isolated colonies have little effect, but interconnected networks cause the steel to become very brittle[3]. Titanium and niobium accelerate σ phase formation, as do common alloying elements and ferrite formers silicon and molybdenum [3,7]. σ phase forms slowly over hundreds of hours and so will not occur during commercial production processes for wrought stainless steels [1,2,3].

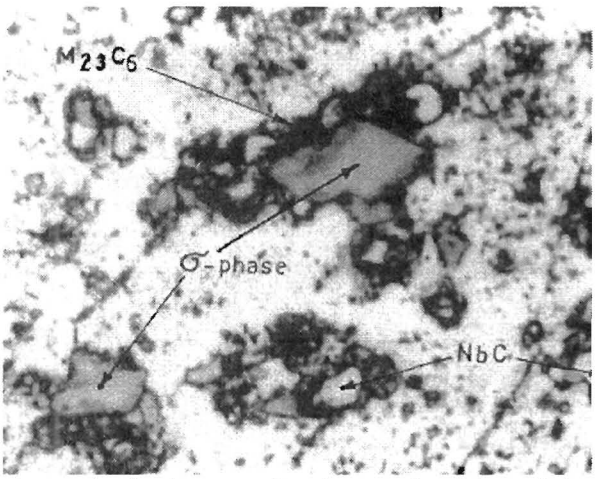

Figure 2.4 An optical micrograph of a cast ferritic stainless steel with niobium additions, (x 1000) from Kuzucu et al. [10]

An example of how σ phase would appear is shown in the optical micrograph in Fig. 2.4 above[10]. This ferritic stainless steel was cast, and the long, slow cooling allowed time for the σ phase tc form.

Another complex embrittling intermetallic phase, χ , with a nominal composition of Fe_2CrMo[3], requires similar precipitation times and temperatures to σ but also significant levels of molybdenum in order to be stable[1] and so will not be seen in 44101.

2.2.5 Stainless Steel Use in Motor Vehicles

Stainless steels have long been used in preference to mild steel for exhaust systems because creep and oxidation resistances are important for a long service life. Most of a stainless steel exhaust pipe is AISI 409, while the hotter end may be AISI 439. Pitting resistance is vital, with the large increase in salt laid on roads during the cold northern hemisphere winters over the last two decades. Exhaust systems are not the only automotive parts increasingly made out of stainless steels. For a typical car in the United States of America, the average amount of stainless steel in a modern motor vehicle is 23kg[11]. The Japanese total average per vehicle is similar, with the exhaust manifold requiring around 5kg[12]. The automotive sector is the best local customer for Columbus Stainless Steel, with the company having supplied more than 31 000 tons of steel to that sector in 1999 and with growth expected to be at least 20% a year[13].

Stainless steel manifolds are much lighter than cast iron manifolds. Lower engine weight is in itself desirable, yet modern engines necessitate exceptional heat resistance. As internal combustion engine efficiencies have increased, as have the temperature of exhaust gases. Stricter regulations in the European Union have also stipulated extended warranties for parts such as environmentally important catalytic converters[14]. Superior dual stabilised ferritic stainless steels were thus designed to replace cast iron engine manifolds. As an engine manifold can reach temperatures of 900°C, this is an extremely demanding application. Thermal shock is also a consideration, as simply driving through water may cause a precipitous drop in temperature[11].

2.2.6 Niobium Additions to Heat Resistant Steels

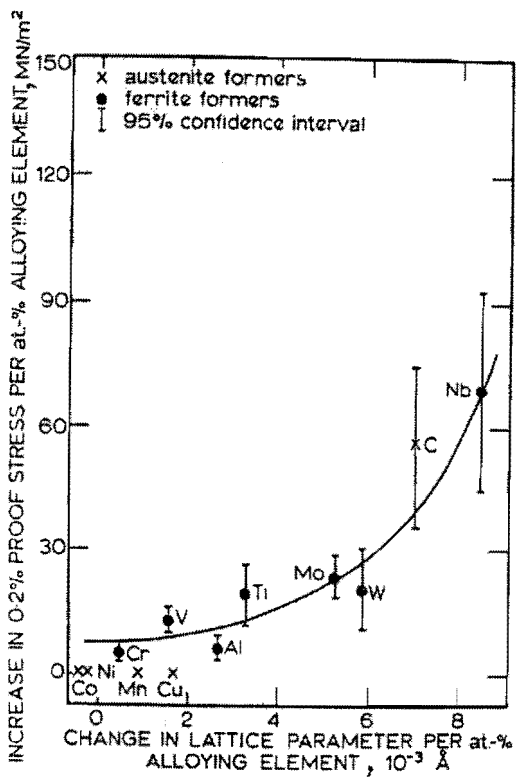

Figure 2.5 Changes in the lattice parameter, due to solute elements, and the resulting increase in the proof stress, from The Metallurgical Evolution of Stainless Steels[3]

The larger atomic size of the substitutionally alloying element,niobium changes the lattice parameter and has a strong influence on solid solution strengthening, as shown in Fig. 2.5 above. 44101 has a nominal 0.5wt% niobium. By increasing the static distortion, alloying decreases the dynamic lattice distortions produced by atomic thermal fluctuations[15]. The root-mean square deviation of the atoms from their

equilibrium positions during thermal oscillations at a given temperature is a definite characteristic of the bond strength. The average interatomic bond strength at high temperature can thus made stronger by alloying [4,15]. Heat resistant steels use niobium additions to improve the hot strength, i.e. yield stress at elevated temperatures.

The decrease in bond strength with increased temperature that would otherwise have occurred is lessened by the presence of the alloying element. Both chromium and niobium have a substantial impact in heat-resistant steels. Increasing interatomic bond strength has the additional benefit of slowing diffusion at high temperatures and hence preserving any metastable microstructural features for longer, which is helpful for creep resistance[15]. (see section 2.2.11)

2.2.7 Niobium and the Hot Strength of a Stabilised Stainless Steel

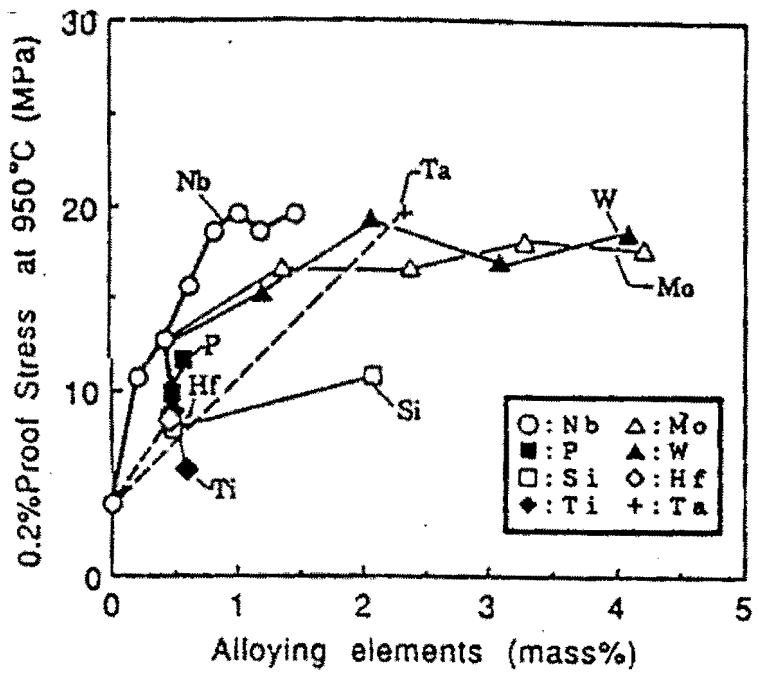

Figure 2.6 The effect of alloying elements on 0.2% proof stress at 950°C for low interstitial steels, according to Fujita[16]

Fujita and co-workers[16] studied the high temperature characteristics of niobium stabilised ferritic stainless steel. They measured the effect of various alloying elements on hot strength at 950°C, as shown above in Fig. 2.6, with niobium having a significant effect at lower concentrations than other possible additions.

If previously annealed at 1250°C, there is a linear relationship between the percentage of niobium added and the 950°C hot strength. However annealing at 1000°C means that there is a saturation in 950°C proof strength above 0.8wt% niobium. During the 1000°C anneal, all niobium up to 0.6wt% is in solid solution. Any higher amounts of niobium form Laves phase. Niobium in solid solution does increase the hot strength. The question is to what extent it remains in solution and what strengthening, if any, is given by the intermetallic phases and carbonitrides.

Since the niobium can not stay in a supersaturated state for long at 950°C after annealing at 1250°C, this increase in strengthening must be due to another cause. Fuijta reports that after annealing at 1000°C of a 0.6%Nb steel, only niobium carbonitrides had formed. Later, after only 0.2% strain had been induced in an interrupted tensile test at 950°C, the Laves phase Fe_2Nb had precipitated along the dislocation networks. Fe_2Nb had formed either in the fifteen minutes prior to testing or under tension. Fujita states that niobium precipitates do strengthen the steel, though probably not the niobium carbonitrides. If the additional hot strength comes from the Laves phase, then Fujita concluded that its major influence is through precipitation on dislocations.

2.2.8 The Nature of Creep

Creep is defined as the process of constant flow for a constant stress over a prolonged period of time. The process of creep has three stages before eventual failure. There will be some initial strain following the application of the load, but the first stage of actual creep will be a rapid, transient period of flow, with the second being one of a linear, steady state. The third and final stage is one of rapidly increasing strain, resulting in eventual fracture[17].

In contrast with the first transient stage, steady state creep increases markedly with temperature and stress. In a metal at high temperatures, the assumption is that the rate of recovery r is sufficiently fast to counteract the rate of work hardening h. That means $d\sigma/dt$ (the decrease in strength) is quick enough to offset $d\sigma/d\varepsilon$ (the rate of work hardening.) The creep rate ($d\varepsilon/d\sigma$) is therefore equal to the ratio of ($d\sigma/dt$) / ($d\sigma/d\varepsilon$), i.e. r/h[17].

2.2.9 The Microstructure during Creep

The microstructure which develops during creep arises from these simultaneous processes of work-hardening and recovery. With the increase in strain, the dislocation density increases. Simultaneously the strain energy is reduced by the mutual annihilation of dislocations and by dislocations forming low-angle boundaries and thereby increasing the network spacing. During constant steady state straining, the refining action balances the growth of the network by recovery. As the creep progresses through steady state, sub-grains form and with increasing deformation, the sub-grain boundary angles increase while the dislocation density remains constant[1,2,17].

The activation energy for steady state creep is that of self-diffusion, due to the need for the edge dislocations to absorb/emit vacancies. Sub-grains do not always form during creep, solute atoms may slow dislocation movement sufficiently such that the steady-state microstructure is a uniform distribution of dislocations[17].

2.2.10 The Role of Grain Boundaries during Creep

Grain boundaries have two different roles to play in creep. They may slide past one another or they may help create vacancies. After a small amount of sliding, grain boundaries are arrested by protuberances and will slide no further until there is plastic flow in these protuberances. Therefore the rate of slip along any given grain boundary is not constant with time. Dislocation pileup at the grain boundaries is followed by some relaxation as dislocations climb towards the grain boundary and this allows further grain boundary movement. Grain boundary precipitation is advantageous in reducing grain boundary sliding.

The grain boundary involvement with the creation and destruction of vacancies is based on the migration of vacancies from one side of a grain to another. This process is termed Herring-Nabarro creep. It occurs at $T= 0.8\ T_m$ and with the stress $\sigma \cong 10$ MPa. Creep through the diffusion of vacancies can occur at temperatures down to 0.5 T_m if vacancies can flow down grain boundaries rather than through the grains. This is termed Coble or grain boundary diffusion creep. Typical Coble creep conditions include temperatures from $0.5T_m$ to $0.6\ T_m$ and low stresses[17].

2.2.11 Creep-Resistant Alloy Design

Designing creep resistant alloys is complex and well designed alloys contain differing constituents in various states of solution and precipitation. There are many factors which affect creep. Creep resistance is often required up to T = 2/3 T_m, yet above T = ½ T_m the solute atoms diffuse as fast as dislocations can move. Therefore solid solution impedance of dislocation movement is secondary during the steady-state stage compared with solute atoms' role in reducing the rate of dislocation cross-slip and climb.

In fact, the most successfully creep resistant metals are fcc metals with low stacking energies and hence dislocations which already readily dissociate, hence discouraging cross-slip and climb. Recovery depends on these processes for dislocations to mutually annihilate and relaxation to occur. With this archetype, niobium's relatively large atomic radius is a key factor, as by lowering the stacking fault energy the separation of partial dislocations is increased and cross-slip and climb is made more difficult.

A good creep resistant alloy, with a solid solution hardened matrix, would also contain a sufficient number of precipitates to force glissile partial dislocations to climb and cross-slip even more in order to circumvent them. In this way precipitates hinder dislocations directly and also have a retarding effect on recovery. This retardation is accomplished through the dislocation network, formed by strain hardening, interconnecting with the particles and thereby being anchored with them[15,16].

For long term effectiveness, precipitates must be stable at service temperatures and finely dispersed. The optimum situation comprises dislocation networks anchored by the precipitates and recovery minimised within a fibrous grain structure. Assuring this state for any given alloy composition is critically dependant on the appropriate thermomechanical processing[4].

Second phase particles also inhibit Coble or grain boundary diffusion creep. These particles are not likely to be affecting the diffusion of vacancies, rather they are affecting the vacancy absorbing capabilities of the grain boundaries. There are

different possible mechanisms for the emission and absorption of vacancies at grain boundaries. However it occurs, both climb and glide of dislocations at the grain boundaries would be involved and would be hindered by particles there[17].

The grain boundaries of fully stabilised ferritic stainless steels are strengthened by the precipitation of iron-niobium intermetallic phases. This beneficial effect can be fully realised if the niobium is taken into solution at high temperatures after cold rolling during production. Intergranular precipitation will then occur at grain boundaries during actual service. Of course, only that niobium not tied up in carbides or nitrides will be available for this purpose[2]. Fujita concluded that Fe_2Nb precipitates are too small to be hindering creep by preventing grain boundary deformation but that the niobium carbonitrides on the titanium nitrides would probably retard grain boundary creep[16].

2.3 Stabilisation of Ferritic Stainless Steels

2.3.1 Sensitisation of Stainless Steels

Stainless steels can become 'sensitised' to corrosion along grain boundaries after exposure to high temperatures. At these high temperatures, the solubility of carbon is great enough for complex chromium carbides to form at grain boundaries. As a substitutional alloying element, chromium diffuses much slower than the interstitial carbon and there may be localised depletion of chromium along the grain boundaries. This may deplete the chromium oxide protective layer to below the level required for the prevention of corrosion. This is 'sensitisation' and regions along the grain boundaries are vulnerable to subsequent corrosion [1,2,3,4,8,11]. The process in ferritic stainless steels is similar to austenitic steels, but sensitisation only occurs above 900°C for ferritics as opposed to 600°C for austenitics. Only at these higher temperatures in the bcc ferritics is the solubility of the interstitial elements sufficient for the formation of chromium carbides [2,3].

2.3.2 Stabilising Additions

Stabilising elements, such as titanium and niobium, are chosen for their carbides' relative stability with respect to chromium carbides. This 'gettering' of the carbon prevents sensitisation [1,2,3,4,8,11]. The lower solubility of carbon in ferritic steels than in austenitic steels makes stabilisers even more necessary. When a stainless steel is

termed 'fully stabilised', this implies that resistance to intergranular corrosion is guaranteed[2].

It should be noted at this point that sensitisation of titanium stabilised steels can occur if exposed to very high temperatures and followed by rapid cooling [8,18]. A possible explanation is that titanium carbide dissolves out of the titanium carbonitrides at high temperatures. The non-equilibrium titanium carbonitrides which form quickly during cooling include some chromium. This leaves the surrounding matrix depleted of chromium. Alternatively, the carbon released by the dissolution of the titanium carbide combines with chromium to form carbides, also leading to localised chromium depletion[8].

2.3.3 Dual Stabilisation

Gordon and Van Bennekom[8] have recently reviewed the subject of stabilisation of ferritic stainless steels. Titanium and niobium are both popular stabilisers and are frequently used in conjunction. Dual stabilisation seeks to minimise the deleterious effects (see section 2.3.4) and maintain the advantages of each stabiliser. AISI 466 is an example of dual stabilisation. It is a corrosion resistant 11wt% chromium steel like AISI 409, yet it has an operating temperature of 50°C to 100°C higher[11].

The advantages of dual stabilisation with titanium and niobium are:

1) Large cuboidal titanium carbonitrides are deleterious for toughness and with fewer forming in dual stabilised steel than in titanium stabilised steel, the toughness is improved[8].
2) Niobium stabilised steels experience weld cracking problems because of long, columnar grain formation and segregation leading to low melting phases at grain boundaries. Titanium nitrides in dual stabilised steels form in the melt and act as heterogeneous nucleation sites, resulting in a fine equi-axed grain structure. Better mechanical properties for the weld result, along with a larger grain boundary area per volume and a consequential lower concentration of tramp elements. Less niobium also directly minimises the possibility of low melting phases at grain boundaries[8].

3) Large titanium nitride particles can cause surface defects in titanium stabilised steels, adding to production costs by increasing the surface grinding required. Dual stabilisation allows for lower overall production costs, as the greater initial cost of niobium is offset by less grinding required for the desired surface finish[9].

2.3.4 Appropriate Stabiliser Levels

Effective stabilisation is achieved through niobium alone with Nb = 10(C +N)[8], which is close to the theoretical prediction of Nb = 7.7(C) + 6.6(N)[2] .
Sufficient titanium levels have been empirically determined as Ti = 0.15wt% + 3.7 (C + N), which is greater than the stoichiometric equation of Ti = 4(C) + 3.4(N)[8].

The optimum dual stabilisation limits have been determined experimentally such that Ti + Nb = 0.2 +4 (C + N) is the minimum and Ti + Nb = 0.8 is the maximum[19]. A ratio of titanium to niobium of 1:2 is ideal[8]. The 44101 samples studied in this project are just within the maximum limit, with the ratio of titanium to niobium being the recommended 1:2.

Apart from the unnecessary additional cost of excess stabilisers, there are adverse consequences. Excessive stabiliser decreases the toughness of welds. The effects of over stabilising with niobium are gradual and not as deleterious or major as those for over stabilising with titanium. Rapid cooling from high temperatures does not cause sensitisation as noticeably as in titanium stabilised steels. It is better to limit stabiliser additions to the optimum levels for the required properties[8].

2.4 Precipitation in Stabilised Ferritic Stainless Steels

2.4.1 Introduction

The nature of the precipitation is a major influence on the mechanical properties of any steel. Precipitation requires lower temperatures and shorter time in ferritic than in austenitic steels owing to the faster atomic diffusion in bcc metals [1,3]. Precipitates and inclusions found in stabilised ferritic stainless steels are very different to those in AISI 430.

During processing, the tendency of the steel to recrystallise is heavily dependent on the nature of the fine precipitates present during the treatment. Recrystallisation is reduced in the titanium stabilised steels and considerably more in the niobium stabilised steels. Recrystallisation is hindered by the abundant precipitation in both[2,20]. Titanium stabilised steels possess titanium phosphides and fine titanium carbides, while their niobium stabilised counterparts contain Fe_2Nb and niobium carbonitrides[2].

2.4.2 Characteristics

The solvus temperatures of probable precipitates in 44101 are included in Fig. 2.7. Some titanium nitrides form in the melt prior to solidification.

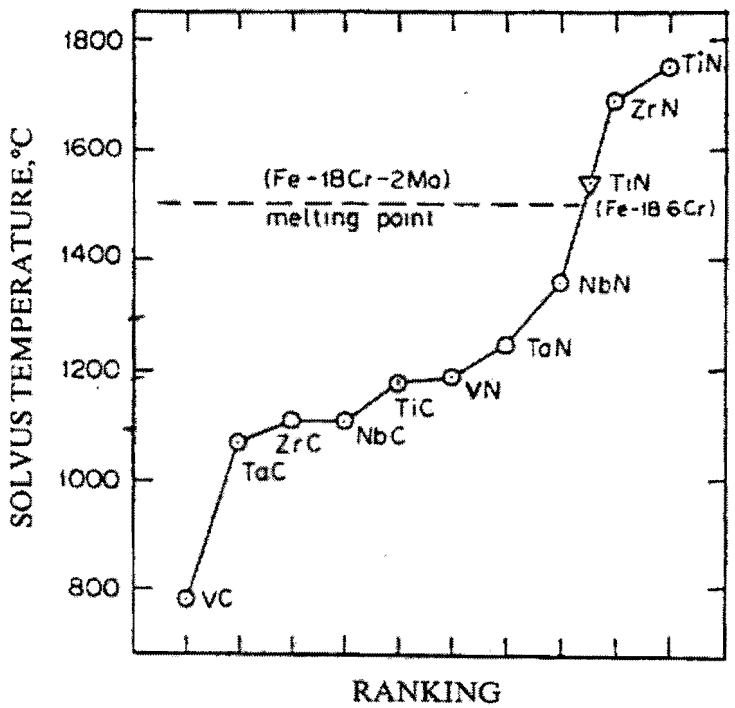

Figure 2.7 The solvus temperatures of precipitates found in stabilised ferritic stainless steels, from the review paper by Gordon and Van Bennekom[8]

The nitrogen precipitates out at higher temperatures as titanium nitrides, which are nuclei for further carbonitride precipitation. When cooled at moderately fast rates, nearly all the carbon is precipitated out while the nitrogen remains in solution. The solubility of carbon is considerably less than of nitrogen in these steels[21].

Inclusions found in stabilised stainless steels are oxides, manganese sulphides and possibly titanium sulphides [1,2,3,8]. In titanium stabilised steels the coarse precipitation, greater than 2μm in size, takes the form of titanium nitrides. These precipitate at grain boundaries with titanium carbide 'belts'. There is fine precipitation of titanium carbides and titanium phosphides between 100nm and 500nm in size, both at grain boundaries and intragranularly[2].

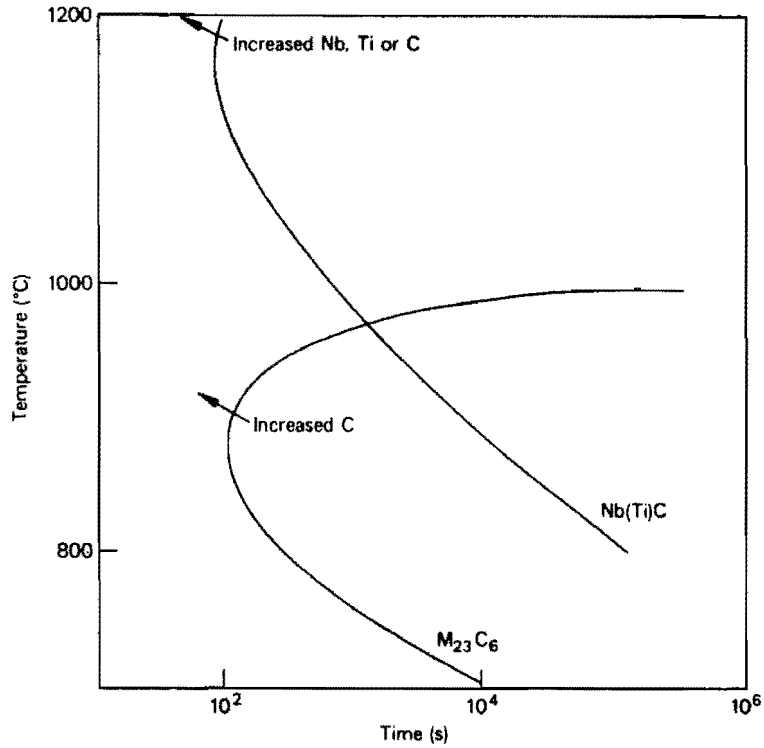

Figure 2.8 Temperature –time growth curves for $M_{23}C_6$ and Nb(Ti)C in Cr-Ni austenitic steels, from Steels – Microstructure and Properties[4]

The precipitation growth curves shown in Fig. 2.8 above were only available for austenitic stainless steels. Precipitation is far slower in austenitic steels than in ferritic steels, approximately by two orders of magnitude.

The packing system for titanium carbides and nitrides is face-centred cubic, with carbon and nitrogen occupying the octahedral sites in the crystal lattice. Titanium carbides and titanium nitrides are mutually soluble. The ratio of titanium nitride to titanium carbide in the precipitate is dependent on the ratio of nitrogen to carbon in the steel. The colour of the precipitate is dependent on this ratio. A yellow/orange colour indicates around only 10% titanium carbide, a red/purple colour 15-22% and a blue/purple colour about 40% titanium carbide[8].

In niobium stabilised steels there are small niobium carbonitrides and iron-niobium intermetallic phases, below 500nm in size[2]. These form small, spherical precipitates which do not decrease the toughness of the alloy significantly, as demonstrated by niobium stabilised steels' greater toughness than titanium stabilised steels[8].

The term 'Laves' phases refers to phases in which two dissimilar types of atoms pack together so closely that the usual co-ordination maximum of 12 atoms is actually exceeded. The two elements must have a size difference of 20-30% in order to pack together, with the elemental ratio being 2:1. For example, in Fe_2Nb each Fe atom has 6 Fe neighbours and 6 Nb neighbours, with each Nb atom having 12 Fe neighbours and 4 Nb neighbours. This means an average co-ordination number of 13.33, i.e. greater than the maximum twelve possible for atoms of equal size.

Fe_2Nb has a structure like that of $MgZn_2$, with the Fe atoms arranged on a space lattice of tetrahedra. In $MgZn_2$, the tetrahedra are joined point-to-point and base-to-base in long chains, called a wurtzite structure. Fe_2Nb has a limited range of homogeneity, not due to any ionic requirements, but because the particular geometry permitting a higher co-ordination number necessitates it[17].

Laves phase precipitates according to Cahn's theory of spinodal decomposition[22]. Spinodal decomposition refers to a sinusoidal distribution of differing composition spontaneously giving rise to precipitates where the matrix composition is extremely close to that of the precipitation. This is in contrast to the nucleation and growth model of precipitation. Transmission electron micrographs show striations in the early stages of decomposition, termed 'tweed' structure[23]. Tweed is a sinusoidal distribution of composition, preceding precipitation. It is accompanied by a softening in Fe-Ti and Fe-Nb binary alloys, for which there is as yet no explanation.

Laves phases form at grain boundaries and dislocations and throughout the matrix, in that order of preference[24]. Precipitate-free zones form adjacent to both grain boundaries and clusters of dislocation-nucleated precipitates[25].

Depending on the nitrogen levels in the steel, rod-like Cr_2N can form. This dissolves above 850°C. Angular Cr_2N precipitates at grain boundaries cause a drastic increase in the impact transition temperatures of 30% chromium alloys[26].

2.4.3 Similar Precipitation in Heat Resistant Steels

Prior to their use in stabilised stainless steels, titanium and niobium had already been added to nickel-containing austenitic steels to improve their heat resistance. While the situation is very different, the precipitates and reasoning behind their use are similar. Therefore this analogous field of research is an alternative source of useful information to the work done on stainless steels.

Lanskaya[15] studied titanium and niobium precipitates in heat-resisting steels. He reported that no single niobium carbonitride phase forms, as it consists of separate phases. Each large carbonitride particle contains a nitride surrounded by carbides. Previous chemical analyses of the phase composition had obtained an average of the data, and researchers had reported it as a single phase. Pure niobium carbides are absent, as they are only found precipitating at nitrides . The composition varies with the nitrogen content. It may typically be $Nb(C_{0.98},N_{0.06})$ or $Nb(C_{0.59},N_{0.37})$ though intermediates are possible.

Lanskaya introduced the use of the Laves phase for structural strengthening in heat resisting steels. It causes no embrittlement and plasticity remains high. An advantage of Laves phase is its relatively large size compared with other precipitates used for similar purposes at high temperatures, such as N_3Ti. Over the long term there is no decline in properties as the precipitates do not coalesce.

Lanskaya found that ageing drastically decreased the hot strength of these heat resistant steels, with precipitation mostly along grain boundaries. Yet, in non-aged specimens, under pressure and operating at simulated service temperatures, Laves phase formed mostly along slip lines, increasing hot strength. Continuous cooling from a solid solution resulted in grain boundary precipitation and did not produce hardening to the extent that isothermal ageing did. The presence of other phases hampered Laves phase formation[15].

2.4.4 A 17%Cr-2%Mo Ferritic Stainless Steel

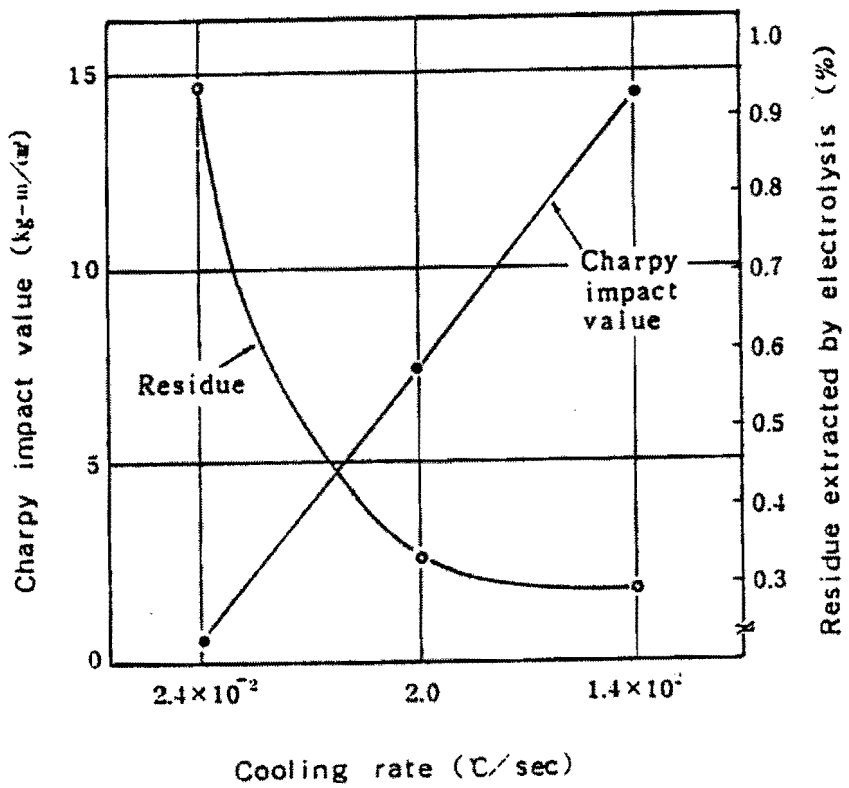

Figure 2.9 The effect of the cooling rate on both the Charpy impact value at room temperature and the electrolytically extracted residue, by Sawatani[27]

Sawatani and co-workers[27] studied a low interstitial 19%Cr-2%Mo ferritic stainless steel and its mechanical property dependence on production processes. The 2% molybdenum allows for the formation of significant Fe_2Mo, a Laves phase. The addition of the molybdenum alone would probably not affect impact toughness. (see section 2.5.2) A large amount of Laves phase precipitates during slow cooling and so decreases the impact toughness, as shown in Fig. 2.9. As-rolled sheets have fine intragranular Laves precipitation, but annealing around 700°C promotes massive precipitation at grain boundaries, as shown in Fig 2.10. Only in the latter case was impact toughness affected. They recommended rapid forced air cooling to ensure avoidance of its formation.

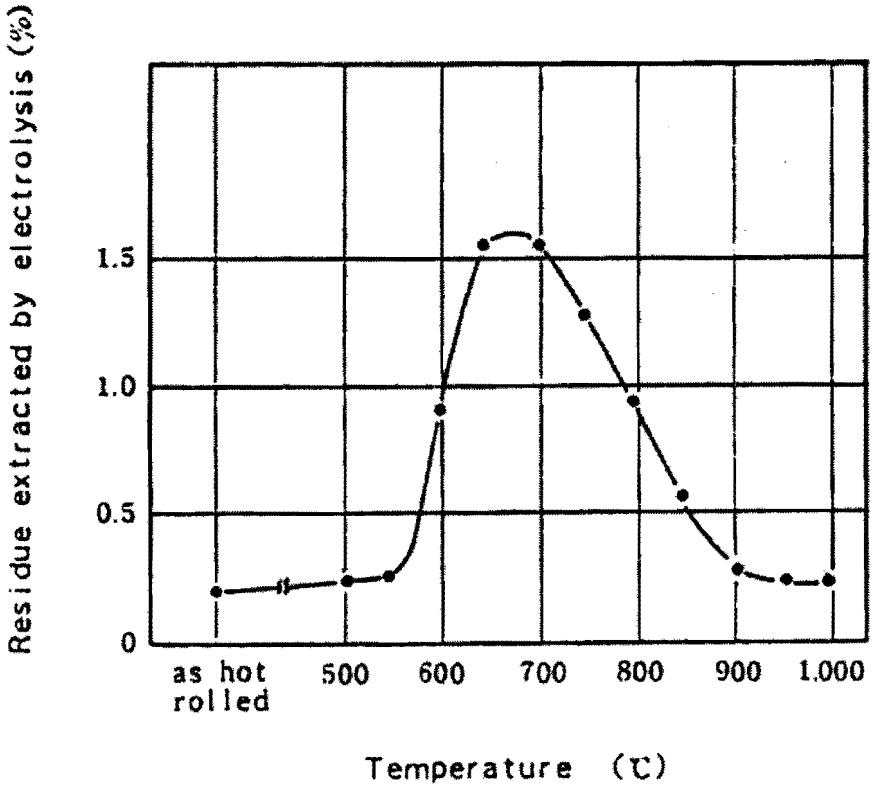

Figure 2.10 Precipitation of the Laves phase after annealing for 1 hour for various temperatures, by Sawatani[27]

2.5 Stabilisers in Low Interstitial Steels

2.5.1 The Ductile to Brittle Transition Temperature

As a notch-sensitive bcc metal, the toughness of ferritic stainless steels exhibits a sharp transition between ductile and brittle behaviour in an impact test. This transition occurs at the ductile-to-brittle transition temperature (DBTT)[1,2]. Typical stainless steel DBTTs have been lowered by decreasing carbon contents. The impact toughness of ferritic stainless steels was vastly improved with the lowering of interstitial levels in the 1970s.

Stabilisation should also improve matters, by eliminating chromium carbides at grain boundaries, but large additions of stabiliser tends to increase the DBTT once more. Grain size is very important for the value of the DBTT and it is difficult to determine what effect other factors such as the precipitation have on the DBTT without understanding how the grain size was affected by the same factors[3].

If the stainless steel has a high DBTT then there is a greater sensitivity to the strain rate during deformation[28]. A high DBTT is not necessarily a problem in the use of the steel, particularly for thin products. The transition from ductile to brittle behaviour varies tremendously with product geometry. Brittle behaviour has never been observed in the case of thin sheets under normal loading conditions, even if their nominal DBTT is higher than room temperature [1,2].

2.5.2 Effect on Impact Toughness of Low Interstitial Content

Plumtree and Gullberg[29] studied the impact toughness of Fe-25%Cr and Fe-18%Cr-2%Mo steels. The steels were quenched in water from high temperatures, so that each were in a similar state with the maximum interstitial content in solution. Otherwise carbides also enhance brittle, cleavage fracture by decreasing the surface energy. It is because of the formation of additional carbides that higher interstitial alloys normally have higher DBTTs. Titanium carbonitrides, and to a lesser extent, niobium carbonitrides are less harmful to the impact toughness of ferritic stainless steels than chromium carbonitrides[30].

Impact transition temperatures (DBTTs) were measured against their interstitial content. The results are shown in Fig. 2.11. For a given interstitial content, the DBTTs or impact shelf energies were not affected by the presence of 2% molybdenum or the change in chromium content from 18% to 25%. This is supported by the findings of Wood[31] that for 18%Cr titanium stabilised stainless steels, 2% molybdenum has no effect on the impact transition temperature.

For a desirably low DBTT and high shelf energy, the combined carbon and nitrogen contents should be kept below 150 ppm, below which further decreases have no further effect. Above 150 ppm, further increases cause a marked increase in DBTT, though once above a certain level (C+N $\cong$ 600 ppm) further increases are not significant. For these stainless steels a room temperature Charpy test value of between 14J to 70J, and above the DBTT a value of 160J would be considered typical[29].

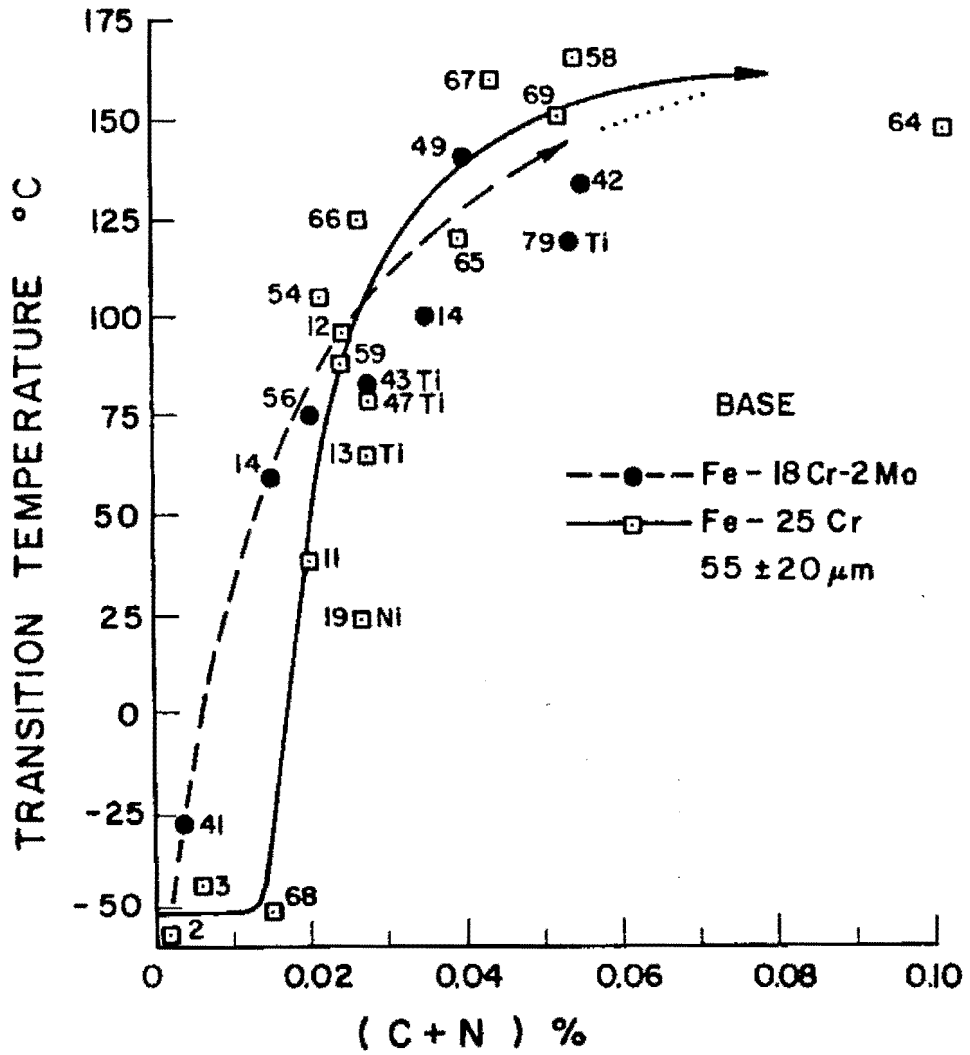

Figure 2.11 The impact transition temperature (DBTT) versus the interstitial content for Fe-18Cr-2Mo and Fe-25Cr ferritic stainless steels, by Plumtree and Gullberg[29]

2.5.3 Effect on Impact Toughness of Dual Stabilisation

Redmond[32] investigated the effect of residual and stabilising elements on the impact toughness of 18%Cr-2%Mo ferritic stainless steels which contained 0.015%C and 0.015%N. Residual elements such as sulphur, silicon and manganese were shown to have minor effects on the DBTT. Niobium stabilised steels have lower transition temperatures than titanium stabilised steels. Trends in the DBTT for niobium and titanium dual stabilised steels, as one element is varied against the other, are shown in Fig. 2.12. For constant niobium levels there is an increase in transition temperature as titanium increases, followed by a slight decrease as more titanium is added. The maximum for 0.44% niobium is at 0.2% titanium, with a transition temperature just

over 30°C. It is not possible to discern any real trend as niobium levels are increased against constant titanium levels.

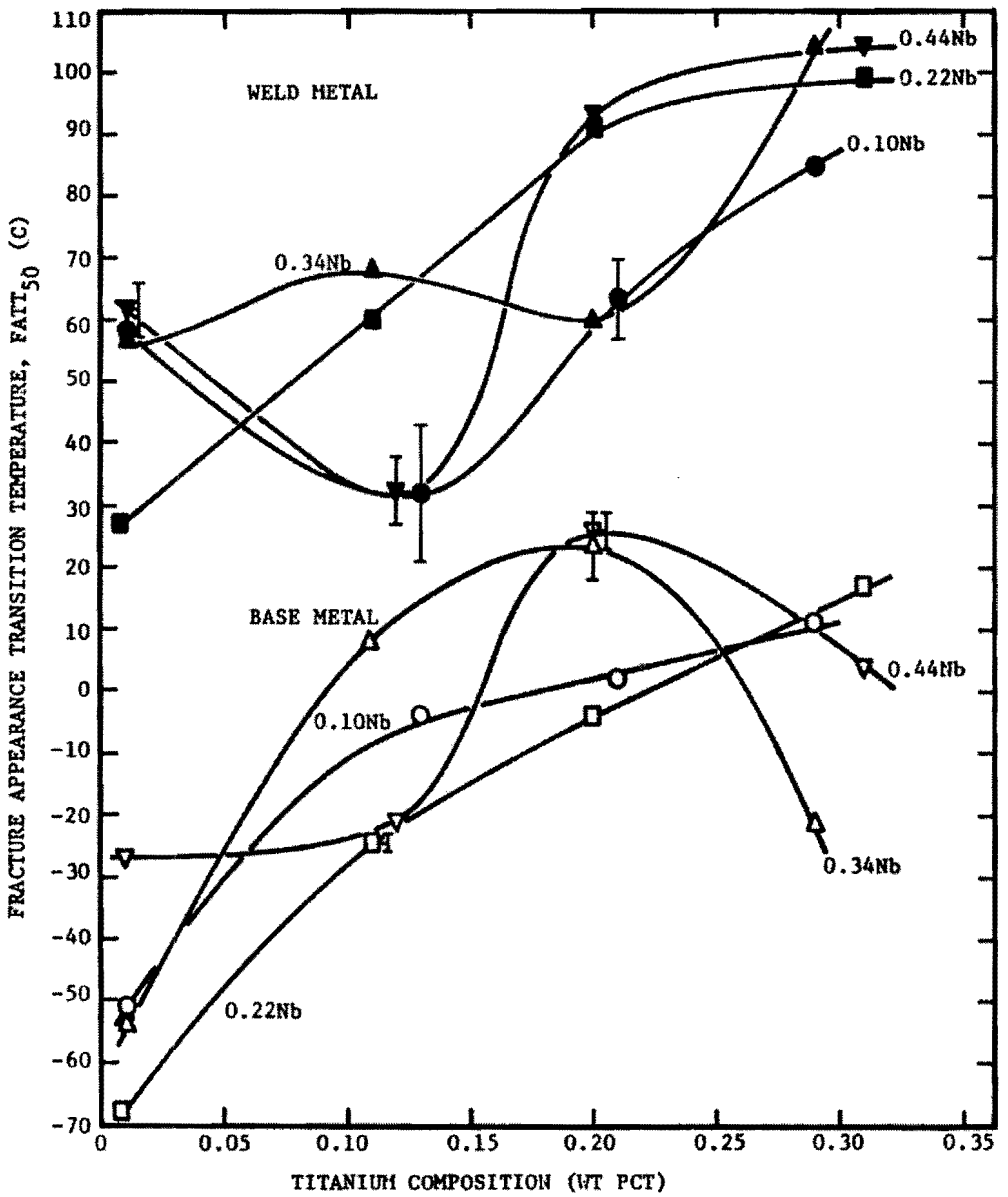

Figure 2.12 The impact toughness of 18Cr-2Mo ferritic stainless steel as a function of niobium and titanium content, by Redmond[32]

2.6 Grain Boundary Effects of Low Interstitial Levels in Iron and Steels

2.6.1 Carbon Segregation to Grain Boundaries

The carbon levels in 44101 are around 0.015wt% to 0.023wt%, which are low. With the addition of stabilisers to 'getter' the carbon, the free carbon in the matrix will fall even lower. Now the role of carbon segregated to grain boundaries has been the subject of much work done over the last half-century. Carbon does segregate preferentially to grain boundaries. It has been difficult to separate the role of carbon from other elements, whether reinforcing or weakening the atomic bonds over the boundary, as even the purest irons contain impurities to some degree [1,4].

It has been known since the 1950s with the work of Rees and Hopkins [33,34], that at extremely low carbon levels (≅ 0.005%), the DBTTs of high purity irons begin to increase again. They believed that, with low levels of carbon, elemental oxygen segregated to grain boundaries, caused grain boundary embrittlement and sharp rises in the DBTT. The intergranular fracture only became apparent at low temperatures. Oxygen was believed to be an embrittling element [33,34,35].

This was investigated in the 1970s with the by-then available Auger Electron Spectroscopy techniques. Powell and co-workers showed that sulphur was segregated to grain boundaries in high purity irons which were experiencing embrittlement[36].

Pichard, Rieu and Goux tested irons with different oxygen contents (see Fig. 2.13), and found that embrittlement was correlated with sulphur segregated to grain boundaries and extremely low carbon levels[37]. Yet sulphur does not segregate in stainless steels, due to its interaction with chromium[4]. In 1997, Matsui and Kimura studied oxygen's decohesiveness effects on grain boundaries in high-purity irons. They found that oxygen segregated to grain boundaries does promote intergranular fracture to some extent, but that only at temperatures of a few tens of Kelvins was it a significant factor[38].

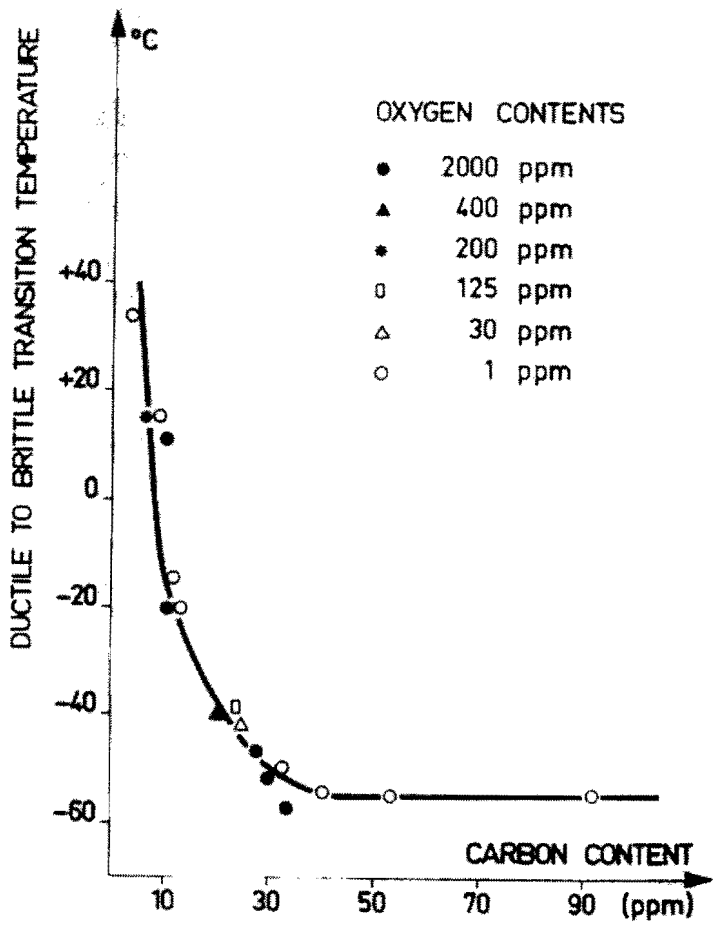

Figure 2.13 The DBTT of high purity irons as a function of carbon content, by Pichard, Rieu and Goux[37]

2.6.2 Intergranular Fracture in Ultra-Low Carbon, Low Alloy Steels

Niikura and co-workers[39] studied ultra-low carbon low-alloy steels with niobium additions and their susceptibility to intergranular fracture (IGF), especially after being reheated into the 600°C to 700°C range as shown in Fig. 2.14. Either a decrease in carbon, or an increase in niobium enhanced the intergranular embrittlement. Intergranular fracture occurred for a critical level of carbon, which increased with niobium content. Carbon segregation was found on prior austenitic grain boundaries and carbon segregation levels were significantly lower for lower-carbon steels and steels containing niobium. There is a consistent correlation between lowering carbon content and intergranular fracture. They concluded that the same mechanism was operating in these steels as in the pure irons in the work discussed in the previous section. In this case, the niobium additions were forming niobium carbonitrides, bringing the carbon in solution to extremely low levels.

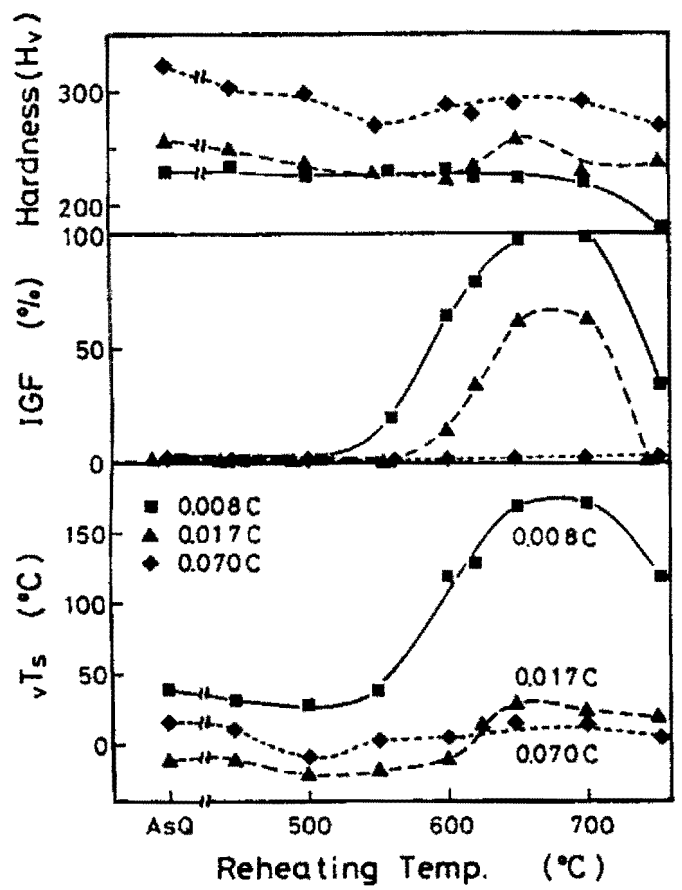

Figure 2.14 The effects of annealing temperature on low alloy steels, with low interstitial levels and niobium additions, by Niikura[39]

C' ›ter 3 Experimental Methods

3.1 Alloy Composition

Samples were supplied by Columbus Stainless of Middelburg. Different heats were sampled, with the following compositions made available for the experiments. Samples from A and C were received hot rolled and annealed and used in the study of the precipitation within the steel, discussed in sections 3.4 and 4.5. Samples from E were supplied cold rolled, but not annealed and were needed for the ageing at 100 hours, see section 3.8 and 4.6. Sample S was a specimen from a shattered coil, with a fractured edge that was examined in the failure analysis, see sections 3.3 and 4.1. Alloy F was not a 44101 sample, but a high carbon and nitrogen AISI 430 ferritic stainless steel used as a comparison with alloy C in the Auger Electron Spectroscopy, described in sections 3.7 and 4.4.

	A	C	E	S	F
Cr	17. 78	17. 73	17. 87	17. 99	16. 756
C	0. 023	0. 014	0. 013	0. 017	0. 057
N	0. 0184	0. 0153	0. 0217	0. 0174	0. 0421
Ti	0. 28	0. 215	0. 208	0. 231	*
Nb	0. 46	0. 529	0. 559	0. 5295	*
Mn	0. 39	0. 44	0. 47	0. 543	0. 6
S	0. 006	0. 0039	0. 001	0. 0016	0. 0169
Si	0. 42	0. 45	0. 49	0. 522	0. 349
Ni	0. 21	0. 17	0. 17	0. 268	0. 161
P	0. 034	0. 03	0. 023	0. 0269	0. 269
Mo	0. 03	0. 02	0. 04	0. 01	0. 01
O	0. 0099	0. 0062	0. 0045	*	*

Figure 3.1 Table of compositions for 44101 heats studied (in weight percent)

3.2 Precipitation Studies

3.2.1 Heat Treatments

Samples of heats A and C were solution treated at 1050°C for two hours, before being annealed at 100°C intervals between 500°C and 900°C for times of one hour, two hours, four hours, eight hours and sixteen hours. Shorter periods of fifteen and thirty minutes at 800°C were also included. This solution treatment temperature of 1050°C is that used by the producer as optimal for grain growth and recrystallisation. The two hour period would certainly ensure that all Laves phase present in the material would go into solution. The solution treatment was done in a Gallenkamp REX-P9 furnace.

The annealing treatments followed, with an immediate transfer to salt baths. There were two salt baths, each from Kilns & Furnaces Manufacturers Pty Ltd of Cape Town. They are type SBF, with a power of 3 kW and an individual capacity of approximately 500cm^3. (They are designed for small experiments of this nature.) The salts were Durferrit® *GS 430* and *GS 540*, manufactured by Degussa[40]. (Though the local agent is now Chemserve Metal Sciences in Epping Industria.) These are non-cyanide containing salts. Baths containing cyanide attack chromium containing steels, as the cyanide oxidation products contain alkaline substances to which the chromium has poor resistance.

One salt bath contained *GS 430*, suitable between 500°C and 700°C while the other contained *GS 540* for between 750°C and 900°C, with the latter including 'inertor' or protective compound *R2*. This inertor compound is in suspension in the *GS 540* and prevents any appreciable decarburisation which would otherwise be evident in steels above 700°C. A low carbon stainless steel is less susceptible, but R2 also decreases carburisation of low carbon steels so it was included as a preventative measure. The salt baths meant that the samples were rapidly at the annealing temperature. Annealing was followed by quenching into water.

3.2.2 Sample Sectioning and Mounting

Samples from each heat supplied were all sectioned using an Al_2O_3 cut-off wheel (Struers, type 03TRE) on a mesotom. This wheel is suitable for the cutting of ordinary steels (Hardness Rockwell C of between 30–45) and was chosen so that damage to the

sample would be minimised. In all such cases, damage is caused to the metallographic structure whenever it is near the cut edge of a sample, and the microstructure within typically 100μm of the edge will be ruined. It is important that the microstructure of the specimen be representative of the sample's bulk structure and it is a function of the grinding step during specimen preparation to reveal that. All specimen surfaces for this precipitation study (see section 4.5) were in the normal/rolling direction plane.

3.2.3 Surface Preparation

Optical and scanning electron microscope specimens need to be ground and polished in order to remove damage from cutting and to render the surface smooth enough for optical microscopy. Traditional methods of grinding and polishing stainless steels have used up to six different progressively finer grit sizes of SiC paper and diamond paste to achieve a well polished surface that after etching will reveal a true reproduction of the microstructure. Generally poor results were achieved using variations on this theme, and after etching it was necessary to begin the process again, ensuring that all traces of the etching were removed. This was time-consuming and mostly unsuccessful, so a very different method was adapted to prepare specimens.

This new method was part of the Struers MD-System[41]. These methods use modern equipment and materials with a different philosophy. They aim to achieve specimen integrity (a faithful reproduction of the material structure) prior to a polishing stage. The system comprises a range of abrasive and polishing pads, able to magnetically fix onto the spinning wheel in the automatic polisher, with a range of abrasives. Preparation of specimens should take fewer steps, with less time and material consumed.

Traditional practice relies on the samples being ground through the series of progressively finer papers to systematically reduce the depth of deformation, with one or two final polishing steps required to produce the final polish. Each step aims at producing a finer finish and aims to remove all deformation introduced by the preceding step. This brute force approach is generally successful over a wide range of metallic alloys and is simple to apply.

Yet the more modern approach is to optimise the specimen preparation according to the alloy's hardness and ductility. It is more concerned with the surface *condition* than with the surface *finish.* Each preparation procedure is intended to employ the least amount of steps or time before achieving specimen integrity. Firstly the specimen must be plane, then each abrasive is chosen such that the residual damage is less than before that step. The time spent on each abrasive is aimed at reducing the amount of deformation to the optimal degree, relating the abrasive functions to 'Z-curves,' rather than seeing the abrasive as producing any given surface finish.

In Fig. 3.2, the 'Z-curves' are used to describe the effect of grinding and polishing a 0.37% carbon steel, using a series of finer SiC papers. This sample would have had 120μm of deformation induced during sectioning. The total deformation depth on the specimen surface is shown on the y-axis, with the preparation time on the x-axis. Each step, grinding with SiC papers and later polishing, initially rapidly reduces the deformation depth but subsequently more slowly increases it. That means that too much grinding at any stage can cause the deformation depth to increase, which is counter productive. Therefore, once the Z-curve of any particular grinding pad or polishing regime is known, then it can be incorporated into a preparation scheme in the optimum way.

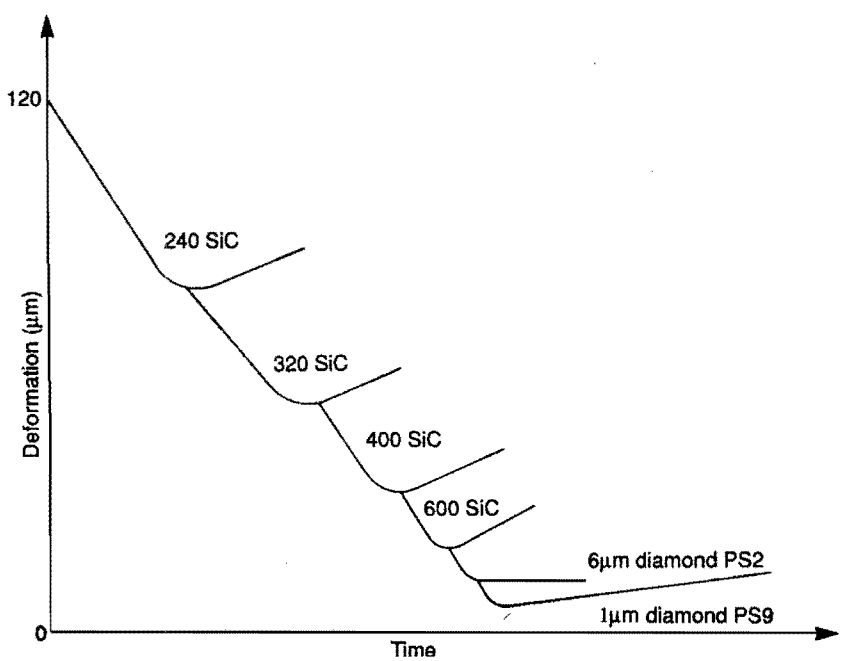

Figure 3-2 The 'Z-curves' of the depth of specimen deformation against the preparation time for a 0.37% carbon steel[41]

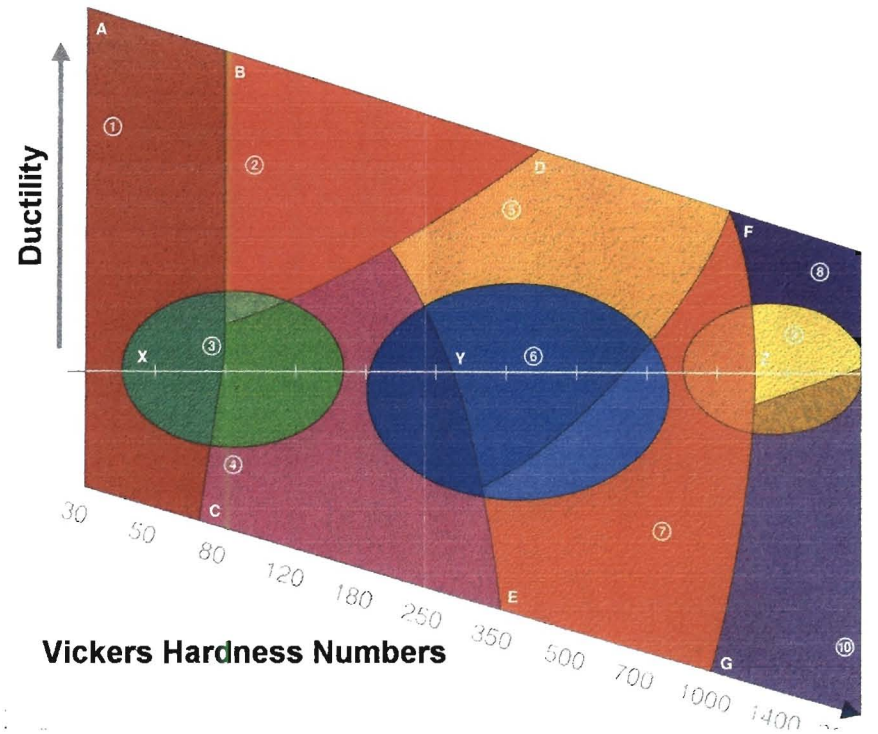

Figure 3.3 The Metalog Preparation Schematic, with specimen ductility against the Vickers Hardness Number, with coloured regions outlining different preparation regimes[42]

Good, reproducible specimen preparation was achieved using method C of Struers' Metalog MD System. This method was tried after similar Struers' schemes (e.g. X and Y) failed to yield as consistent a surface finish. Which method is used depends on the hardness and ductility of the specimen. Method C is advised for alloys such as medium carbon steels and cast brass. (See the Metalog Preparation Schematic in Fig. 3.3) The method was adapted slightly, in that longer periods of time (shown in brackets) were more effective for the Fine Grinding and DP steps.

Step:	Plane Grinding	Fine Grinding	DP	OP
Surface: (Trade Name)	MD-Primo	MD-Largo	MD-Dac	MD-Nap
Abrasive:	SiC	9μm DP-Suspension	3μm DP-Suspension	Colloidal Silica
Revolutions per Minute:	300	150	150	150
Force: (N)	20N	30N	30N	10N
Time: (min)	Until plane	5 (8)	5 (7)	1

Figure 3.4 Preparation details for method C in the Struers Metalog MD System[42]

3.2.4 Etching

Chemical etchants were used, based on hydrochloric acid and nitric acid. This combination is frequently used by metallurgists and is called aqua-regia[43]. The first variant used was glyceregia, which is hydrochloric acid and nitric acid moderated with glycerine. It was used for the fractography (see section 4.1) and early investigations of precipitation. Glyceregia varies in the ratio of its three constituents. The composition used was concentrated HCl, glycerine and HNO_3 in the ratio 3:2:1 by volume. The HCl and glycerine were first mixed thoroughly, before adding the HNO_3. The etchant then sat for half-an-hour before being swabbed onto the specimen. It was found that the etching was quicker and more even if the specimen had been warmed previously. The specimen was washed in hot water, then methanol and dried. Glyceregia is a 'clean' etchant , outlining precipitates and inclusions and producing surface relief for twins and grains. Only fresh glyceregia could be used, as it is not stable and after three to four hours, older glyceregia does have a tendency to pit. Glyceregia produces explosive esters and has been known to explode if kept in storage and so was discarded immediately after use.

Once the specimen preparation method had been optimised, then it was found that a stronger etchant could be used. Previously any imperfection was ruthlessly etched, so glyceregia was more appropriate. The images in section 4-5 and 4-6 are etched by

H_20, HCl and HNO_3 in a 3:2:1 ratio. It produced similar results to glyceregia, but took only 10-45 seconds. Specimens were placed in the etchant in the ultrasonic bath to ensure a free flow of etchant over the surface.

The image in Fig. 3.5 shows a fully hand-polished specimen, with Nomarski interference contrast used to emphasise surface relief. The difference in height from grain to grain is clear, with the grain boundaries very prominent. The harder precipitates stand proud of the specimen, with the matrix immediately behind them being protected. This means that a perfectly even polished surface is difficult to achieve. Another difficulty is that many tiny precipitates are removed and roll about, scratching the surface very badly unless great care is taken during the final polishing steps.

3.2.5 Optical Microscopy

A Reichert MeF3-A light microscope was used in brightfield mode, with some use of Nomarski interference contrast. This was in conjunction with a Digital Camera Leica DC 100, with attendant software. All images were stored and manipulated digitally, with micron markers drawn in Paint Shop Pro™ and then printed on a Hewlett-Packard 2000CN colour printer at the Electron Microscope Unit at UCT.

3.3 Fractography with the Scanning Electron Microscope

A sample of the fracture surface from a coil that had fractured after hot rolling was provided by Columbus Stainless. It was examined using the Leica 440 Scanning Electron Microscope at the Electron Microscope Unit at UCT. The failure had occurred straight across the width of the coil, in the transverse direction. Images of the fracture surface were therefore taken in the normal transverse plane. A sample of the fracture surface was sectioned halfway through its thickness, with the new surface then polished. This provided a view in the plane of the transverse and rolling directions of the area alongside the fracture surface. Secondary electron images were also obtained of tensile test fracture surfaces, allowing comparisons to be made between the modes of fracture of embrittled (alloy S) and unembrittled (alloy C) steels.

3.4 Scanning Electron Microscopy of Precipitation

Specimens were ground and polished as for the optical microscopy. The Leica 440 Scanning Electron Microscope, at the Electron Microscope Unit at UCT, was used to study the precipitation, in both the secondary electron and backscattered electron modes. Specimens were carbon coated, as this was preferable to metallic coatings for the backscattered mode. Secondary electron images are determined by the topography of the specimen, while the backscattered electron images are also heavily dependant on the atomic number of the elements present [44,45]. Hence the brightness of each part of a backscattered electron image is dependant on the atomic number of the elements present. Early prepared specimens suffered from SiC contamination from the grinding papers, which was less of a problem once the switch had been made to the MD-Struers system.

Secondary electron images provided clear views of the precipitates at very high magnifications. Backscattered electron images were useful in differentiating between different precipitates. The probe current was 500pA, on medium gain with a careful optimisation of brightness and contrast. The Leica 440 could acquire images with a 'negative' (i.e. less than one) 0.2 gamma potential. This accentuated the visual contrast between the precipitates and the background, in the backscattered images of Figs. 4.58-59.

3.5 X-Ray Mapping

Mapping of the elemental composition of a large grain boundary precipitate was achieved using Energy Dispersive Spectroscopy (EDS) in a point-by-point analysis, with the EDS attachment to the Leica 440 Scanning Electron Microscope being made by Kevex Instruments.

3.6 Tensile Testing

Tensile tests were performed using a Zwick 1484 Universal Tensile Tester controlled by a personal computer with the data manipulated in Microsoft Excel. The specimens conformed to the dimensions prescribed for flat subsize sheet specimens in ASTM E8[46]. The gauge length was 25mm and the width was 6.25mm. The alloy C specimens were 4mm thick, while the embrittled alloy S specimens were 5mm thick. The tensile axis was in the transverse direction. The strain rate was $0.001s^{-1}$. For those specimens which were tested 'under constraint', a short, rounded gauge length of 4mm was cut within the stipulated gauge length. The centre of the inner gauge length was now only 3.25mm wide.

A fractured tensile specimen of the embrittled alloy S was ground, polished and etched so that it may be examined using optical microscopy. The orientation and form of the cracks in the specimen were then investigated.

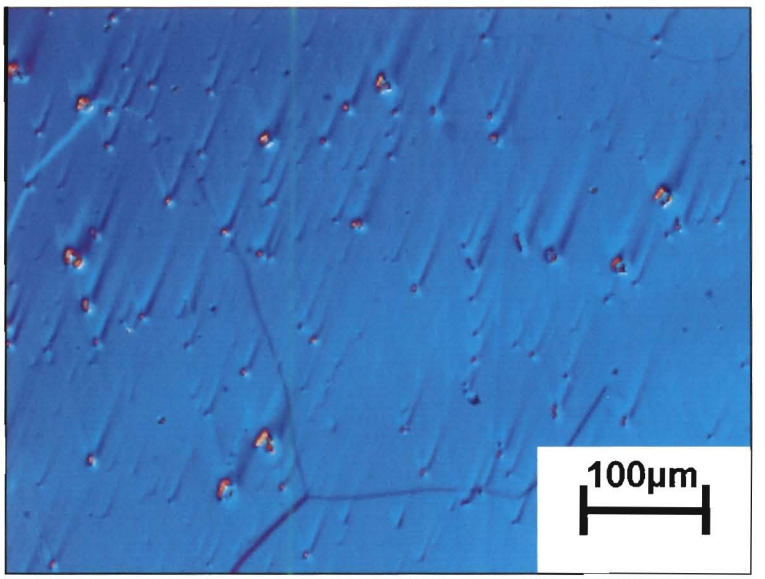

Figure 3.5

A after 4 hours at 600°C

Polished only, obtained using Nomarski interference contrast

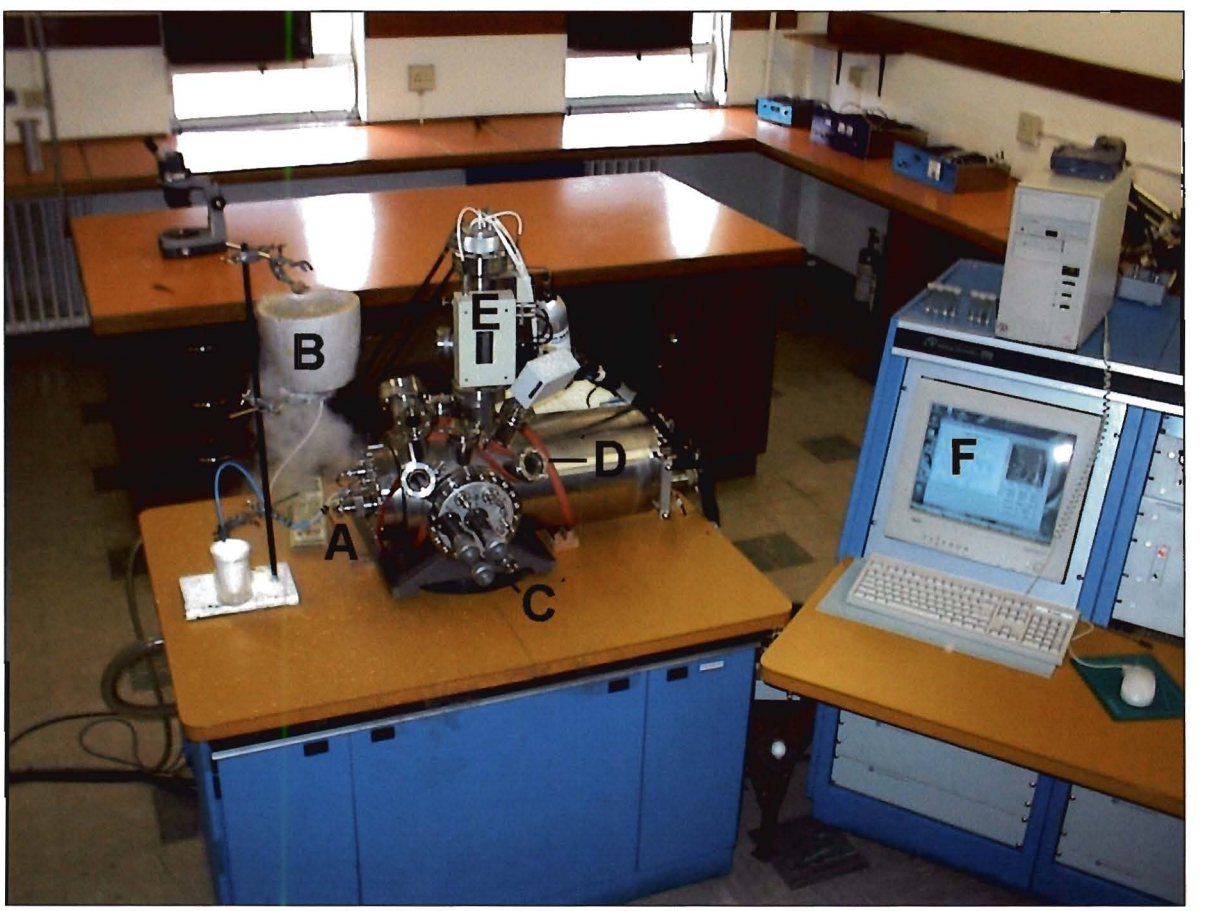

Figure 3.6 The Scanning Auger Microscope

A: Specimen Stage, B: Liquid Nitrogen Coolant, C: Specimen Position Adjusters

D: Viewport, E: Detector, F: Software Interface

3.7 Auger Electron Spectroscopy

The elemental composition of the atomic layers closest to the grain boundary may not be the same as that of the bulk of the material. When the grain boundary composition differs from the matrix, it is a form of surface segregation. This may be a transient state but if at equilibrium, surface segregation implies a lower energy state has been attained than for an identical composition for both the surface and the bulk. Even if only involving several layers of atoms, grain boundary segregation affects many chemical, mechanical and electrical properties. It was only with the development of Auger Electron Spectroscopy (AES) in 1968 that direct measurements of surface segregation became possible[47].

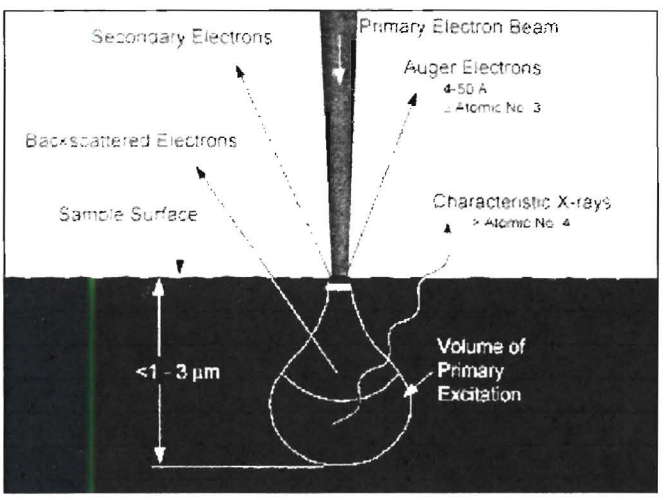

Figure 3.7 The interaction between an incident electron beam and a solid sample, showing the interaction volumes for Auger electrons, secondary electrons, backscattered electrons and x-ray fluorescence

AES depends on the release of Auger electrons from the sample under an electron beam, the energies of which are indicative of the presence of an element. Ionisation is the removal of an electron from an atom, and if an inner electron shell loses an electron, an outer electron drops into that inner shell, leaving a vacancy. An amount of energy, equivalent to the energy difference between those two levels, is released. This can take one of two forms: either the entire energy is released as an X-Ray photon or another electron is emitted from an outer orbit. The difference between that electron's own ionisation energy and the freed energy becomes the escaping electron's kinetic energy[48]. These Auger electrons have low kinetic energies and are not able to penetrate the metal further than 0.1µm. Fig. 3.7 shows the different interaction

volumes for Auger, secondary and backscattered electrons, with that for Auger electrons being very small. This lack of penetrating ability is an asset when analysing the atomic layers of the surface. As the Auger electrons are guaranteed to be from the first few atomic layers, any compositional difference with the bulk material is not overwhelmed in the signal.

For the majority of metallurgical problems, such as this one, it is necessary to investigate the composition of internal interfaces such as grain boundaries and particle/matrix interfaces. The samples must be fractured in an ultrahigh vacuum in the spectrometer, otherwise there would be carbon and oxygen adsorption from the atmosphere. This would mask the true composition of the interface. This has limited the use of AES, since to be useful the interface of interest must be coincident with the fracture surface. If the fracture is not intergranular, then methods must be employed to induce intergranular fracture. These can include hydrogen charging and the use of high temperature stages[49]. In 44101, which has exhibited grain boundary weakness, intergranular fracture was encouraged by the use of very low temperatures.

The standard Auger spectra plots the derivative of the number of electrons with respect to energy as a function of the energy[50]. The derivative is used in place of the actual number of electrons, because the number of electrons is very small in comparison to the background and so using the derivative helps to emphasise the signal. Also, in metallurgical applications it is common to use the changes in peak height ratios to express the changes in composition. It is hard to obtain accurate compositions with AES from compositionally simple, well-prepared surfaces. For multicomponent, rough fracture surfaces it is impossible.

The equipment used for this work, at the Department of Physics at the University of the Orange Free State, was a Scanning Auger Microscope, a Perkin Elmer Physical Electronics Model 590. It is operated by PhD student J..J. Terblans. It uses a single pass analyser, rather than a double, resulting in less energy resolution but greater peak heights. As a scanning microscope, it uses an electron beam less than 1μm in diameter to form an image of the fracture surface. This enabled us to see different areas of the fracture in the microscope and to adjust the position of the scanning beam so that the precise location of the signal origin could be adjusted and recorded.

3.8 Ageing at 850°C Investigation

An investigation was conducted into the effect of grain size on the precipitation distribution after 100 hours at 850°C, the results of which are discussed in section 4.6. Samples were needed with the same level of initial precipitation but different grain sizes, for it to be the key factor for the 100 hours of ageing at 850°C. A cold-rolled, but not annealed, sheet of 44101 was obtained. Therefore it possessed elongated grains, with a high dislocation density. (This dislocation density would otherwise be decreased by the post cold rolling anneal.) This high dislocation density would drive recrystallisation at a high enough temperature.

Three samples were prepared before ageing, at 10 minutes at 950°C, 10 minutes at 1050°C and 2 hours at 1050°. These would cause recrystallisation, with larger grain sizes at the higher temperature and longer time. Yet 10 minutes would not be long enough for much precipitation to form prior to the next stage in the experimental treatment, the 100 hour ageing at 850°C. Some precipitation would be present in all three samples, before the 100 hour ageing. Only the third, with 2 hours at 1050°C would have significant additional precipitation from the first experimental step. This specimen was included to see if this had an effect, along with an even greater grain size.

All three specimens were aged at 850°C for 100 hours. It had been found that 10 minutes at 950°C provided for recrystallisation of the steel, with 850°C being too low a temperature. Each was treated differently beforehand:

Specimen E1 ... 10 minutes at 950°C

Specimen E2 ... 10 minutes at 1050°C

Specimen E3 ... 2 hours at 1050°C

The higher temperature or longer time meant greater grain growth in the specimen, before the ageing treatment. The specimens were ground, polished and etched as explained in section 3.2.3-4. They were then studied using the optical and electron microscopy methods detailed in sections 3.2.5 and 3.4.

Chapter 4 Analysis and Discussion

4.1 Fractography

4.1.1 Context of the Failure Investigation

Production heats of this stainless steel had on occasion failed mechanically during manufacture, with a subsequent loss of material and production time. The failures occurred at the same stage in production, after hot rolling and prior to the subsequent annealing. A sample from a production heat which had experienced failure was examined, in order to investigate the causes of this failure.

The modern understanding of fractography is advanced and was used as a guide to examining the fracture surface. Fractography is the study of the appearance of metallic failures in order to explain the failure mechanism[51].. Coupled with a knowledge of the microstructure and the distribution of impurities in the stainless steel, it should be possible to deduce the cause of the failures[52]. Once understood, the thermomechanical processing or steel composition could be altered to avoid future problems.

4.1.2 Failure Occurrence during Production

Columbus Stainless continuously cast the stainless steel into 20 tonne slabs. The cast slab is reheated at approximately 1100°C for three hours, before hot rolling at between 900°C to 950°C, then cold rolled to its final gauge. Following both hot and cold rolling, the heat is annealed at 1050°C for 30 seconds before pickling. 1050°C is the optimum temperature for grain growth and recrystallisation.

Following hot rolling and prior to annealing, the steel is coiled and cools to ambient temperature while coiled. The cooling rate in the coil depends on the distance from the surface of the coil, from 2°C/min in the outer laps to 15°C-20°C/min deep within the coil. It must then be uncoiled before passing through the annealing and pickling process. It was during this uncoiling and straightening at ambient temperature that failures in 44101 were experienced.

The failure occurred across the width of the steel sheet, in the plane of the normal and transverse directions. It occurred predominately in one of the outer laps of the coil. After such a failure, the entire coil must be scrapped, at considerable expense. Repeated coiling and uncoiling is part of the production process of every stainless steel, with the same stresses being experienced by each heat. Yet only 44101 experiences failure in this way. Therefore an unknown metallurgical factor or deleterious combination of factors must be responsible for these premature failures.

4.1.3 The Fracture Surface

While being uncoiled at ambient temperature, the steel is plastically deformed as it is unbent and straightened out of the coil. The inner part of the lap would be under tension while the outer part would be under contraction, with a neutral zone along the centre of the lap. There would also be some tension in the rolling direction through the entire thickness of the sheet immediately after unbending, as the straightened sheet is pulled out of the coil.

The fracture surface is shown in Fig. 4.1. At first sight it is a classic brittle failure, being bright, shiny and multi-faceted. The regions originally under compression or tension are marked on Fig 4.1 and show clear differences in their appearance. Only the one region was initially under tension, but the final fracture stress must have been tensile across the entire fracture surface, so that this brittle fracture could result, with the sheet shattering right across its width.

Final failure by separation in metals occurs under tension before it would under contraction[53] and there is no evidence of ductile deformation under compression. This implies that the initial failure occurred in the region under tension, with a brittle failure spreading rapidly across the central axis and into the region previously under compression. These regions experienced sudden failure as the crack expanded.

Different features of the fracture surface will be discussed in turn below, yet from the above reasoning it can be argued that the clues to the causes of the failure will be found where the failure first began, in the region initially under tension in bending. It is here that the cracks began, before the rapid final fracture.

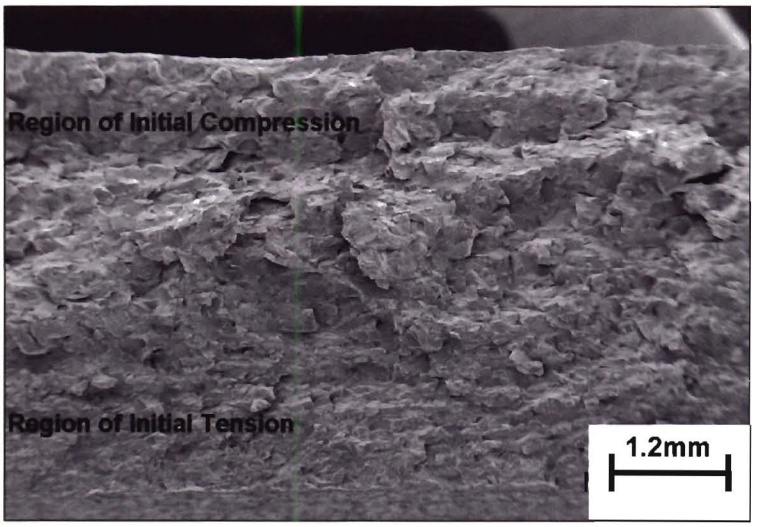

Figure 4.1

The fracture surface of the shattered coil

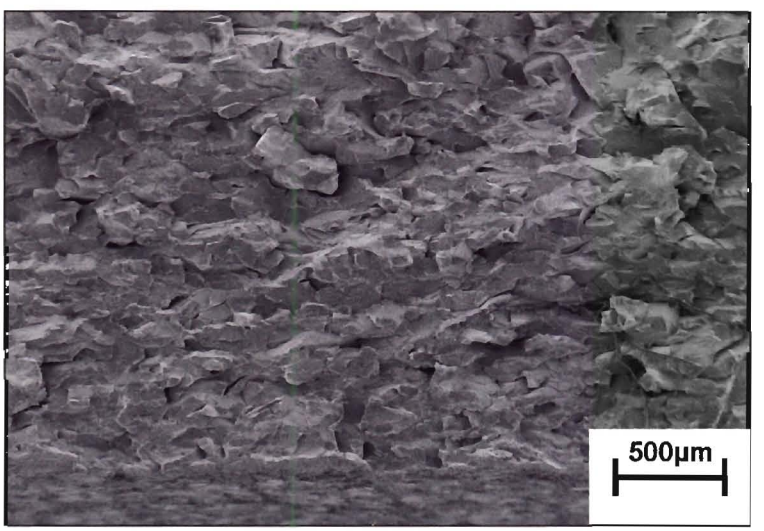

Figure 4.2

The region of the fracture surface initially under tension, with numerous tiny cracks extending into the fracture surface

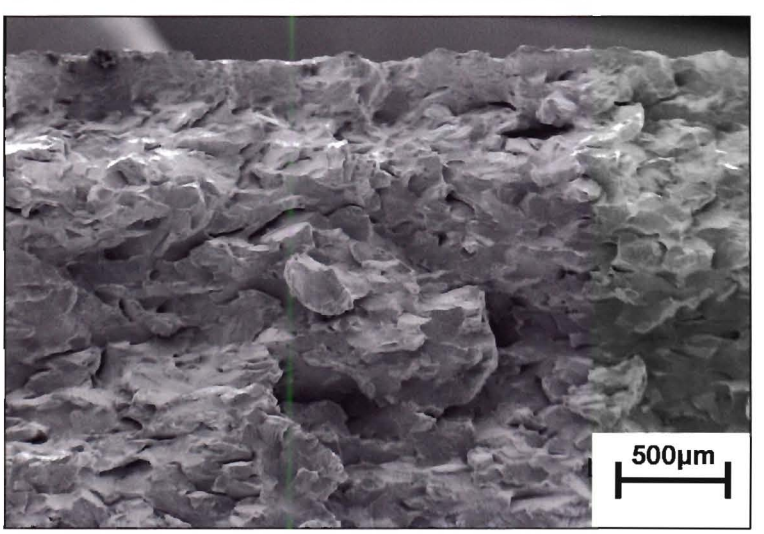

Figure 4.3

The region of the fracture surface initially under compression

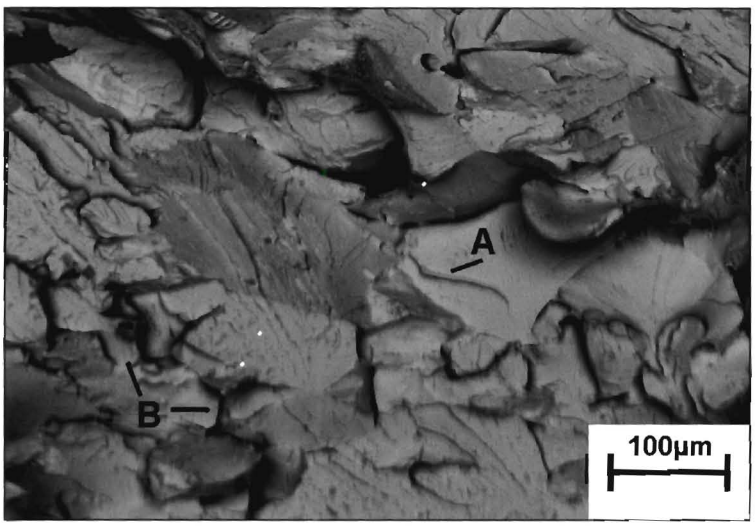

Figure 4.4

A backscattered electron image in the region where failure initially occurred

A: transgranular cleavage

B: cracks into the surface

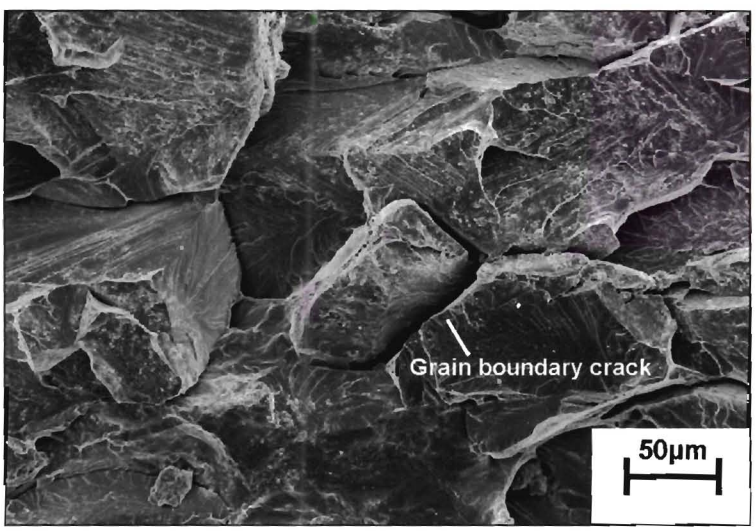

Figure 4.5

In the region of initial failure, an example of a grain separated from its neighbours

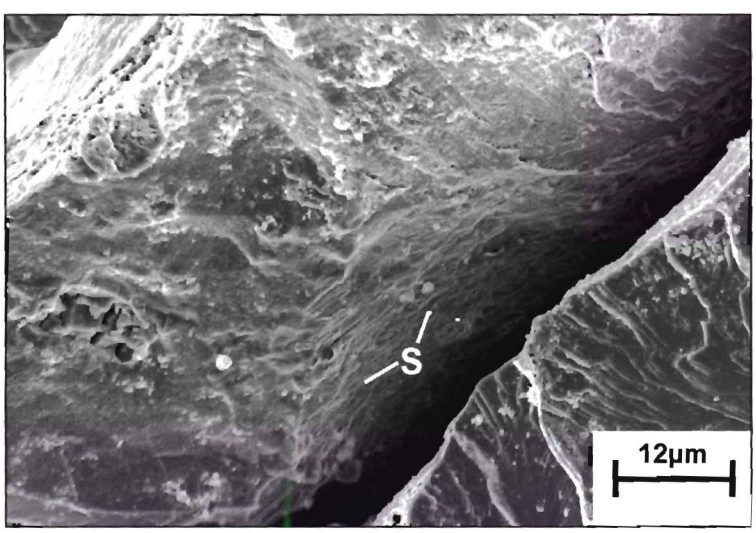

Figure 4.6

Looking into the cleft between the grains in Fig. 4.5 above

S: Wavy slip lines indicating plasticity

4.1.4 The Region Initially Under Tension

This region, shown in Fig. 4.2, is where the initial cracks are believed to have originated. It is far less irregular than the jagged regions where sudden catastrophic failure occurred. The region exhibits transgranular fracture, with the direction of the cleavage planes changing at grain boundaries. The cleavage planes are flat and smooth, though they can propagate undisturbed only within a single grain. A fine example is seen at A in Fig. 4.4 in the region initially under tension. The single right-angled step present here is clearly visible as a dark line across the grain. In a secondary electron image that line appears very bright, owing to the 'edge effect.' This backscattered electron image avoids that, which can overemphasise that minor cleavage step.

The cracks noted in Fig. 4.2 are very evident in this image, with B indicating how the deepest appear to follow grain boundaries into the fracture surface. The sheer number of similar clefts is a noticeable feature of the fracture surface. This seems to indicate that the grain boundaries have separated prior to or during failure. The region exhibits a clear transition in the transverse direction along the fracture surface, between it and the centre of the sheet. This indicates a change in the fracture process, from the initial crack which developed in the region under tension and then the final catastrophic shattering. Some grains, as in the centre of Fig. 4.5, are noticeably separate from their surroundings, which typically exhibit transgranular fracture. This grain may have experienced further 'pullout' during failure and this is an opportunity to look into one of the gaps in the fracture surface in Fig. 4.6. The point S indicates where wavy slip lines show the crack formation involved plasticity[54].

4.1.5 Brittle Cleavage on the Fracture Surface

On the larger scale the surface is very uneven, with the steel sheet having shattered apart extremely violently. But, on the microscale, cleavage is visible across much of the brittle fracture surface. Cleavage, a distinctive form of transcrystalline fracture, proceeds along crystallographic planes of low indices, i.e. high atomic density, with little plastic deformation. It is typical of bcc metals such as this ferritic stainless steel, rather than its fcc austenitic counterparts[51]. Transgranular fracture is visible across most of Fig. 4.3.

This behaviour is found so often in iron and steel that it was long assumed to be intrinsic to ferritic irons and steels. However it is now known that highly-purified zone-refined irons are extremely ductile, including very pure iron-chromium alloys to very low temperatures[55]. With increasing interstitial carbon and nitrogen, the transition from ductile to brittle behaviour increases with temperature.

Propagation of a cleavage crack requires much less energy than a ductile crack. This can be clearly demonstrated using a Charpy or Izod impact tester, where a ductile break in a steel will absorb far more energy than a brittle, cleavage dominated fracture[51,53].

Cleavage is not the only fracture mode visible on the surface. Fig. 4.7 includes quasi-cleavage fracture around C. Quasi-cleavage fracture shows clear features of ductile flow on a microscopic scale, but on a macroscopic one shows very little deformation. The 'cleavage' plane at the centre of Fig. 4.7 is rounded upwards at the edges like a bowl. Quasi-cleavage fracture is composed of curved or bowed facets and rosette surfaces such as these, having no orientation relationship with the underlying crystallographic planes. Quasi-cleavage is typically found in low-alloy heat-treatable steels, tested at low temperatures[51].

When a cleavage plane crosses a grain boundary, as shown at D in Fig. 4.7, it subdivides into a number of parallel, subsidiary cracks. This is because of the orientation difference between the grains. As propagation continues, they may reunite but while separate they are divided by almost right-angled steps. Small areas of ductile failure, such as at E in Fig. 4.7, are also visible.

Twins are a common feature on the cleavage planes of bcc metals, e.g. iron and carbon steels[51] but are not visible on this fracture surface, since stainless steels, heavily alloyed with chromium, do not display twinning[4].

4.1.6 The Interior of the Shattered Specimen

The deep cracks in the fracture surface have been exposed in Fig. 4.8 by cutting the shattered steel sample in midsection (M) in the plane of the rolling and transverse directions. Once the initial crack had spread across the steel sheet in the region under tension, the rest reverberated in an very violent sudden failure, resulting in a brittle 'biscuit' fracture as seen here. These cracks (N) are hence the result of, rather than the cause of the failure.

In Fig. 4.9, a crack in the interior of the same specimen follows a grain boundary until it splits (O) and cleaves the grains transgranularly. The cracks in Fig. 4.2 may have begun at the grain boundaries but may have diverted at a precipitate or grain boundary triple point into transgranular fracture in this way. Though most of the transgranular fracture in the region under tension would probably only have occurred once the steel had begun to fail on a larger scale with rapid propagation of cracks.

In the optical micrograph in Fig. 4.10 the grain boundaries are clearly delineated, showing how the irregularly-shaped grains are elongated in the rolling direction. Large precipitates (probably titanium nitrides, see section 2.4.2) are visible at the grain boundaries. At a higher magnification in Fig. 4.11, the grain boundaries can be seen as flecked with tiny dark precipitates, along with intragranular precipitation.

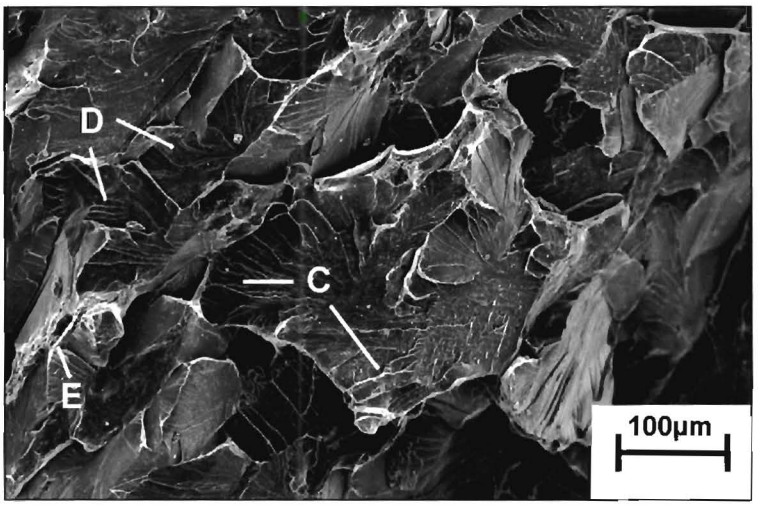

Figure 4.7

Example of the mixed modes of fracture exhibited by the region at the central axis of the sheet

C: Quasi-cleavage fracture

D: Cleavage fracture

E: Ductile failure

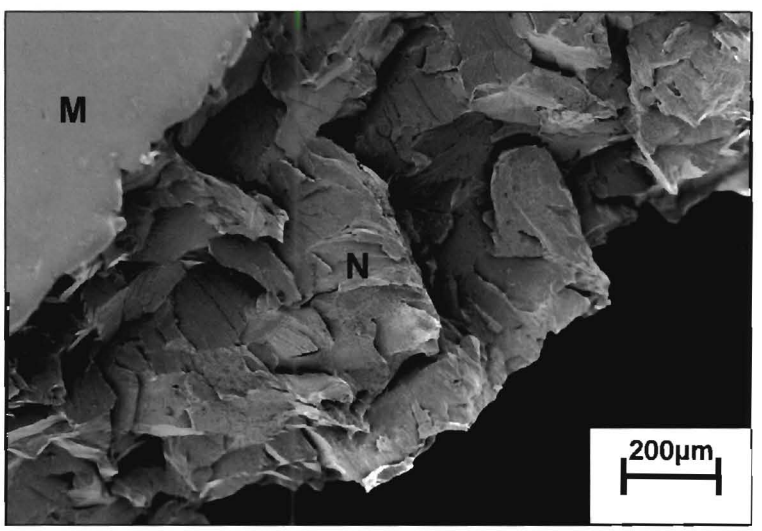

Figure 4.8

The fracture, once sectioned midway though in the rolling plane

M: Prepared surface shown below

N: Brittle cracks from final shattering

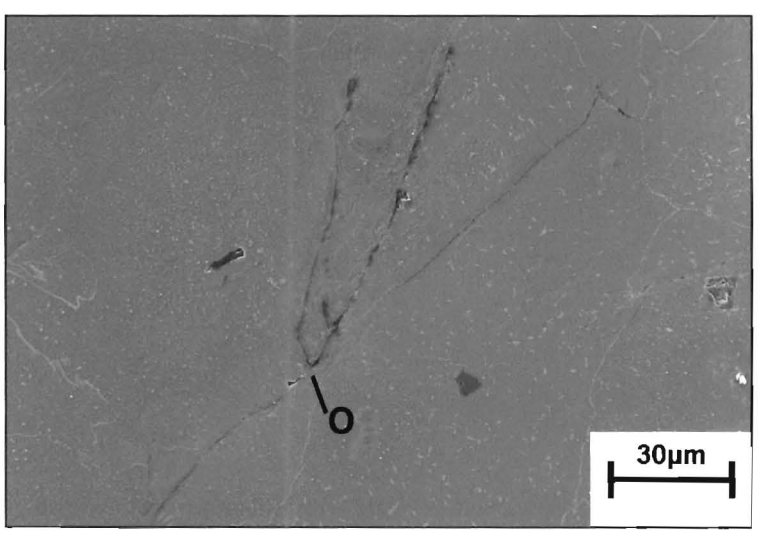

Figure 4.9

A crack upon the above sectioned surface M, about 300µm from the fracture

O: An intergranular crack splits and diverts transgranularly

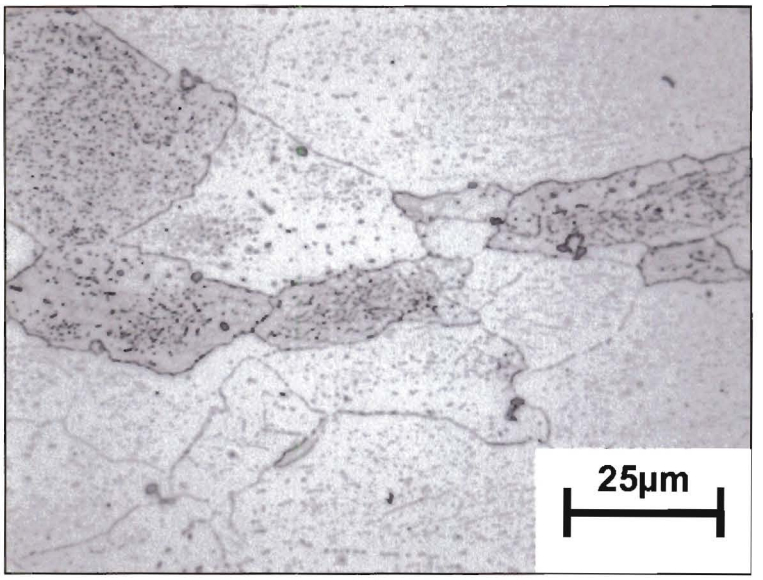

Figure 4.10

S (Embrittled)

The microstructure of the shattered specimen, with the grains elongated in the rolling direction

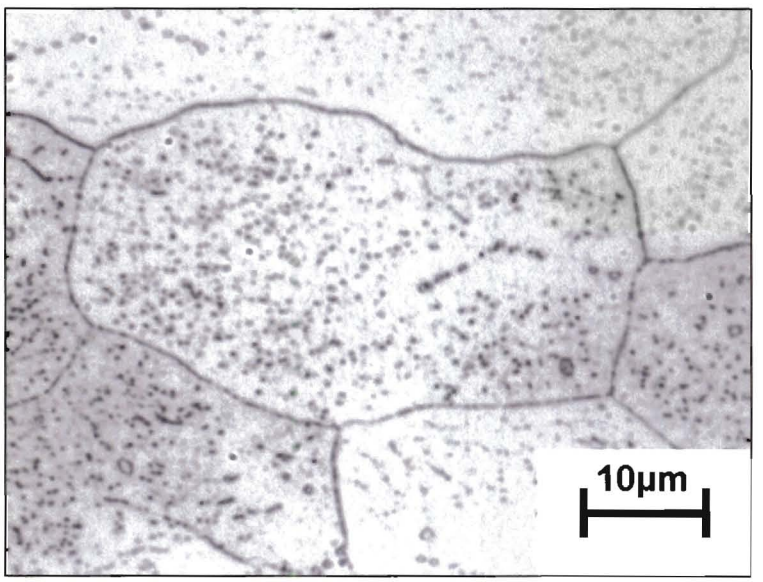

Figure 4.11

S (Embrittled)

A typical grain within the shattered steel

4.2 Failure Analysis

4.2.1 A Brittle Fracture

The fracture surface under investigation is a bright, shiny fracture. Brittle fracture is characterised by its sudden occurrence and the absence of deformation as the crack advances. There is no permanent deformation to be seen over the majority of the fracture surface. The stainless steel sheet undergoes plastic deformation as it is straightened out of the coil. No necking has occurred, with the sheet the same thickness right up to the fracture surface. A brittle fracture surface is always perpendicular to the principal tensile stress, which means that the final fracture stress was in the rolling direction.

Well-known causes of stainless steel embrittlement include 475°C embrittlement and σ phase, but as discussed in section 2.2.3-4, these are not likely to be a concern during commercial production processes. The formation of martensite after hot rolling, mentioned in section 2.1.5, is not likely for this fully stabilised ferritic stainless steel, formulated to have no dual-phase regions at high temperatures.

An immediate hypothesis could be that the embrittled 44101 is simply far more brittle than other stainless steels. Some form of embrittlement has made the stainless steel's yield stress exceed its ultimate tensile stress, causing the strain induced in the steel to cause stress greater than the ultimate tensile stress, without any plastic deformation to relieve that strain. The embrittled steel may be unusually incompatible with plastic yielding specifically while under constraint (see the next section) to such a degree that it breaks in a brittle fashion before it has yielded. To test this, tensile tests of the embrittled and unembrittled heats were conducted.

4.2.2 Tensile Tests: As Received vs. Embrittled

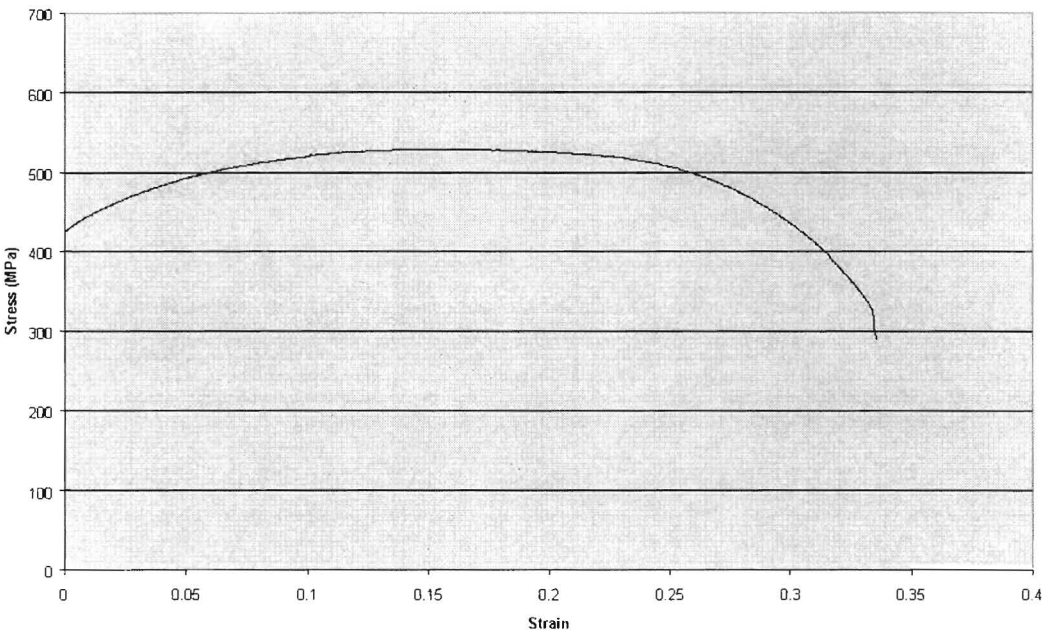

Figure 4.12 A tensile test of a subsize specimen of as received steel C.

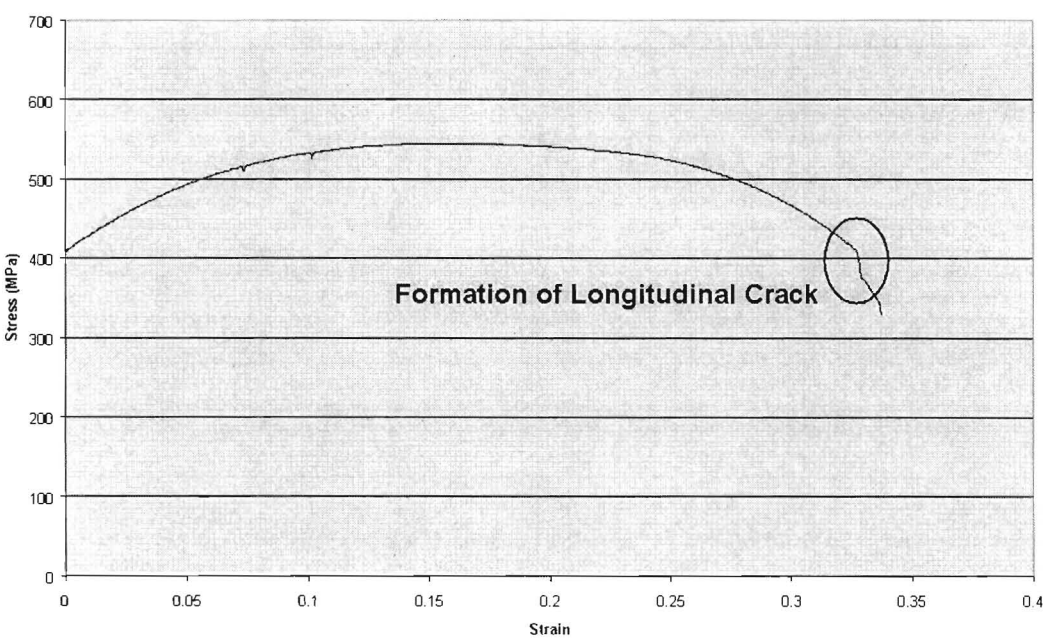

Figure 4.13 A tensile test of a subsize specimen of the embrittled steel S which failed in production

Tensile test results for specimens of successfully rolled heat C and failed heat S are compared in Figs. 4.12-13. S, the embrittled 44101, is not lacking in strength or ductility in comparison to C. Yet something in their microstructure is sufficiently different to make S liable to failure. Though yielding similar data above, the S specimens broke in a very different manner from C. A crack, running lengthways, formed midway through the specimen shortly before the final fracture. The fracture surface also looked very different. (see Figs.4.16-21)

Standard tensile specimens are punched or machined such that the volume of metal under strain is not 'under constraint' in any direction. Metal alongside a sudden increase in gauge in a specimen would be constrained against yield by the adjacent metal in the thicker section. This additional influence would make specimens yield at some higher stress, depending on the specimen geometry.

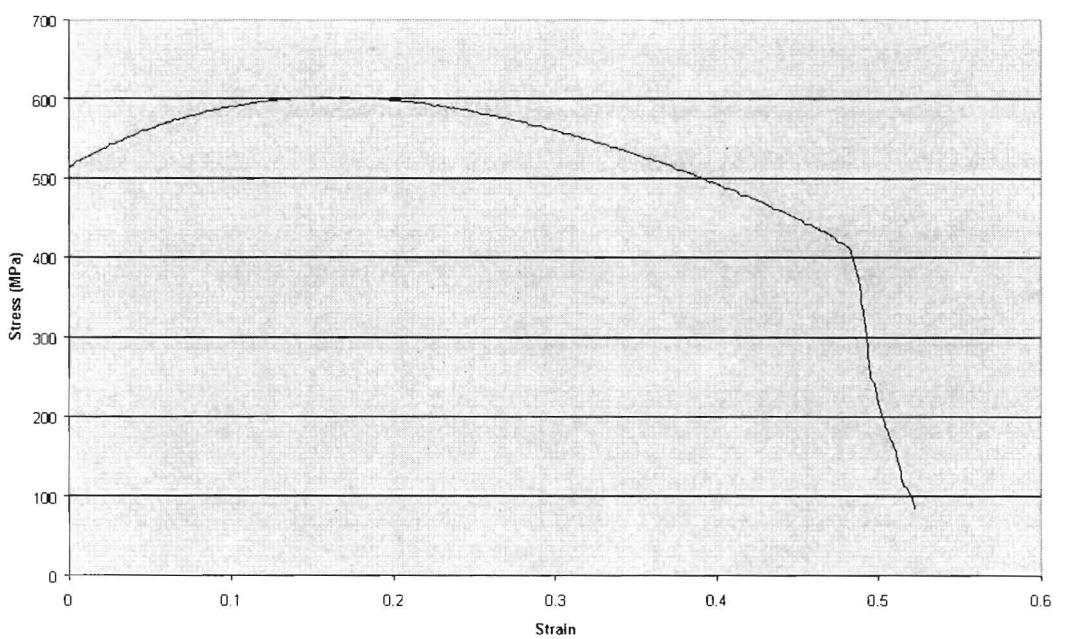

Figure 4.14 A tensile test of a specimen 'under constraint' of as-received heat C.

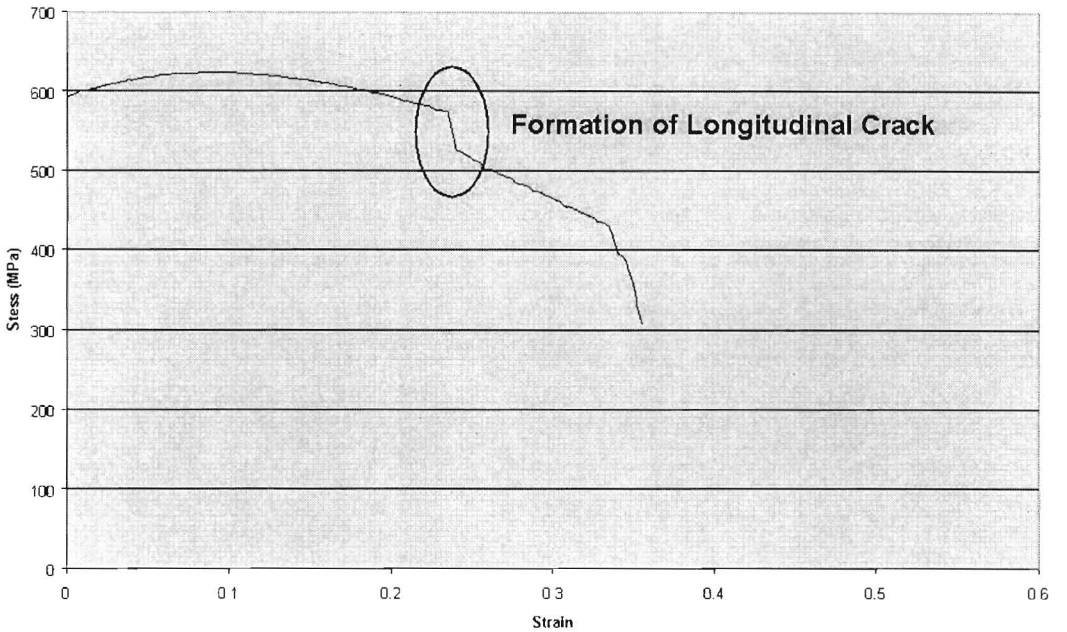

Figure 4.15 A tensile test of a specimen 'under constraint' of the embrittled heat S.

During production, the uncoiling sheet is under constraint across its width. Its two metre width is sufficient to make it difficult for the steel to contract in the transverse direction. This increases the apparent yield stress of the steel. This difference was simulated for these two steels by inducing constraint into tensile specimens. Within the subsize tensile specimens stipulated gauge length, a shorter, narrower gauge length was machined. The steel at the centre was constrained by the thicker, standard gauge width steel on either side. (see section 3.6)

Under this constraint, the specimens did behave very differently. The cracks observed in the standard subsize S tensile specimens were again observed. Their formation is associated with the sudden drops in stress after necking observed in Fig. 4.15 and to a lesser extent in Fig. 4.13. The embrittled specimen is far less ductile than heat C, with a total elongation to fracture of approximately a third less. The longitudinal cracks form in S at half the plastic elongation before ultimate failure in C. Their formation in S in the standard subsize specimen is not in itself sufficient in a tensile test to significantly affect the elongation. Yet under constraint, S is far more vulnerable.

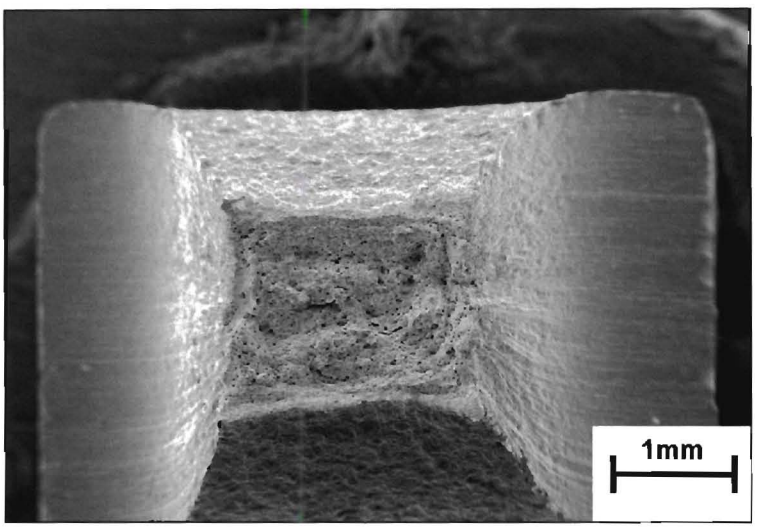

Figure 4.16

C (as received)

The fracture surface of the as-received tensile test specimen under constraint

Secondary electron image

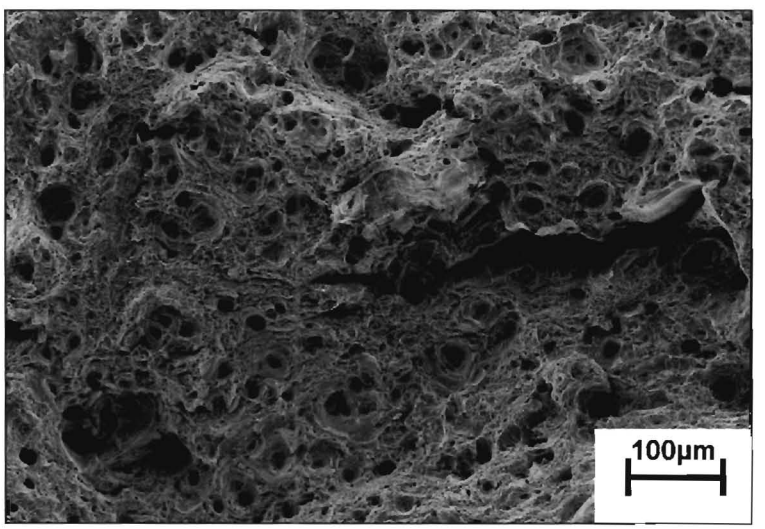

Figure 4.17

C (as received)

The above ductile fracture surface at a higher magnification

Secondary electron image

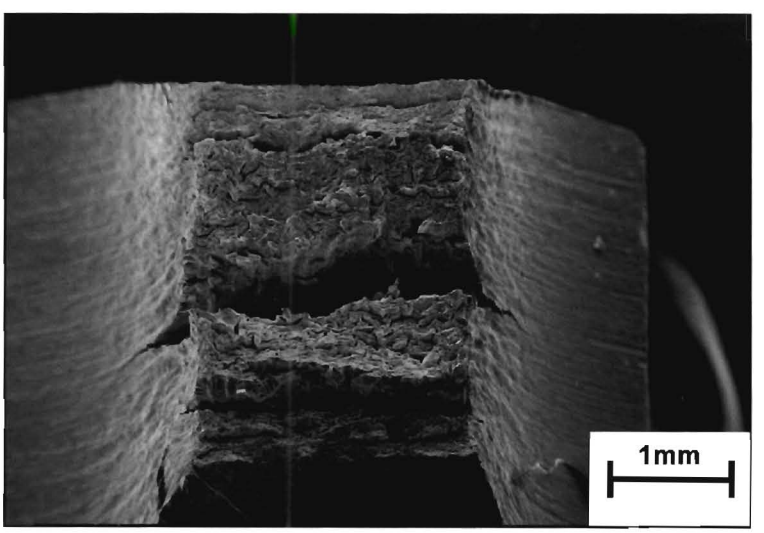

Figure 4.18

S (embrittled)

The fracture surface of an embrittled tensile test specimen

Secondary electron image

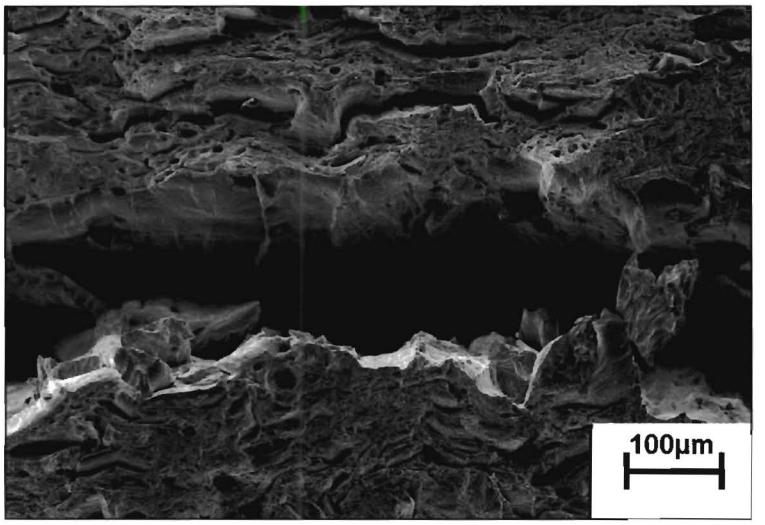

Figure 4.19

S (embrittled)

A crack into the embrittled tensile test specimen's fracture surface

Secondary electron image

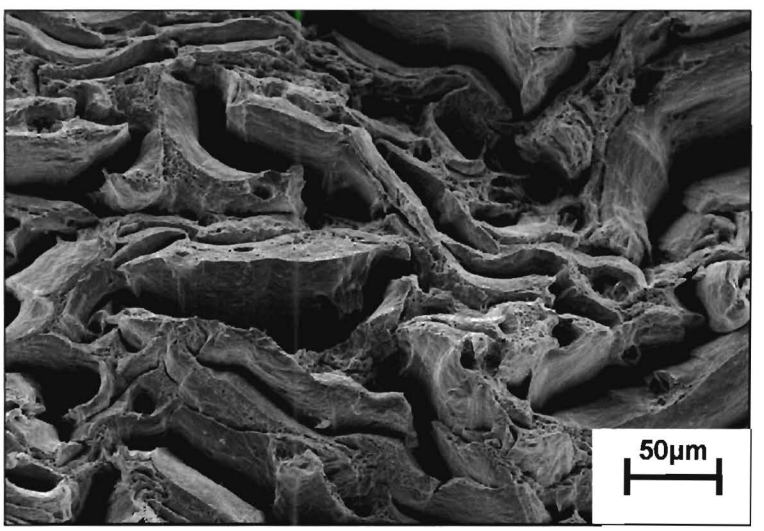

Figure 4.20

S (embrittled)

The myriad of tiny cracks in the fracture surface, alongside the large crack in the image above

Secondary electron image

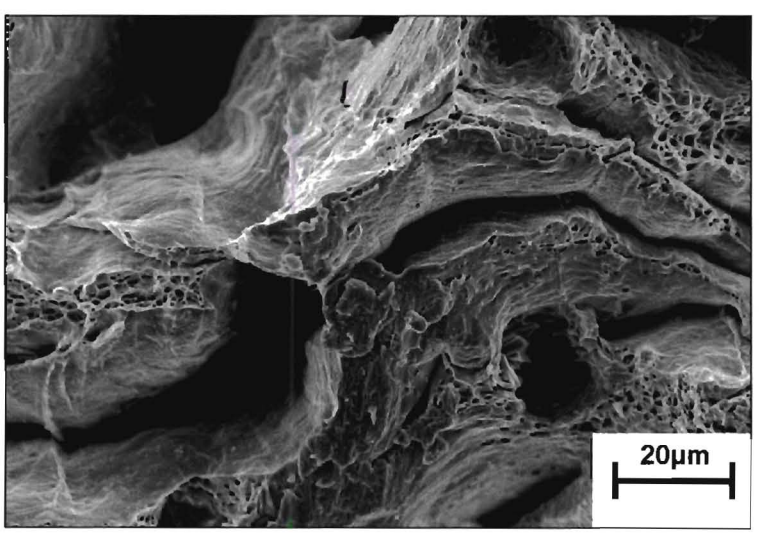

Figure 4.21

S (embrittled)

The dimples show evidence of the final ductile failure around the many tiny cracks

Secondary electron image

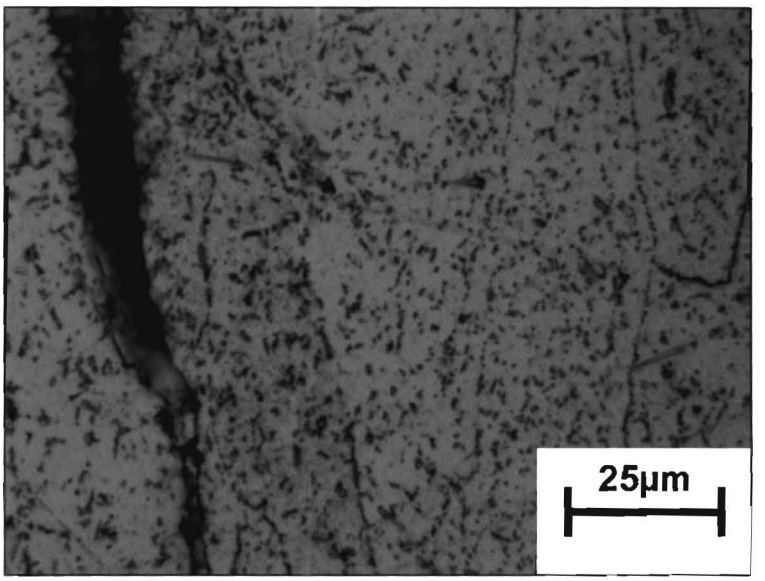

Fig. 4.22

S (embrittled)

A microcrack within the bulk of the tensile test specimen runs parallel to the grain boundaries which are delineated by precipitates

Optical micrograph

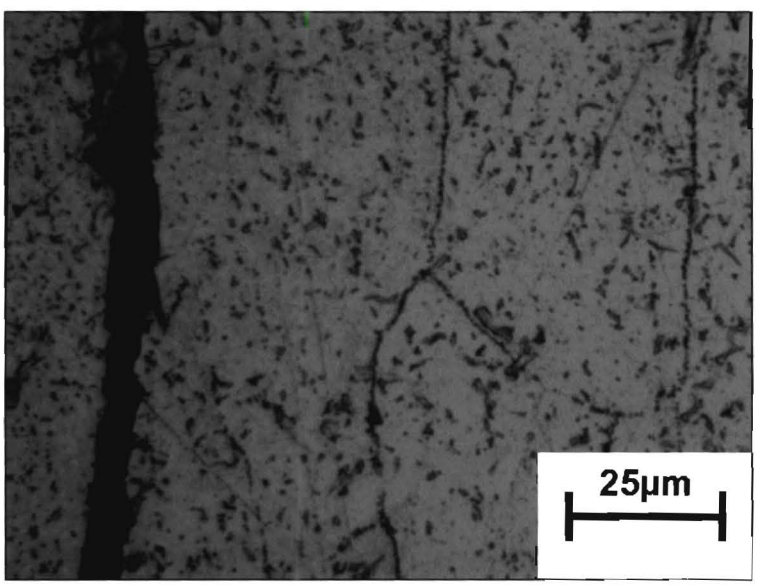

Fig. 4.23

S (Embrittled)

The cracks during the tensile test suggest that the grains are separating

Optical micrograph

Internal cracks and other internal stress raisers can produce such tri-axial stress states. An example is a notch in the plane surface of a material and this always causes a tri-axial stress state. The same metal, tested twice under tension, will fracture with deformation if there is no notch, while the specimen with a notch will break in a brittle fashion, especially for a sharp notch. A state of plane strain (equivalent to a tri-axial stress state) will always occur near cracks in thick specimens because transverse plastic flow can not occur at the crack tip[53]. The steel sheet is very wide, so that transverse plastic flow is already hindered in this dimension.

There are a number of other factors which could favour sudden brittle failure over a ductile one. Brittle fracture is encouraged by low temperatures and high velocity loading[17]. Yet in the circumstances of this production failure or the tensile tests, the temperature and loading conditions were no different.

4.2.4 Cracks

In a ductile material such as a stainless steel and for low velocities, new cracks can form once the yield point is reached, either for the material as a whole or at a stress raiser. Cracks form through a process of dislocation movement allowing plastic deformation. This is a different scenario from that of a high-velocity impact, during which, however the cracks are initiated, the dislocations do not have sufficient time to allow plastic deformation to subsequently blunt the crack.

Under sufficient stress at a far lower velocity, plastic deformation can crack second phase particles and these microcracks can then propagate. For example, this is important in carbon steels containing cementite particles or lamellae. Brittle inclusions such as alumina particles can also be a source of crack nuclei in steels[4].

The mechanical behaviour of this stainless steel, as a bcc metal, is very temperature dependent. This is true for the nucleation of cracks before failure, whether under impact or low velocity loading. As temperatures decrease in body-centred-cubic metals, the yield point increases sharply. The velocity of dislocation movement is proportional to the stress. With a greater yield stress at lower temperatures, when the

In Figs. 4.16-17, the secondary electron images of the unembrittled C tensile specimen depict a very ductile failure. Each of the dimples is associated with a precipitate. The larger dimples probably contained a titanium nitride, with the smaller ones forming around carbonitrides or Laves phases.

The embrittled S specimen in Fig. 4.18 looks very different, with a dark, ridged surface with deep cracks. Fig. 4.19 shows how one of these cracks, seen forming during the tensile test, cuts deeply into the specimen. Alongside the crack is an unusual fracture pattern, coruscated waves of high crests and deep troughs. At a higher magnification in Fig. 4.20, the crests look sharp, with smooth, dark cracks snaking all over. In Fig. 4.21, the cracks can be seen to have dimpled tips. A myriad of these tiny cracks had formed and were enlarging along the tensile axis. Then the ductile surrounding matrix thinned and finally broke. These cracks are an experimental version of what occurred in the region under tension in the bending sheet. The embrittled metal may have been no less ductile, but once the cracks had formed the overall area upon which force was applied rapidly diminished as each connecting ribbon necked individually.

Optical micrographs of the embrittled specimen S were taken from side-on of these cracks. The cracks ran parallel to the grain boundaries, which are clearly delineated in the micrographs by the presence of small precipitates. Figs. 4.22-23 are representative of the cracks, which appeared to follow the grain boundaries exclusively. This was whether they were large or small, clefts into the fracture surface or microcracks within the bulk of the specimen.

4.2.3 Tri-Axial Stress States

The embrittled steel broke in tension because it could withstand far less elongation under constraint than other unembrittled heats such as C. In the steel sheet under tension in bending, any such separation would form a stress concentration. That stress concentration may be large enough to be a critical flaw in terms of fracture mechanics. By definition a multi- (tri) axial stress state, this would make it very difficult for the stress to be released through plastic deformation. In this scenario, the steel sheet would then break, shattering violently right through.

dislocations do begin to move, their velocity is high and localised dislocation pileups at obstacles becomes likely. Cracks are known to nucleate at such dislocation pileups[4,17].

If the bcc steel is breaking in a brittle fashion because the temperature is low or that precipitates are cracking, then a smaller grain size would be helpful. The shear stress at the head of a dislocation pileup is $\eta\tau$, where η is the number of dislocations and τ is the shear stress in the slip direction. The smaller the grain size, the smaller the number of dislocations in the pileup when a slip band arrives at a boundary. Hence, as grain size is reduced, η will be smaller and there will be less crack nuclei, regardless of whether they are forming through dislocation coalescence or by dislocation pileups causing precipitates to crack[4]. Failure through cracking must first have the cracks nucleate (i.e. form) before they propagate through the steel. In certain circumstances that propagation may become unstable and explosively rapid. Fast fracture occurs most frequently in ceramics, with no dislocations present to allow for plastic deformation and stress relief[17]. Yet it is not limited to such materials and the necessary steps to the fast fracture of this steel will now be discussed.

4.2.5 Crack Nucleation

Nucleation occurs when a critical value of the effective shear stress is reached, at a critical grouping of dislocations which can create that crack nucleus. Grain boundaries, hard particles, inclusions and grain boundary carbides act as barriers to dislocation movement, encouraging crack initiation. A cleavage crack is nucleated when the concentrated stresses at the tip of that blocked dislocation band equal the cohesive stress:

$$\tau_N \mathbf{nb} \approx 2\gamma_T + \tau_i \mathbf{nb}$$

where:

τ_N = shear stress for crack nucleation

τ_i = friction shear stress

$\mathbf{n}$ = number of dislocations in the pileup

$\mathbf{b}$ = burgers vector

γ_T = true surface energy

This means that the work done by the applied shear stress (the product of τ_N and a displacement of **nb**) equals the combined work of moving the dislocations against the friction stress (the product of τ_N and the displacement of **nb**) and the work done in creating new fracture surfaces ($2\gamma_T$). For most metals, γ_T (true surface energy) is replaced by a more general γ term, which includes the fact that some plastic relaxation occurs around the dislocation band[17].

The value of γ is reduced by the presence of intergranular carbides. With grain boundary precipitation, crack nucleation is facilitated because the precipitates prevent much stress relaxation at the tip of the blocked slipband and γ decreases, i.e. the work done for crack initiation is small. This is in contrast to the effect of small, well distributed particles throughout the matrix. Dislocation bands pile-up at grain boundaries, whereas intragranular precipitates offer more opportunities for dislocations to circumvent through cross-slip. Thus cracks initiate more easily at grain boundaries, even though the resulting cracks are probably transgranular and not intergranular. Therefore alloys with homogeneous (intragranular) second-phase distribution are tougher than those with heterogeneous precipitation along grain boundaries [4,17].

4.2.6 Crack Propagation

The propagation of a crack depends on the magnitude of the local tensile stress, which must reach σ_f. This critical tensile stress is not temperature dependent. At low temperatures, the yield stress is higher but the plastic zone at the crack tip is smaller, while at higher temperatures the larger plastic zone is offset by the lower yield stress.

$$\sigma_f = \sqrt{\frac{\pi E \gamma}{1-\upsilon}\frac{1}{c}}$$

where:
E: Young's Modulus
υ: Poisson's Ratio
γ: the effective surface energy associated with the propagation of the crack [4,56]

Under certain conditions, dependent on the stress intensity and the fracture toughness, cracks do not propagate linearly with increasing stress but develop spontaneously into an unstable, rapidly propagating crack. Unstable crack propagation is hindered by grain boundaries since the crack must adapt itself to each new crystal orientation of each succeeding grain by subdividing itself into a number of subsidiary cracks at each grain boundary. The separation energy is then larger than with one crystal plane alone, as in coarse grains which allow the unhindered propagation of cracks over large distances. Fine grained metals are therefore less susceptible to brittle fracture and to rapid crack propagation than coarse-grained ones[17].

A ferritic stainless steel is resistant to crack initiation, yet it is not particularly resistant to crack propagation. Ferritic stainless steels are notoriously vulnerable to cracks, as they have poorer fracture toughness than austenitic stainless steels. Once a crack long and sharp enough is present then the bcc matrix is vulnerable to cleavage of its crystal planes [1,2]. Research into the poor impact toughness of stabilised ferritic stainless steels has focused on the possible role of precipitates in crack initiation, rather than into the fracture toughness of the ferritic stainless steel. The resistance to crack propagation of this bcc steel would be expected to be relatively poor, it is rather how the cracks initiate that is the issue with regards to low toughness.

4.3 Failure Causes and Explanation

4.3.1 Possibilities for Crack Initiation

Possible ways in which cracks may be initiated, especially at grain boundaries, have been put forward and studied by researchers interested in the impact toughness of stabilised ferritic stainless steels [57,58,59]. When studying impact toughness, they are not concerned with plastic deformation causing cracks to form (as in section 4.4.2) because during impact there is insufficient time for dislocations to start moving. Yet their work is relevant, in as much as there may be a relationship between the poor impact resistance and the brittle failures during production. The origin of the cracks during impact may be similar in nature. This view is encouraged by the following facts.

Early production heats of 44101 manufactured by Columbus had a high DBTT, at 70-80°C. Later production refinements brought it down to 20-30 °C, in line with other ferritic stainless steels. Subsize Charpy impact tests of the 44101 samples used in this project gave 3.8 J/mm^2 energy absorption at room temperature, which is very low. Annealing at 670°C for 16h increased the Charpy impact value to 9.5 J/mm^2, possibly due to the relaxation of strain fields surrounding the precipitates[60].

This stabilised stainless steel could be expected to have a higher DBTT than other titanium and niobium stainless steels with similar interstitial contents. This is according to the work done by Redmond[32] (see section 2.5.3), where additions of 0.25wt% titanium and 0.45wt% niobium produced the highest DBTT for a dual stabilised 17%Cr ferritic stainless steel. It seems possible that the lower toughness may have a similar basis as the embrittlement, with crack initiation being the common thread.

Under impact conditions, brittle cracks in ferritic stainless steels initiate mainly at grain boundaries. Some start at the intersection of grain boundaries or at inclusions on the grain boundary. Impact differs from low velocity loading in that there is insufficient time for crack growth to be blunted by plastic deformation.

The original cracks under impact are probably short, sharp cracks formed in association with the precipitates, according to Plumtree and Gullberg[29]. Either the hard precipitates are fracturing in a brittle fashion and the cracks then extend into the more ductile matrix, or the precipitates act as stress raisers, in themselves sufficient to initiate failure.

The first possibility was considered but no cracks were noted extending from any precipitates into the matrix. A few specimens displayed broken TiN particles, but none had any cracks extending into the matrix. As for the second possibility, voids do form through plastic deformation around the precipitates in the tensile tests. But any initial crack between matrix and precipitate is blunted through plastic deformation into a rounded void. This prevents the first cracks forming from rapidly spreading, though ultimately they are responsible for failure. Yet there is a marked difference between Figs. 4.16-17, where this has happened, and Figs. 4.18-21 for the embrittled specimen. Therefore under low-velocity loading, precipitates are not simply stress raisers as angular precipitates could be under impact.

Or may there be microcracks present at large precipitates from rapid cooling? Pollard[21] regarded these prior cracks around titanium nitride precipitates as responsible for ultimate tensile failure in stabilised stainless steels. However these microcracks around larger precipitates were only seen in specimens rapidly water cooled and not in Pollard's slowly cooled specimens. None were seen in any impact or production specimens in the present work.

The intergranular cracks observed on the fracture surface are consistent with intergranular cracks observed in stabilised ferritic stainless steels by Kinoshita[57]. Even at cryogenic temperatures, Kinoshita observed brittle cracks at grain boundaries forming in bent specimens. He believed that these cracks were associated with tiny grain boundary precipitates, but was unable to determine exactly what role they played.

Intergranular microcracks were also found to be associated with titanium stabilised steels with increased brittleness by Grubb, Wright and Farrer[28]. They demonstrated

that in steels of interstitial levels of around 75 ppm, titanium stabilisation raised the DBTT. They theorised that it was due to the embrittling effect of titanium segregated on grain boundaries, or that oxygen segregation was the cause of the embrittlement. They pointed out that the extra low carbon levels in the matrix, due to the initial low levels with extensive 'gettering' by the titanium, could be low enough to allow for the intergranular embrittlement previously only observed in high-purity irons.

4.3.2 The Role of Precipitation

Precipitates at the grain boundary, such as chromium nitrides, decrease the ultimate tensile stress of ferritic stainless steels substantially, even if the steel contains extra-low interstitial levels. They provide nucleation sites for cracks, as discussed in section 4.2.5. Grain boundary precipitation does not affect the steel's yield stress[21]. Crack propagation is further favoured by the presence of precipitates, in that they lower the energy required to create the new surfaces[4].

The addition of stabilising elements prevents the formation of chromium carbonitrides at the grain boundaries. Therefore the fracture stress is far higher than in an unstabilised steel with the same carbon and nitrogen levels. The yield stress would be decreased only slightly by the removal of carbon and nitrogen from the matrix[21].

Large volumes of precipitation, perhaps carbonitrides in this 44101, would lower the fracture stress. If the fracture stress dropped to similar levels to the yield stress, the steel may very well become truly brittle. (see section 4.2.1) Yet the embrittled tensile specimens showed much ductility before final failure. Truly brittle results for ferritic stainless steels were also not observed by Pollard. He showed that stabilising precipitates could lower the fracture stress in a ferritic stainless steel substantially, but not to the extent that no plastic deformation was possible[21].

If the grain boundary precipitation is considerable, then a sizeable crack may nucleate within the precipitation, which has a far lower value of γ. (see section 4.2.5) If very extensive, a network of precipitates at grain boundaries could have a brittle failure running through it, resulting in a type of intergranular fracture[4]. This extreme example was not probably the case in 44101 as the precipitation at the grain boundaries was

never sufficient for a crack to grow any significant length within the precipitation alone. The precipitation is not continuous, as shown in Fig. 4.57. The Laves phase does not form a continuous film of precipitation, and with niobium only 0.5wt% of the steel, the total volume fraction at grain boundaries is small.

4.3.3 How Failure Occurred

The evidence that the cracks originate at the grain boundaries, with separation occurring between grains or between grain boundary precipitates and the matrix has been discussed. Therefore nucleation probably occurs at grain boundary precipitation, with the crack propagation occurring along grain boundaries. These cracks grow, with the clefts in the fracture surface (see Figs. 4.2 and 4.4) being remnants. These clefts are the surface result of microcracks in the bulk of the material. These microcracks would appear to follow the grain boundaries. They are the stress raisers which caused the stress intensity factor to reach the critical level which lead to rapid crack growth.

How these microcracks form in tension tests in shown in section 4.2.2. The cracks into the surface of the specimen follow grain boundaries, as in Figs. 4.22-23. In contrast, in unembrittled C in Figs. 4.16-17, the separation around intragranular precipitates in tension forms voids, with coalescence leading to a true ductile failure.

In the coil, the cracks form between the grains. They do not become blunted within the matrix but instead follow the grain boundaries for some distance. They can achieve some length by following grain boundaries. Then they may veer suddenly into the grain. (see Fig 4.9) This sudden change of direction may be due to a precipitate, inclusion or extremely irregular grain shapes which may exacerbate a stress concentration. It may be that triple-points, where three grains meet, are especially susceptible. Ferritic stainless steels are prone to stress concentrations at grain boundaries, with their grain growth leading to irregular grain boundary shapes. If that is true for any ferritic stainless steel, then this may exacerbate the stress concentration for a crack at grain boundaries.

Cracks, especially sharp cracks, produce tri-axial stress states. Grains can not deform in the transverse direction as the width of the sheet provides constraint. Some cracks

coalesce sufficiently to make their crack long enough to fulfil the criterion for fast fracture. This fracture then extends rapidly through the region in tension. Then the region initially under tension is akin briefly to one large notch in the plane surface of the sheet. The rest of the steel sheet then rapidly shatters from the stress intensity factor, which the fracture toughness of the steel is not sufficient to withstand.

4.3.4 The Roots of this Failure

The evidence shows that at a microscopic level grain boundaries were delaminating enough for dangerously long cracks to form. There are two fundamental factors which may have been involved. Firstly, precipitation at the grain boundaries and secondly, poor cohesiveness between the intergranular precipitation and the matrix or the grain boundaries themselves.

The first aspect, that of the precipitation, implies that the problem may be mitigated by avoiding precipitation at the grain boundaries. The role of the precipitation in encouraging crack initiation at the grain boundaries has been discussed in sections 4.2.4-5. It is necessary to understand the time and temperature requirements for precipitation. With that information, some guidelines would be available as to the cooling rates needed to avoid deleterious precipitation. Acquiring that data would be the first step in testing that part of the hypothesis. If faster cooling rates can decrease or even prevent precipitation and there are material property benefits, then that would support the above reasoning.

The interface between the precipitates and the grain boundary may indeed have a lower cohesivity. Evidence for this would require sophisticated analysis of the interface. Any difference would be in composition of the surface layer from the bulk of the matrix. It was decided to investigate this possibility using Auger Electron Spectroscopy. This technique can give a qualitative elemental composition of the two to three atoms thick surface layer at grain boundaries.

4.3.5 Practical Problem Solution

The shattering of these coiled stainless steels was eventually avoided by diminishing the embrittlement of the steel, by altering the production process. A method known as 'Run Out Table Cooling' (ROTC) was used to swiftly cool the hot rolled material, prior to coiling. The last pass temperature is 900°C before the material is rolled out onto a run out table. Across this table, several curtains of water fall onto the steel, cooling it rapidly down to 600°C, prior to coiling. Once coiled, the steel is allowed to cool by normal heat loss down to approximately 50°C before further processing.

ROTC is a common practice, used in the production of difficult grades of stainless steel. An example is the Duplex steels, where in their case the rapid cooling is required to avoid the formation of the brittle σ phase. (see section 2.2.4) Certain ferritic grades also require its use, so that grain growth is inhibited and the DBTT is decreased. This technique of rapid cooling increases the steel's impact toughness at room temperature. The shattering occurrences appear to have been prevented in the same way. The ROTC adaptation to the production process has been a great success, as the production line alteration costs are certainly small in comparison to the savings in the prevention of production losses[60].

The rapid cooling is believed to prevent significant precipitation at the grain boundaries. This technique also prevents grain growth in the steel as it cools between 900°C and 600°C. Smaller grain sizes would mean that the stresses due to dislocation pileup at the grain boundaries are less, meaning less likelihood of crack initiation at the grain boundaries.

4.4 The Grain Boundaries Investigated

4.4.1 The Significance of Extra-Low Carbon Levels

The ferritic stainless steel has low carbon levels and the amount of free carbon is further lowered by the formation of stabilising carbides. Carbon does segregate to grain boundaries in high purity iron and steels and it is believed to improve the cohesiveness of the grain boundaries, either directly or indirectly by supplanting other embrittling segregating elements. Sulphur was shown to be the embrittling element in high-purity irons by Pichard, Rieu and Goux[37], yet sulphur does not segregate to grain boundaries in stainless steels due to its interaction with chromium[4]. Therefore it is not likely to be the problem with this stainless steel.

Grubb, Wright and Farrar[28] had suggested that titanium segregated to grain boundaries had embrittled the ferritic stainless steels in their investigation. They also believed that the extremely low carbon levels had an effect. Yet, with or without titanium segregation, determining whether there is any appreciable carbon segregation to grain boundaries would alone be of interest.

Intergranular fracture was encouraged in low-carbon low-alloy steels studied by Niikura and co-workers[39] by the addition of niobium. (see section 2.6.2) While the exact mechanism was not known to them, it is possible that a similar situation is occurring in this ferritic stainless steel.

It is improbable that only one factor, such as extremely low carbon levels or titanium segregation, is responsible for the intergranular fractures found in the sample from the rolling mill. The ferritic stainless steel also has precipitation along the grain boundaries. The precipitation may encourage the separation of grain boundaries. The cohesiveness between the bulk matrix and the precipitates may be affected by the interface composition.

It was decided to investigate this possibility in 44101. Titanium segregation to the grain boundaries may be weakening their cohesiveness. This would be an analogous situation to those described above. Yet it has not been demonstrated in a ferritic

stainless steel. Therefore, in order to explore the hypothesis that the grain boundary composition was substantially different from the matrix, it was decided to employ Auger Electron Spectroscopy.

4.4.2 Applying Auger Electron Spectroscopy

This ferritic stainless steel had exhibited crack formation at the grain boundaries, owing to unknown causes. Now intergranular embrittlement or weakness of some nature has been studied in a number of alloy systems, such as tin and low- alloy steels. In these cases preferential elemental segregation to the grain boundaries was the cause of the problems. For many years these explanations had been only conjectural, but with the development of Auger Electron Spectroscopy around 1970, experimental evidence began to collect in support. These studies emphasised how the macroscopic material properties could be strongly influenced by the composition of the grain boundaries, even if the segregated layer was only atoms thick [47,49]. Auger Electron Spectroscopy will not explain any mechanism on an atomic level, but will only show the composition at that interface[49].

4.4.3 Scanning Auger Microscope Results

Two specimens from each of the two alloys were fractured and analysed using this equipment. The first alloy was a sample of AISI 430 ferritic stainless steel and was used as a control sample. The second group of specimens were of alloy C, an unembrittled 44101 heat. The intention was to compare a non-stabilised ferritic stainless steel with relatively high interstitial levels with the stabilised steel. The secondary electron images of the two fractured samples are shown on the next page.

The samples were broken at –90°C in a high vacuum by impact with a small bar. Unfortunately neither specimen exhibited a true intergranular fracture and some ductility remained, even at this low temperature. The low temperature of testing was intended to encourage intergranular fracture. Yet, even with a sharp impact, the fractures were not purely brittle and exhibited some ductility. It is possible that if the testing apparatus was able to reach truly cryogenic temperatures as intended, at around –190°C, then a partly intergranular brittle fracture would have occurred. It was originally intended to fracture the specimens at this temperature, but this would have required modification of the equipment which was not a feasible option.

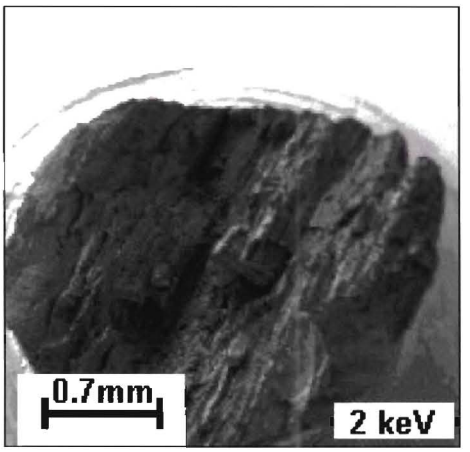

Figure 4.24 An AISI 430 specimen

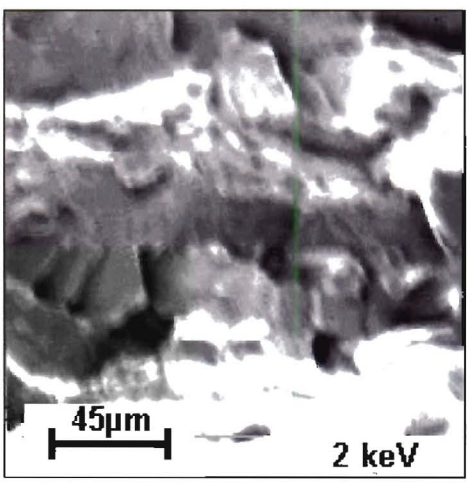

Figure 4.25 The fracture surface of the AISI 430 specimen

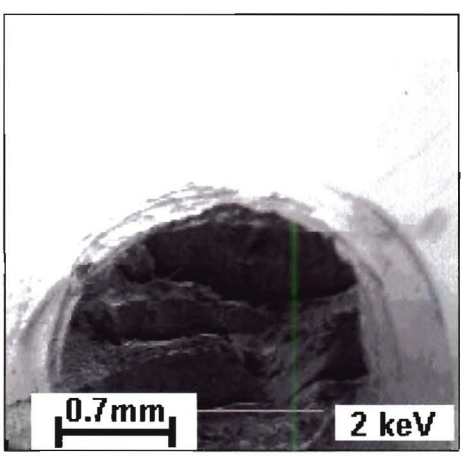

Figure 4.26 An alloy C specimen

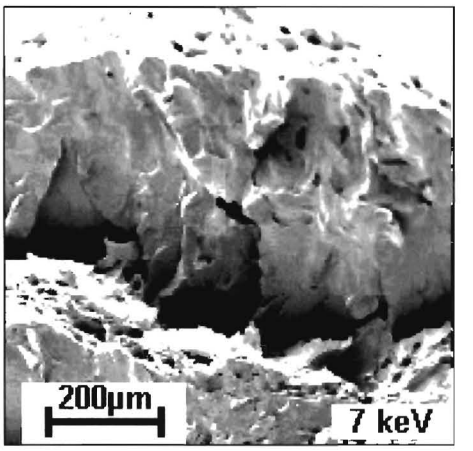

Figure 4. 27 Alloy C – mixed mode of fracture

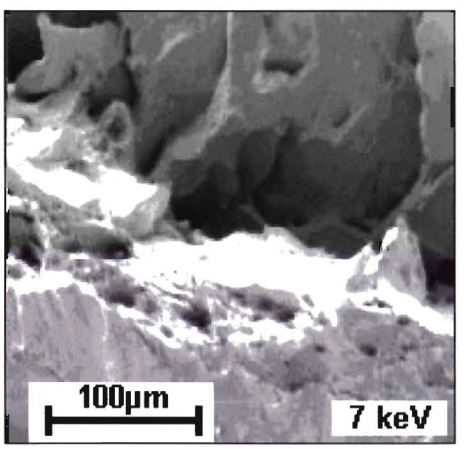

Figure 4.28 The above area at a higher magnification

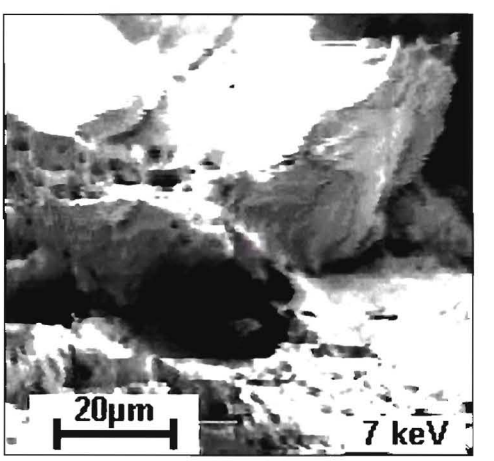

Figure 4.29 A precipitate in a dimple

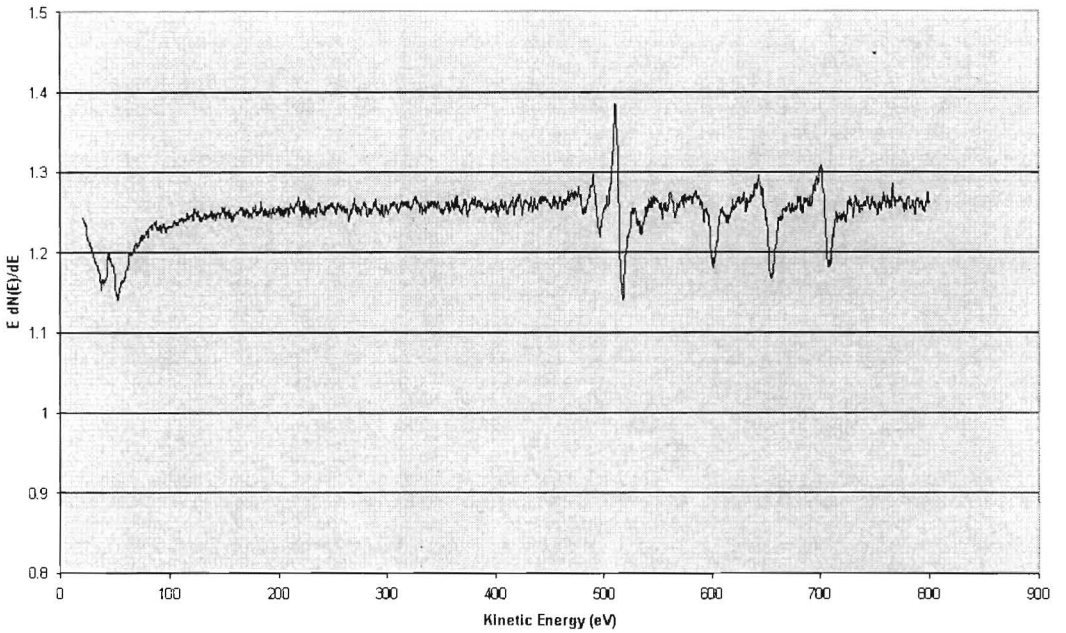

Figure 4.30 The AISI 430 control sample with the background peaks due to iron and chromium only

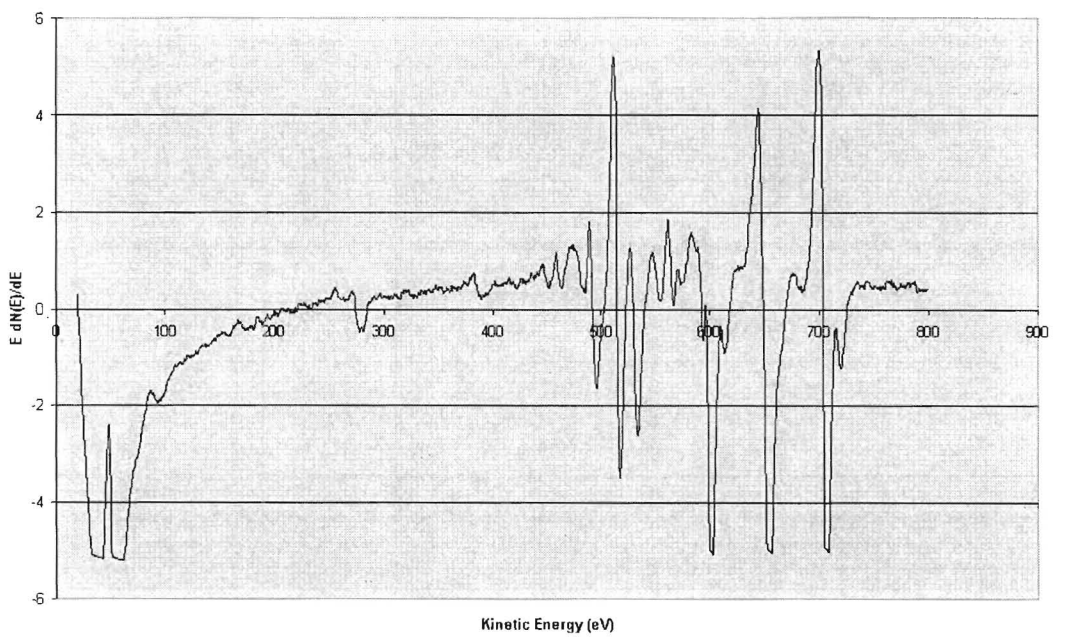

Figure 4.31 After approximately an hour, then the carbon and oxygen has settled to a measurable extent on the specimen of 44101

<u>Peaks of Interest:</u> Carbon at 275 eV and Oxygen at 510 eV

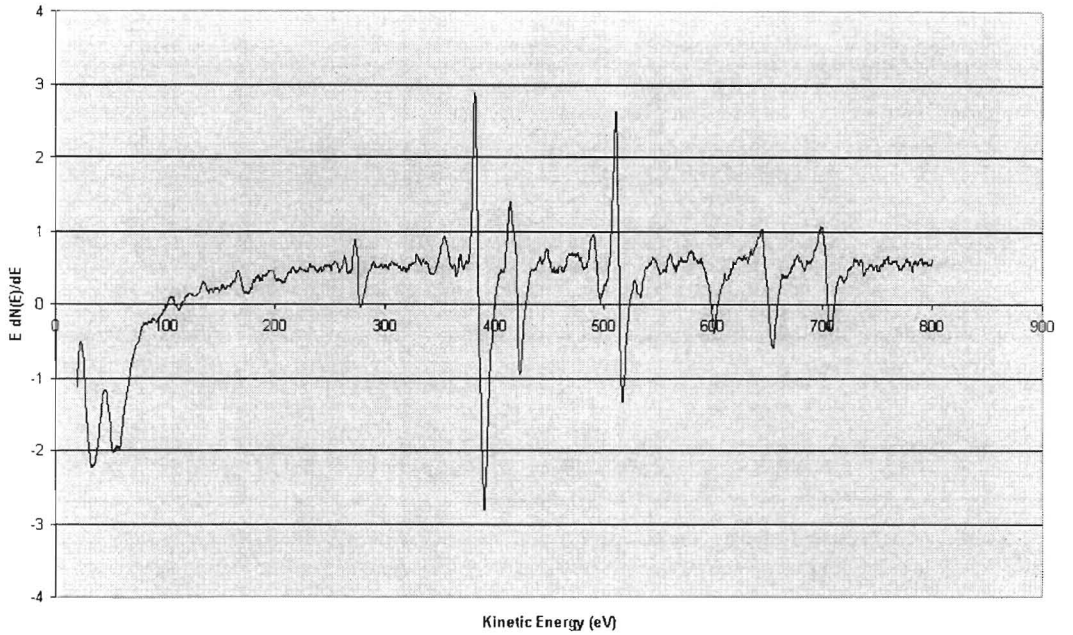

Figure 4.32 The composition of the precipitation in Fig. 29

Peaks of Interest: Niobium at 109,146,170 eV; Carbon at 275 eV; Titanium at 357, 390, 421 eV; Nitrogen at 389 eV

Over a hundred spot analyses were done on the four samples, two samples each of the two alloys. There was little of interest on the AISI 430 samples. Initial analyses of the first AISI 430 sample in Figs. 4.24-25 showed that only iron and chromium were present. This confirmed that the experimental vacuum was sufficiently high to prevent immediate contamination of the fracture surface with atmospheric elements. (see Fig 4.30) After about an hour contaminants such as carbon and oxygen would have settled in detectable quantities onto the fracture surface as shown in Fig. 4.31. Analyses taken repeatedly in the same region also tended to show a strong presence of oxygen. This was due to the formation of a fine layer of chromium oxide. The chromium atoms were oxidised by the electron beam when used in its scanning mode for image acquisition.

The samples of the stabilised stainless steel did not exhibit intergranular fracture either. The mode of fracture was mixed-mode, with the characteristic dimples of ductile failure alongside cleavage planes, as shown in Figs. 4.27-28. This prevented an analysis of any clearly defined grain boundary.

A precipitate is shown in Fig.4.29, which, from the elemental composition, is probably a titanium nitride with niobium carbonitride alongside. The titanium and nitrogen peaks are very strong, with smaller niobium and carbon peaks. Though the Auger electron signal is only from the topmost atoms, the area analysed is 1 μm across and both types of precipitation may have been analysed. These larger titanium nitride precipitates are found predominately at grain boundaries and this suggests that this line of ductile dimples is following a grain boundary, with the cleavage planes cutting across the grains themselves. Yet this is only a supposition from circumstantial evidence and would be difficult to corroborate.

4.5 The Appearance of Precipitation

4.5.1 As-Received and Solution Treated Specimens

The samples which were received for experimentation had been hot rolled and then annealed at 1050°C for 30s. A typical micrograph depicting their microstructure is shown in Fig. 4.33. This shows how the grains are still elongated in the direction of rolling. Recrystallisation has not begun and the grains are irregularly shaped. The titanium nitride particles are spread out, not just at grain boundaries. Smaller, black precipitates are visible throughout. These are probably niobium carbonitrides, since the annealing process was significantly higher than the dissolution temperature for the Laves phase, Fe_2Nb. There is no immediately noticeable precipitation along the grain boundaries.

In order to allow the Laves phase which may have formed during annealing to go into solution, the as received steel was solution treated at 1050°C for a further two hours. A solution treated specimen is shown in Fig. 4.34. The titanium nitride precipitates are still present, while the rest of the steel is relatively precipitation free, including the grain boundaries. The grain size is much larger after the 2 hours at 1050°C in comparison with the as received specimen in Fig. 4.33.

A large precipitate typically found at the grain boundaries is shown in a backscattered electron image in Fig. 4.35. This accentuates the difference in composition between the central precipitate and the additional precipitate around it. X-Ray mappings were done of the precipitation, for elements such as iron, chromium, titanium and niobium. The matrix was unsurprisingly constituted of iron and chromium. The central precipitate was rich in titanium (see Fig. 4.36) with the surrounding precipitation rich in niobium (see Fig. 4.37) This would support the expectation raised by previous work done on stabilised steels' precipitation (see section 2.4.2) that this is a titanium nitride, surrounded by niobium carbonitrides. Niobium rich Laves phase would have gone into solution at the annealing temperature of 1050°C[2].

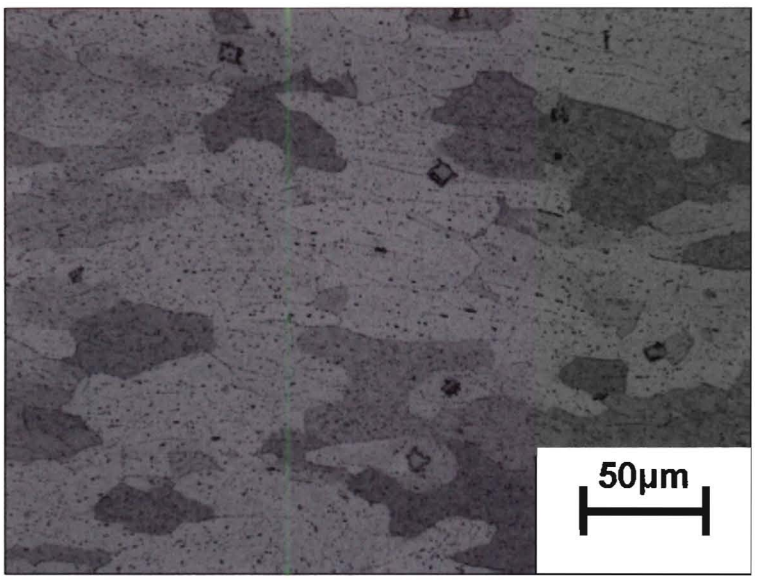

Figure 4.33

C (as received)

hot rolled and annealed

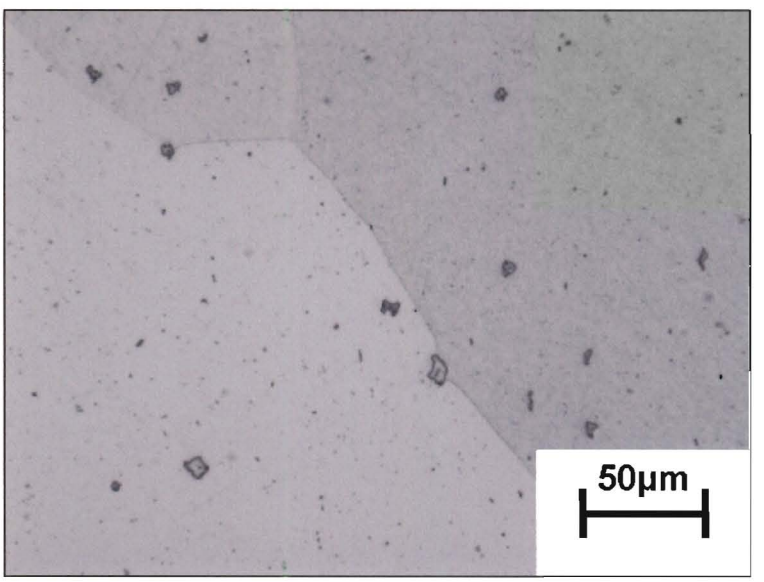

Figure 4.34

A (solution treated)

after 2 hours at 1050°C

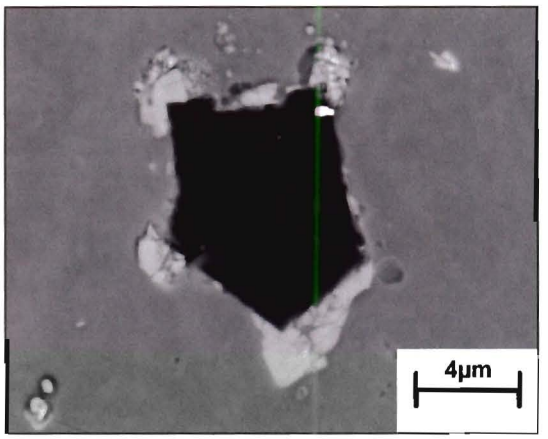

Figure 4.35

A typical large titanium nitride precipitate, as found often at grain boundaries

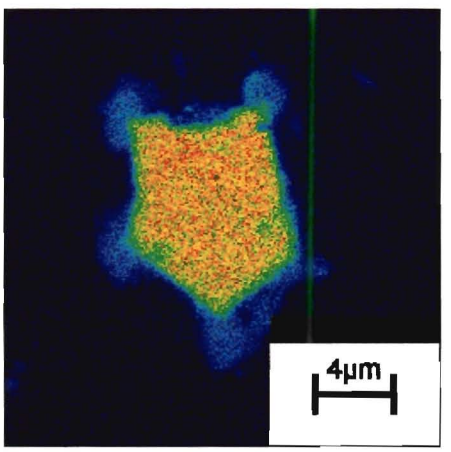

Figure 4.36

An X-ray map for titanium

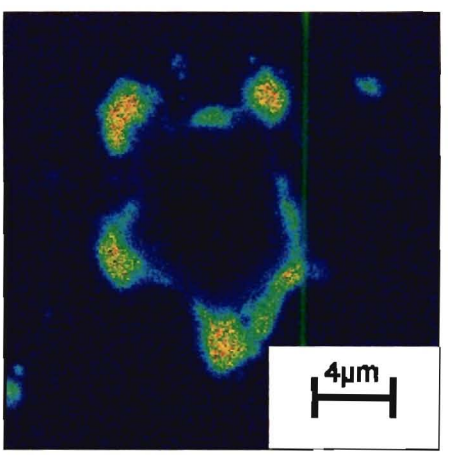

Figure 4.37

An X-ray map for niobium

4.5.2 A Range of Times and Temperatures

These images are of samples which were first solution treated at 1050°C for 2 hours, before being aged at temperatures between 500°C and 900°C and times ranging from 1 hour to 16 hours. These particular ones shown and discussed individually were chosen as being representative of the results of the experimental investigation.

In Fig. 4.38 after only one hour at 900°C, the grain boundaries are clearly delineated with intragranular precipitation throughout the grains in some profusion. In Fig. 4.39, after four hours at 900°C, there is as great a profusion of intragranular precipitation. Some precipitation growth has occurred, with some precipitates being distinctly larger. Along the grain boundary in the lower part of the image, individual precipitates can be discerned along the grain boundaries.

After only 15 minutes at 800°C, not much precipitation has had time to occur in Fig. 4.40. Yet after 15 minutes more, in Fig 4.41, there are a multitude of smaller precipitates. In Fig 4.42, after one hour at 800°C, there is much intergranular precipitation and tiny precipitates are visible along the grain boundaries. Many intragranular precipitates are bigger, as seen in Fig. 4.39, which was after four hours at 900°C. After four hours at 800°C in Fig. 4.43, the intragranular precipitation is very dense. The picture is similar for Fig. 4.44, after eight hours at 800°C.

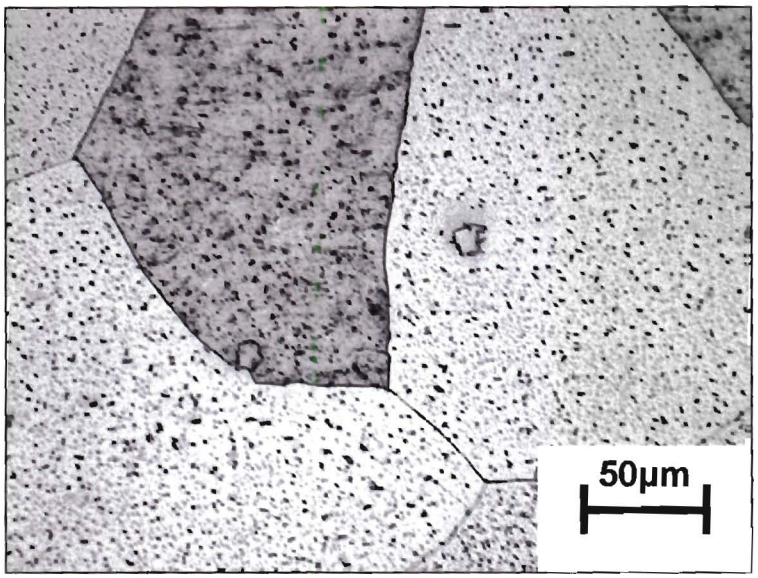

Figure 4.38

A after 1 hour at 900°C

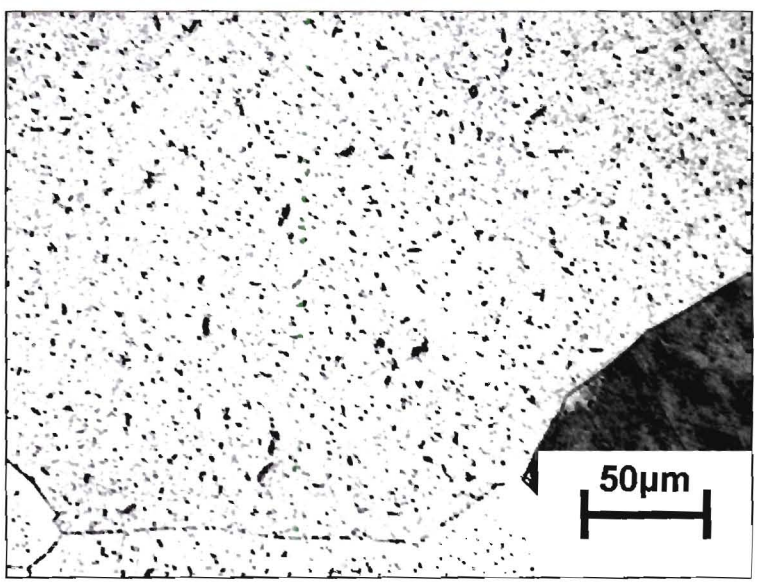

Figure 4.39

A after 4 hours at 900°C

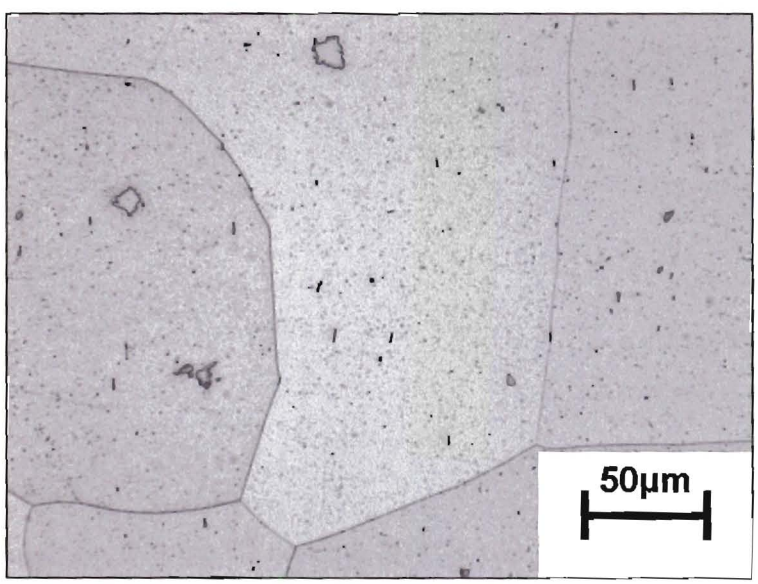

Figure 4.40

A after 15 min at 800°C

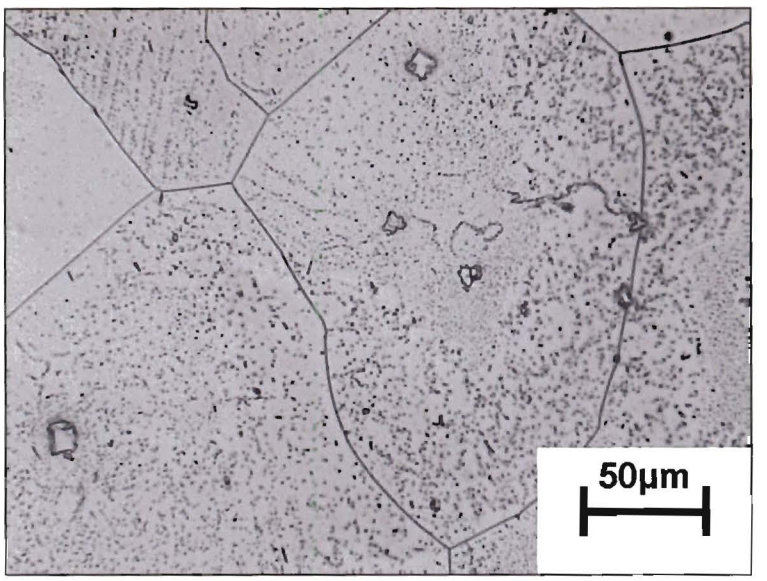

Figure 4.41

A after 30 min at 800°C

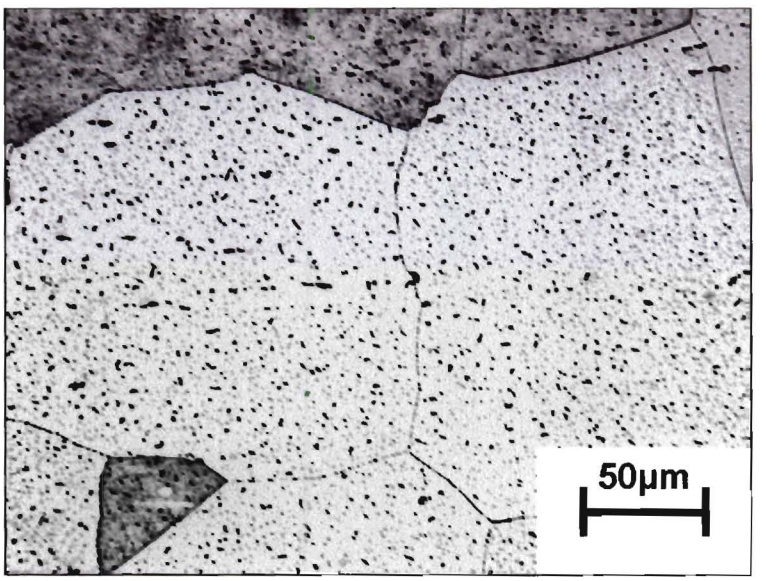

Figure 4.42

A after 1 hour at 800°C

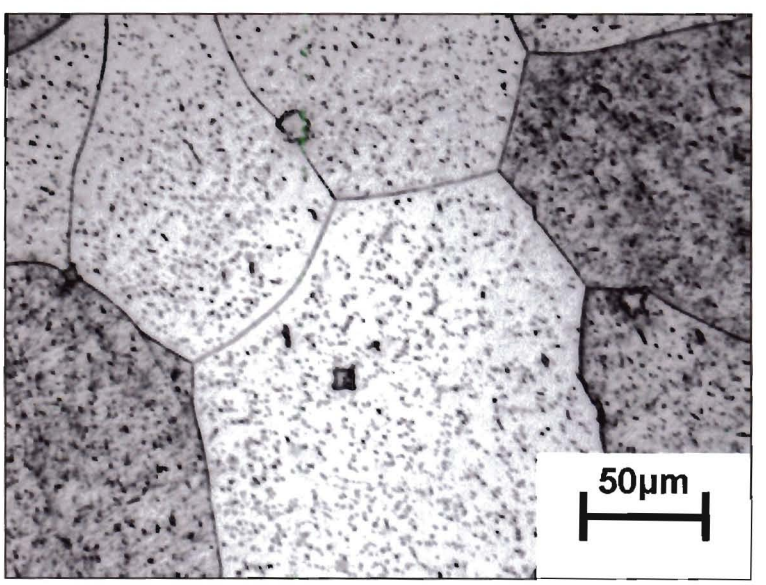

Figure 4.43

A after 4 hours at 800°C

Even after eight hours at 700°C there is very little precipitation visible in Fig.4.45. While after 16 hours at 700°C in Fig. 4.46 there has been a remarkable transformation, with heavy precipitation throughout the specimen. The precipitation is dissimilar to that at higher temperatures in that its arrangement is more regular; frequently in strings, like beads on a necklace. The precipitation may be the same carbonitrides as at 800°C and 900°C, but forming differently or it may have a different composition. A spinodal, rather than a nucleation and growth, formation would be more likely to result in such structures[23].

In Fig. 4.47, after 8 hours at 600°C there has been no additional precipitation. After sixteen hours at 600°C, there is very little precipitation present in Fig. 4.48. Even in a heavily etched sample such as this it is clearly less than that in Fig. 4.46, after sixteen hours at 700°C.

After sixteen hours at 500°C in Fig. 4.49, there has been no intergranular precipitation. Therefore it can be concluded that the precipitation of interest is therefore occurring at higher temperatures. The sixteen hours at 500°C is theoretically just long enough for the formation of chromium-rich α' phase, but even if 475°C embrittlement (see section 2.2.3) has begun to occur, the separate phases would not be distinguishable in an optical microscope.

The occurrence of precipitation has been summarised in Fig. 4.50, where it can be seen that the bulk of the precipitation occurs at greater than 800°C.

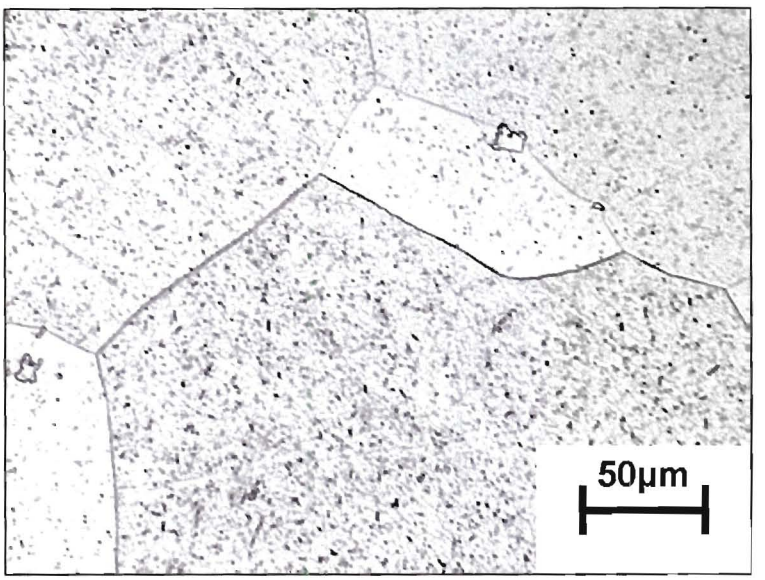

Figure 4.44

A after 8 hours at 800°C

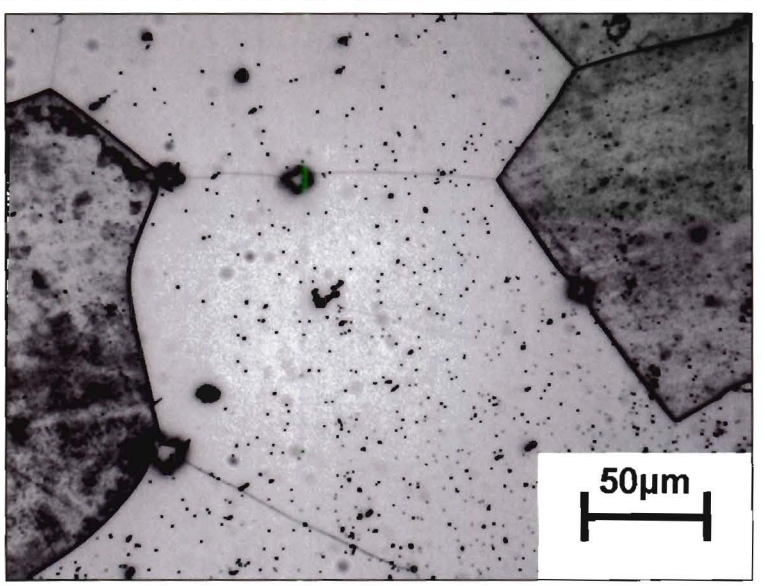

Figure 4.45

A after 8 hours at 700°C

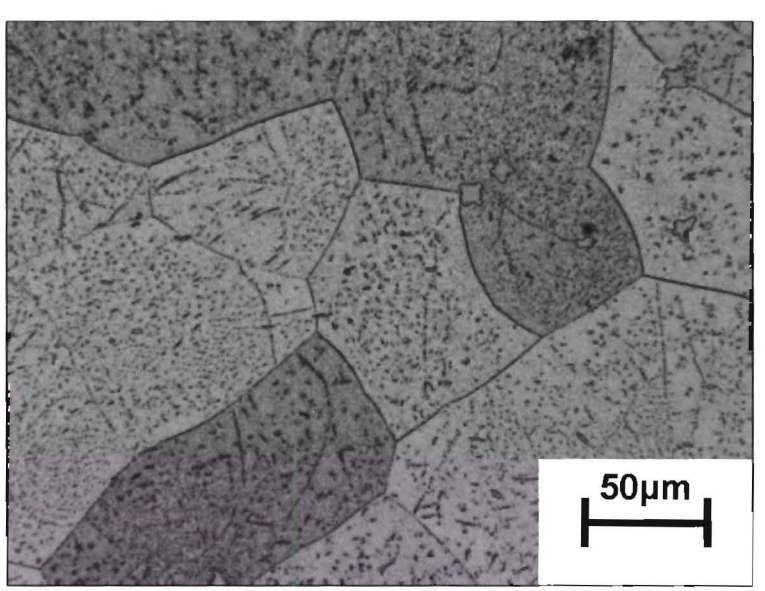

Figure 4.46

A after 16 hours at 700°C

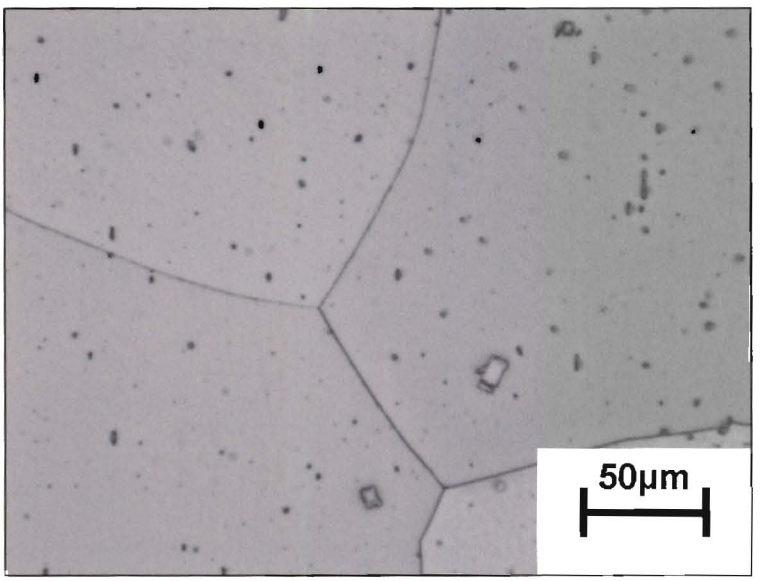

Figure 4.47

A after 8 hours at 600°C

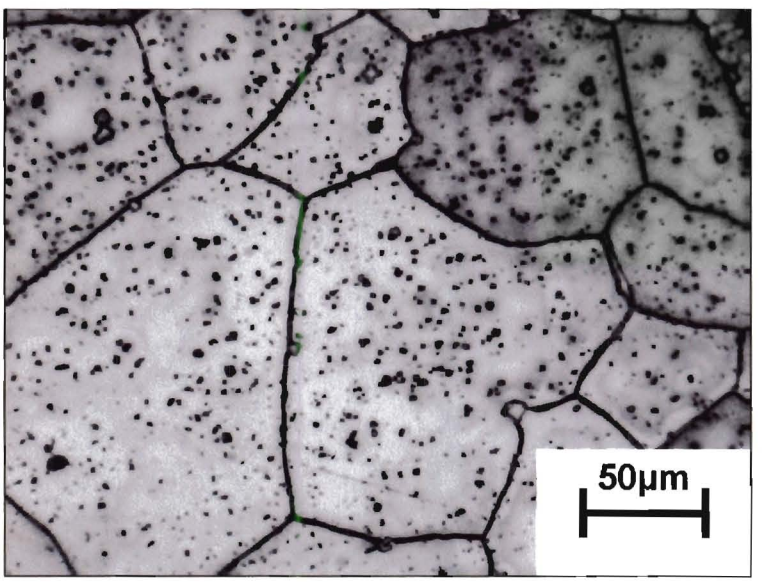

Figure 4.48

A after 16 hours at 600°C

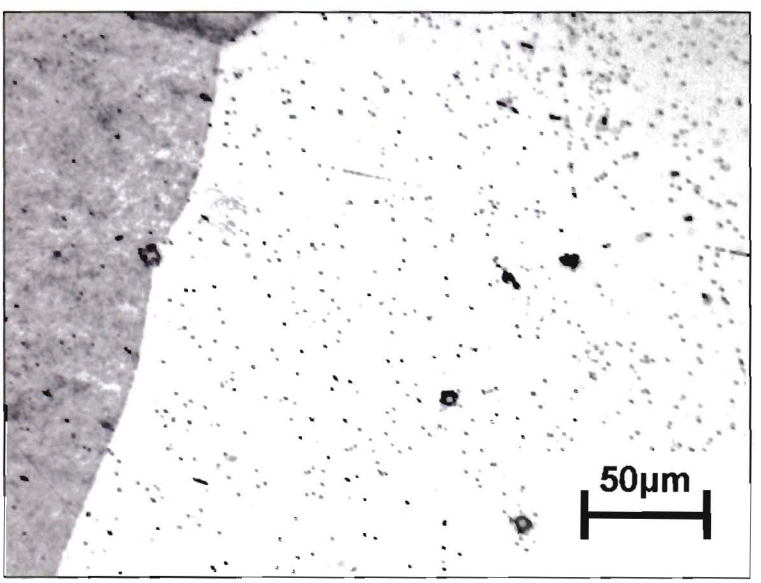

Fig. 4.49

A after 16 hours at 500°C

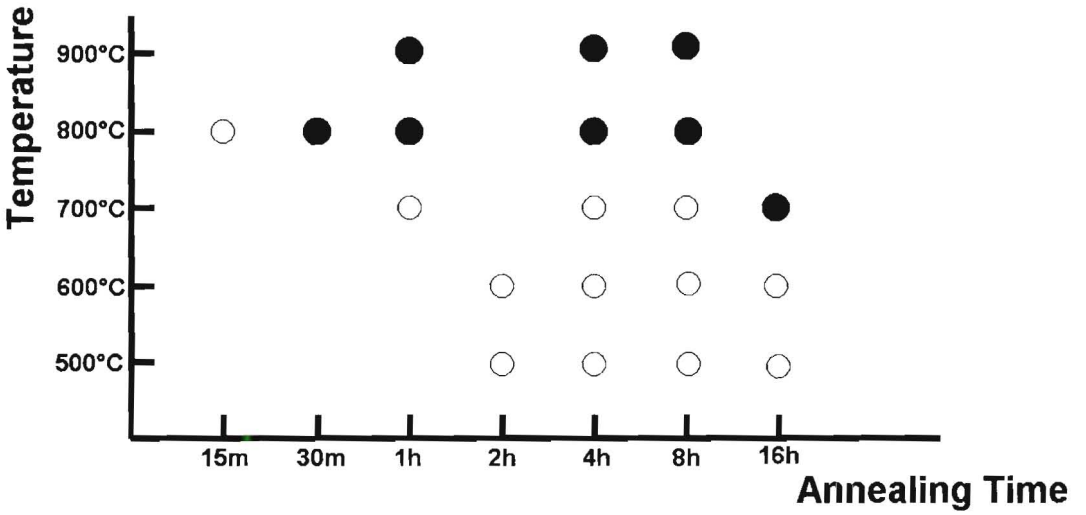

Figure 4.50 The occurrence of precipitation for different annealing temperatures and times

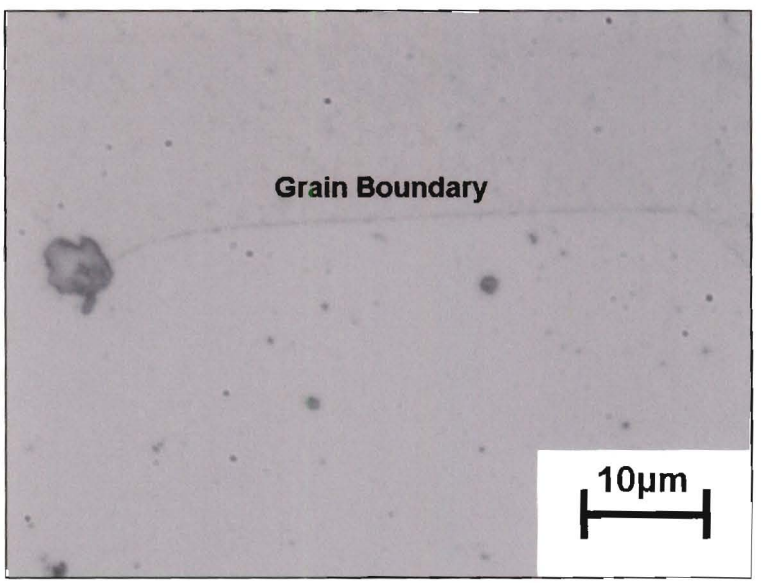

Figure 4.51

A (solution treated)

after 2 hours at 1050°C

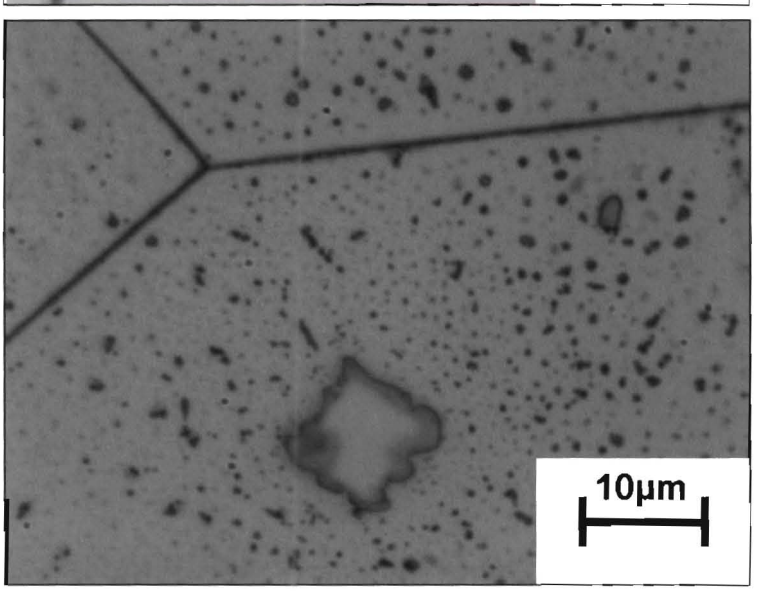

Figure 4.52

A after 30 minutes at 800°C

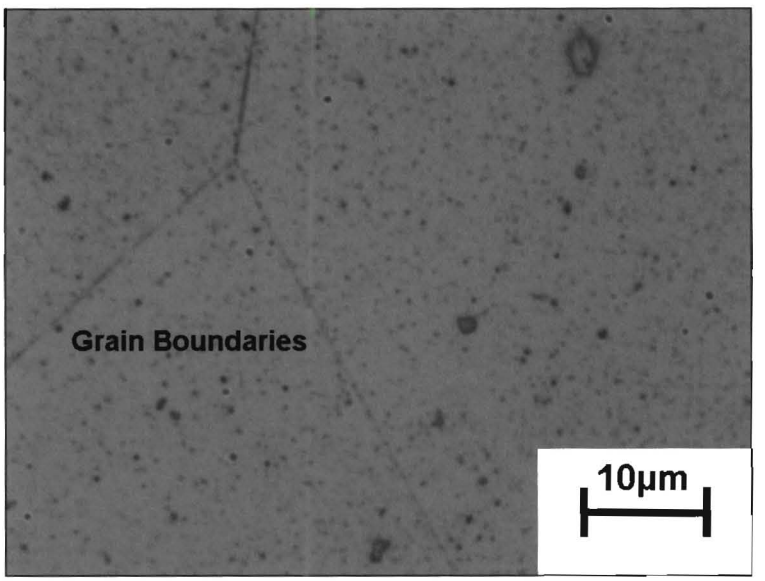

Figure 4.53

A after 4 hours at 700°C

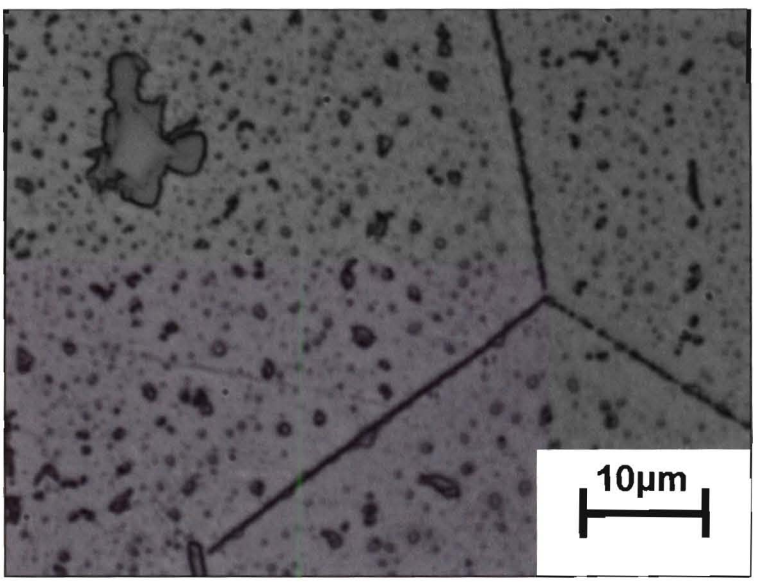

Figure 4.54

A after 1 hour at 800°C

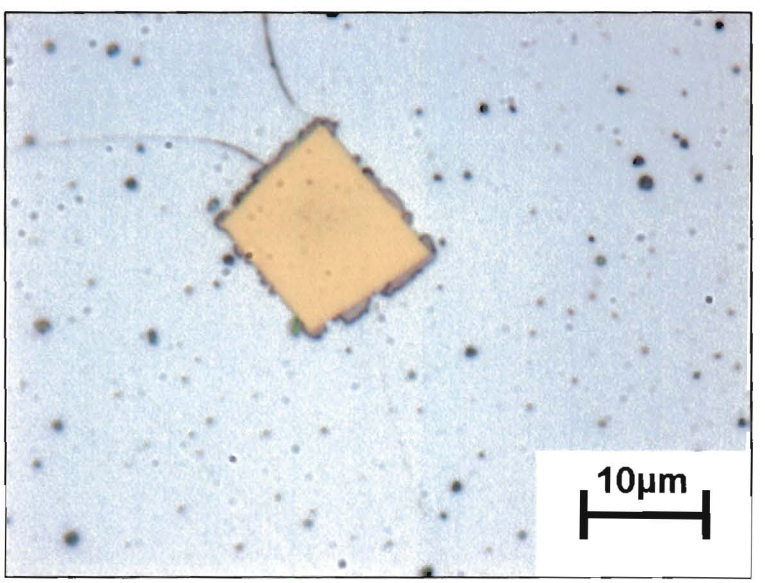

Figure 4.55

A after 1 hour at 700°C

A yellow titanium nitride precipitate, with niobium carbonitride precipitated around it

4.5.3 Intergranular Precipitation

The failure analysis and theory in sections 4.1-4.3 mentions how the precipitation at the grain boundary may be influential. It is also of importance for the creep resistance of the stainless steel at high temperatures, as discussed in sections 2.2.8-11. Therefore the grain boundaries were investigated at a higher magnification and pertinent images are shown in figures 4.51-55. The titanium nitride precipitates are often found at the grain boundaries. Now we refer specifically to the smaller precipitation spread along the grain boundaries. After solution treatment at 1050°C for two hours, there is no precipitation evident at the grain boundaries in Fig. 4.51.

After 30 minutes at 800°C, shown in Fig. 4.52, the grain boundaries are heavily etched, suggesting that intergranular precipitation is present. As there was none after the solution treatment during which Laves phase would dissolved, this is probably the formation of Fe_2Nb. This is in sharp contrast to the situation at 700°C, where even after four hours in Fig. 4.53, there is very little or no intergranular precipitation. Once a full hour has passed at 800°C, in Fig. 4.54, then the intergranular precipitation is very prominent. The titanium nitride precipitate in Fig. 4.55 is very yellow, typical of those found in these steels, indicating that its composition is about 10% TiC and 90% TiN. (see section 2.4.2)

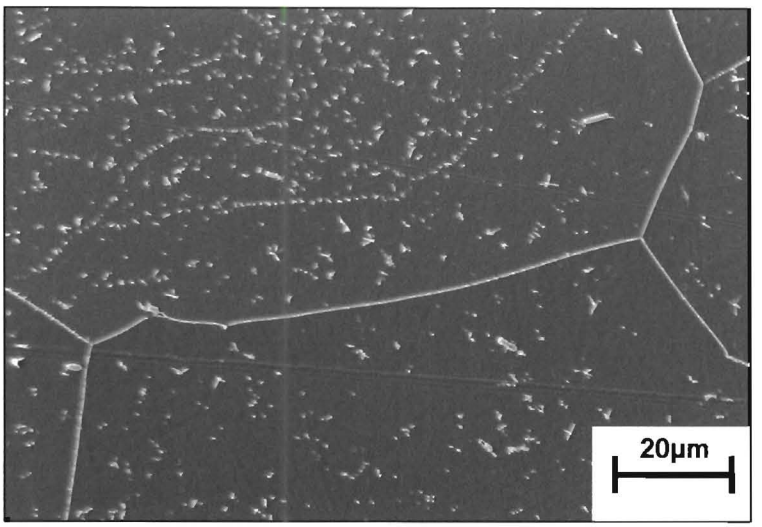

Figure 4.56

A after 2 hours at 800°C

Secondary electron image

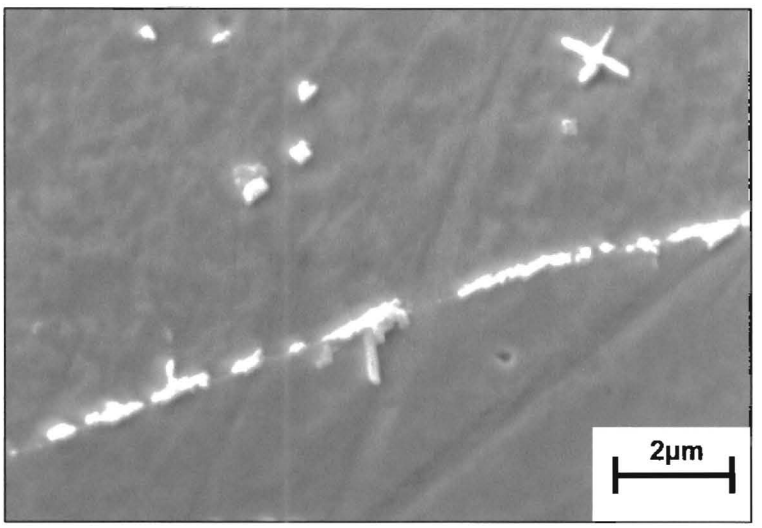

Figure 4.57

A after 2 hours at 800°C

Secondary electron image

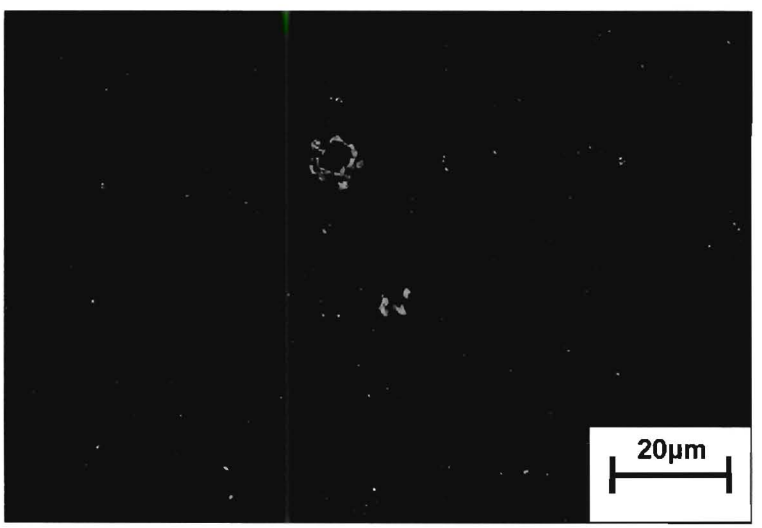

Figure 4.58

C after 4 hours at 500°C

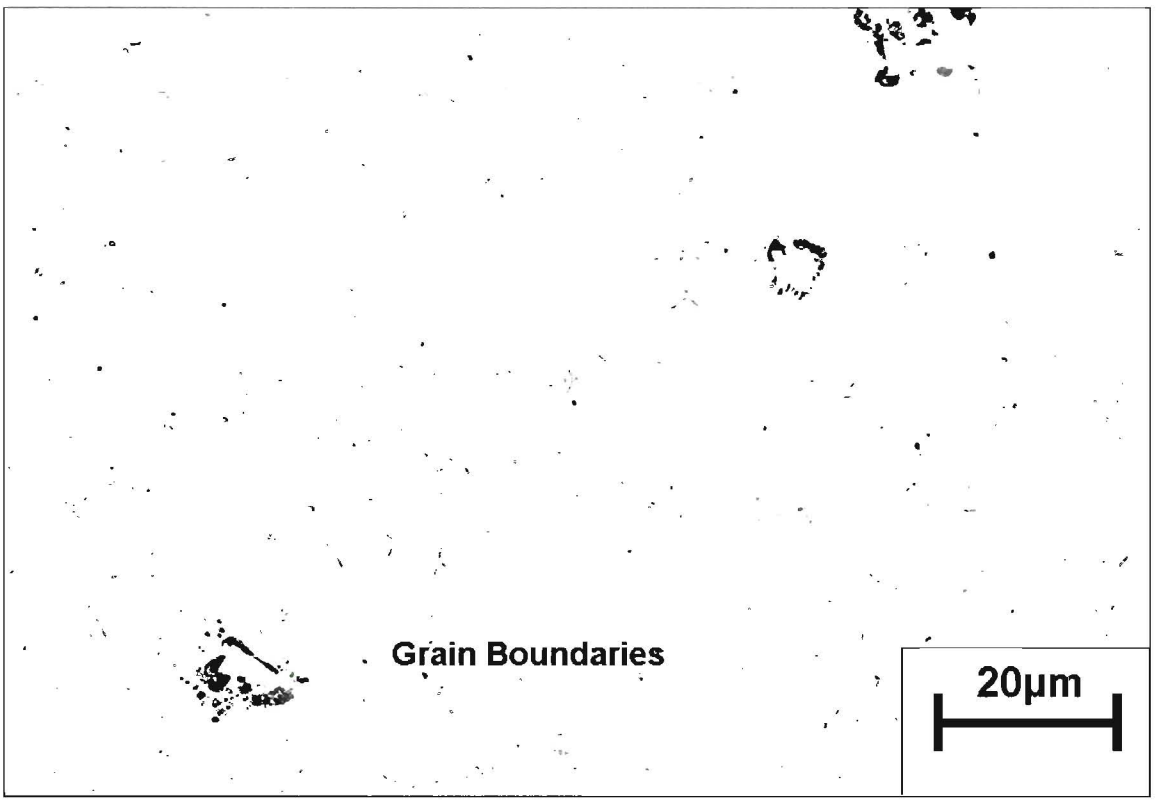

Figure 4. 59 A negative of a backscattered electron image of C after 4 hours at 800°C, with niobium-rich grain boundaries now clearly distinguishable

4.5.4 Electron Microscopy

Scanning electron microscopy has provided an alternative view of the distribution of the precipitation. In Fig. 4.56, the tiny white precipitates are highly contrasted with the matrix. The grain boundaries here are very clear, partly because of precipitation along the grain boundaries but also because etching around these precipitates and along the grain boundaries creates an 'edge effect' for this secondary electron image. An edge releases secondary electrons from both sides, so that small area will appear brighter than it otherwise would.

The micrograph in Fig. 4.56 shows the precipitation very clearly, with the smallest of the precipitates, which would be on the limits of optical resolution, being distinguishable. The areas alongside grain boundaries are relatively precipitate free, as would be expected if the grain boundaries were favoured for formation[25]. The larger precipitates are many different shapes, with the smallest precipitation forming strings. These strings are good evidence of a spinodal form of precipitation[23]. Laves phase forms through spinodal decomposition and these equidistant, tiny precipitates are probably Laves phase. However it is not sufficient to prove this as a periodically fluctuating composition could also have lead to carbonitrides forming in a nucleation and growth manner. Yet the precipitates in these strings have not undergone much growth, which also implies an Fe_2Nb composition[15].

In Fig. 4.57 the precipitates along the grain boundary are shown in a secondary electron image, which is possible at a far higher magnification than for the optical micrographs of Figs. 4.51-55. These precipitates are smaller than 1μm across and do not encompass the entire grain boundary. Many, including the very smallest, are rectangular in shape. The scratches may have formed from detached precipitates rolling across the specimen during the polishing process, of which the difficulty in avoiding is mentioned in section 3.2.3.

The backscattered electron images in Figs. 4.58-59 show very bright precipitates against a very dark background. These backscattered electron images depend on atomic number contrast and so niobium rich precipitates such as niobium

carbonitrides and Fe_2Nb show up strongly against the matrix. Fig. 4.58 has niobium carbonitrides surrounding a titanium nitride, which is not discernible, along with a few niobium carbonitrides through the matrix. These would have been already present after the solution treatment at 1050°C.

In Fig. 4.59, after four hours at 800°C, there are more niobium-rich precipitates throughout the matrix. Of more interest, is the sprinkling of niobium-rich precipitation along the grain boundaries. This precipitation was conspicuous after etching in the optical micrograph in Fig. 4.54. This precipitation was too small to have the composition determined through EDS, yet these backscattered images are able to confirm that they are niobium rich.

4.6 Ageing at 850°C for 100 Hours

4.6.1 Experimental Context

The volume and distribution of precipitation in this stainless steel is of some importance when considering its creep resistance. In section 4.5 this thesis has shown and discussed the precipitation occurring over a wide range of temperatures and times. However to gain insight into aspects of the role of the precipitation in creep, it is necessary to study the precipitation occurring at high temperatures over a much longer time frame.

The producer of 44101 had been concerned with the degree of sagging, i.e. creep, experienced by 44101 when undergoing a standard test. This test consists of a standard tensile test blank held at 850°C for a hundred hours under its own weight alone. When allowing for the gauge, there is a limit set as to the degree of acceptable sagging. Research by Columbus Stainless had been done on the influence of grain size and the role of the precipitation. As would be expected from the roles of grain size and precipitation during creep, as discussed in sections 2.2.8-11, grains had to be a certain maximum size and a certain degree of precipitation present to ensure that the creep resistance was adequate[60].

4.6.2 Grain Size Influence on Precipitation

If the grain size is too small, the surface area of grain boundaries per volume of material is too high for good creep resistance. Yet the greater the amount of precipitation at the grain boundaries, the better for creep resistance. The precipitation at the grain boundaries was forming at 850°C during the creep tests. Specimens, solution treated at 1050°C, had more grain boundary precipitation during ageing at 850°C and greater creep resistance than specimens allowed to cool slowly from hot rolling.

If the grain size is smaller, then grain boundary precipitation would be encouraged. This potentially greater precipitation may then offset the inherent disadvantage of a smaller grain size. It was decided to investigate this possibility. The experimental approach has been detailed in section 3.8.

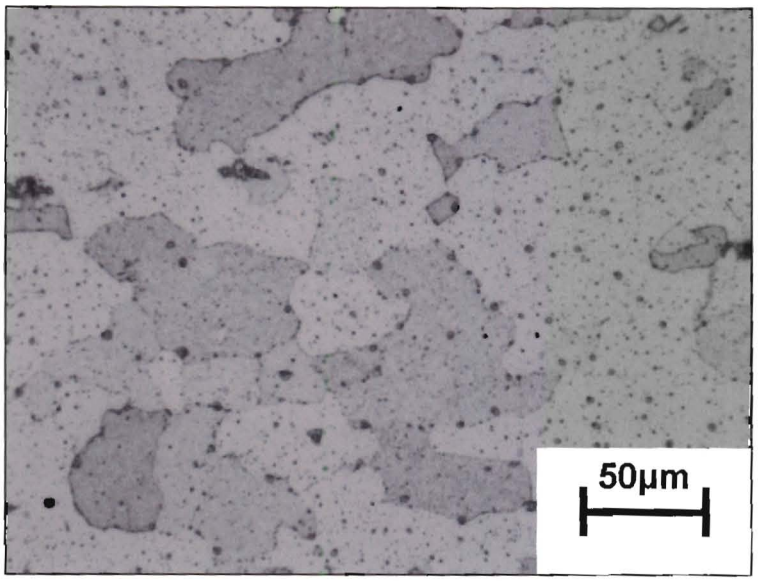

Figure 4.60

E1

after 10 minutes at 950°C

and 100 hours at 850°C

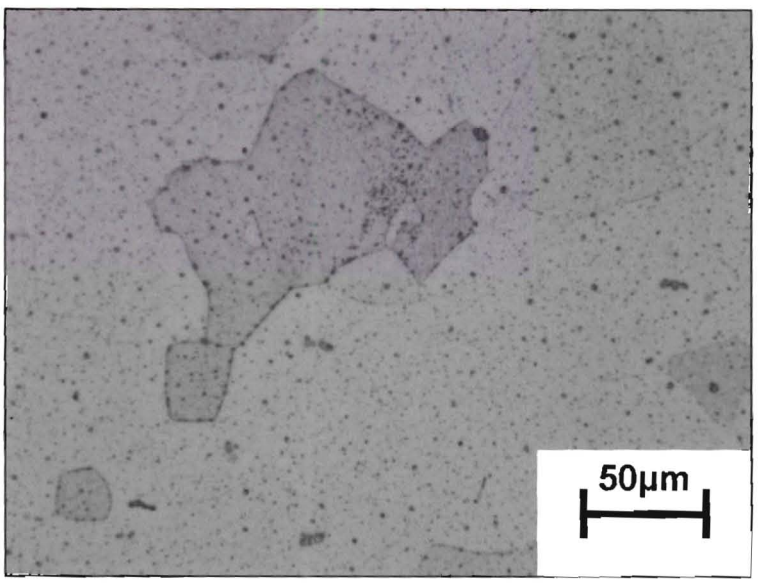

Figure 4.61

E2

after 10 minutes at 1050°C

and 100 hours at 850°C

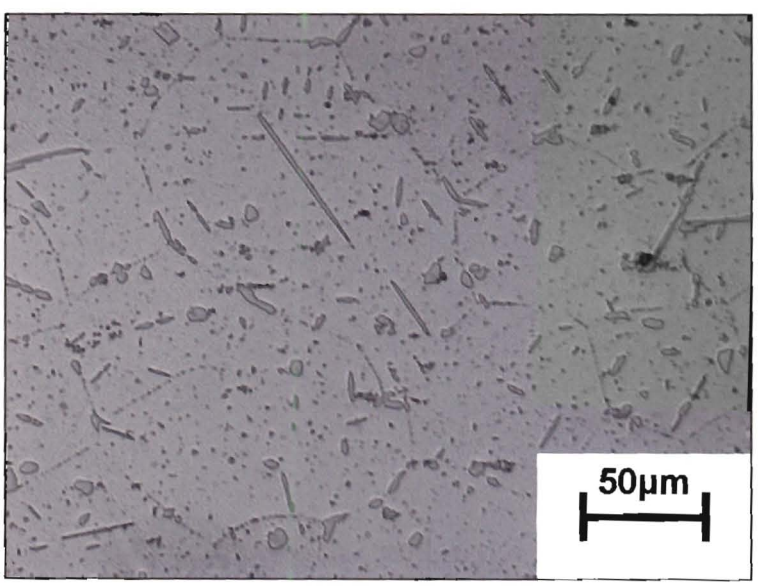

Figure 4.62

E3

after 2 hours at 1050°C

and 100 hours at 850°C

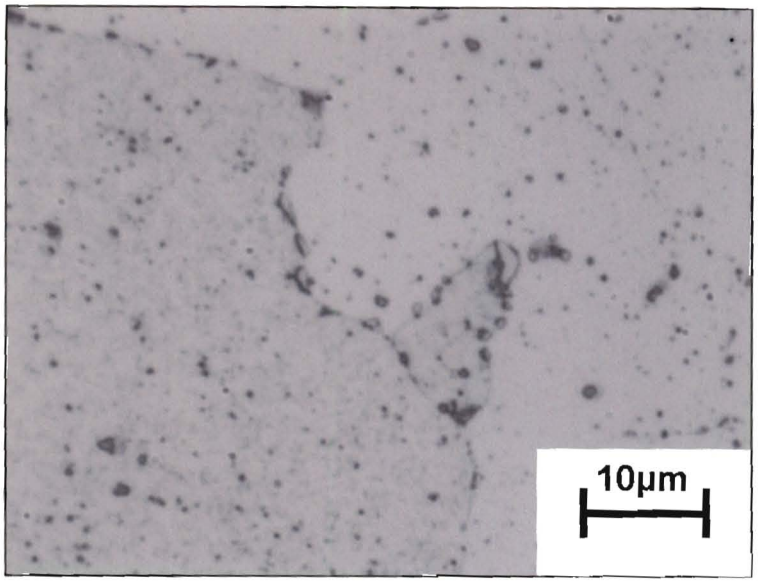

Figure 4.63

E1

after 10 minutes at 950°C

and 100 hours at 850°C

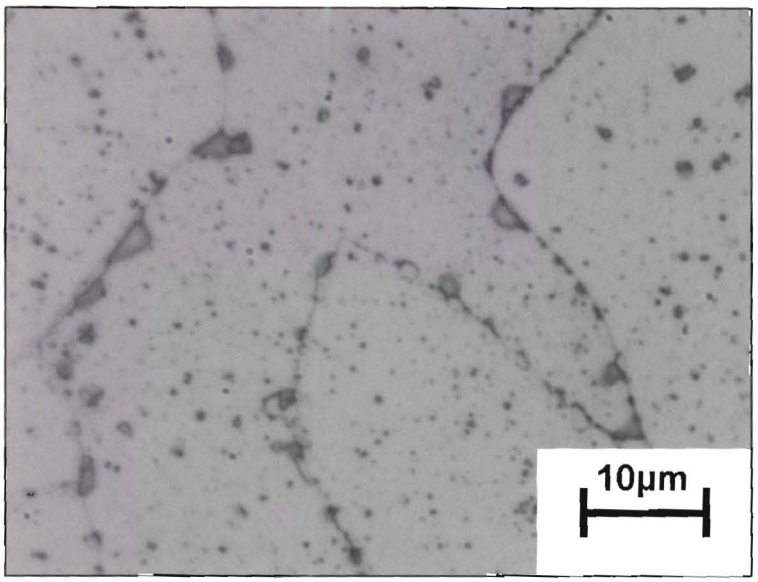

Figure 4.64

E2

after 10 minutes at 1050°C

and 100 hours at 850°C

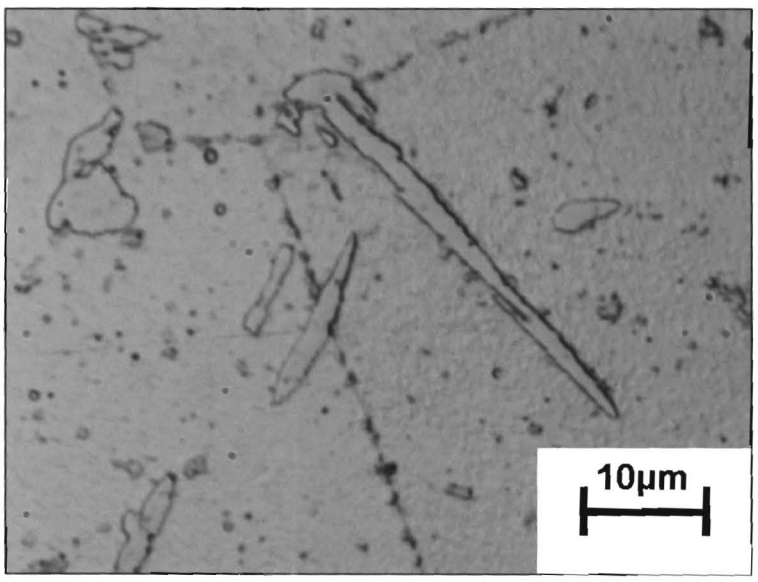

Figure 4.65

E3

after 2 hours at 1050°C

and 100 hours at 850°C

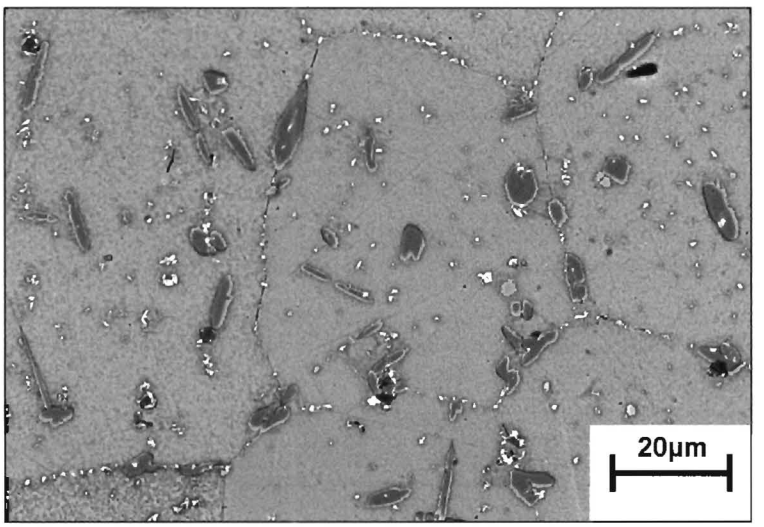

Figure 4.66

E3

after 2 hours at 1050°C

and 100h at 850°C

Backscattered electron image

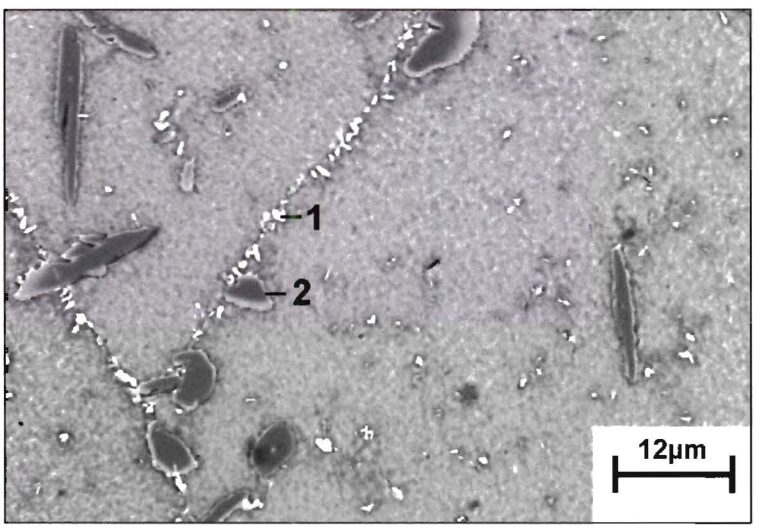

Figure 4.67

E3

after 2 hours at 1050°C

and 100 hours at 850°C

Backscattered electron image

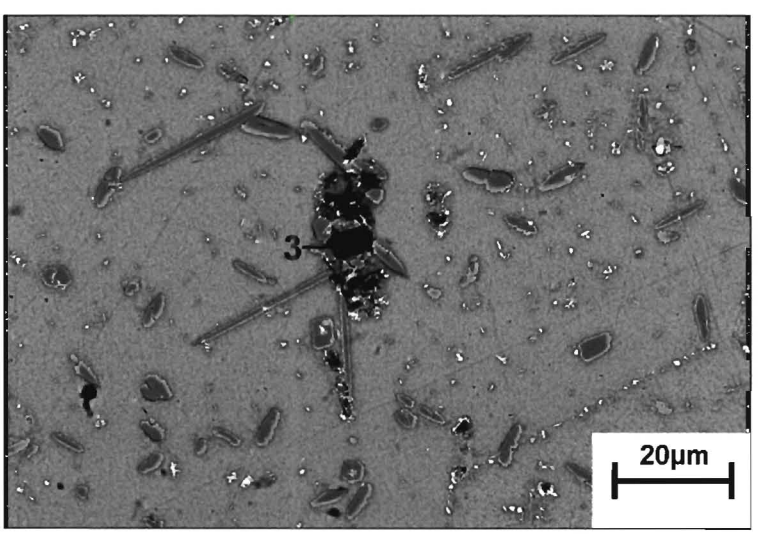

Figure 4.68

E3

after 2 hours at 1050°C

and 100 hours at 850°C

Backscattered electron image

4.6.3 Nature and Appearance of Precipitation

Specimen E1 has the smallest grains, with specimen E3 having the largest. The optical micrographs in Figs. 4.60-62 show the differing grain sizes between the specimens, as the grain size increases with time and temperature. In E1, recrystallisation has begun, while in E2 it is nearly complete, with E3 showing how the grains grew during the two hours at 1050°C, forming an equi-axed structure. Ferritic steels can experience grain growth as low as 600°C but grain growth for the three specimens would be the same during the 100 hour ageing.

In Fig. 4.60 of specimen E1, there are large precipitates visible at grain boundaries, and similarly in specimen E2 in Fig. 4.61. Yet the latter has far more medium sized precipitates strung like beads along grain boundaries. This difference is clearer in Figs. 4.63-64 at a higher magnification, where the grain boundaries in specimen E1 are devoid of the sizeable grain boundary precipitates in E2. This difference between E1 and E2 is also seen in backscattered electron images of grain boundaries in E1 and E2, so it is not an artefact of optical microscopy. The higher temperature prior to the 100 hours treatment has had an effect, probably by putting precipitation into solution, which reforms at grain boundaries during the 100 hours at 850°C.

The specimen E3 in Fig. 4.62, which underwent a full two hours at 1050°C, exhibits very different precipitation. Large precipitates predominate, with smaller, darker precipitates are also present in some profusion. Many of the larger precipitates are very angular, long and thin. At a higher magnification in Fig. 4.65, these two types of precipitation are distinguishable. Both the larger and smaller precipitates favour the grain boundaries, with the larger precipitates then growing into the grains.

The larger precipitates in specimen E3 are distinguishable in the backscattered electron images in Fig. 4.66-68, with the tiny white precipitates now concentrated heavily along the grain boundaries. The backscattered electron images are affected by atomic number contrast and the different precipitates of differing composition show different tones. In Fig. 4.66 it is emphasised how much the precipitates favour the grain boundaries for their formation, with the grain structure defined impressively by

the various types. The small grain boundary precipitates are more numerous in E3 than in E2 or E1. They are probably of importance in obstructing the flow of vacancies down grain boundaries, a prerequisite of the Coble creep mechanism. This would raise the temperature at which creep through the diffusion of vacancies could occur, by restricting it to a Herring-Nabarro type mechanism. (see section 2.2.10)

The image contrast on these images had to be increased sharply to accentuate the atomic number contrast between the precipitates and the matrix. This immediately suggested that the new precipitates had a different composition to the titanium nitrides and especially niobium-rich carbonitrides. The morphology of the larger precipitates, being long and angular rather than blocky, is different from that of the titanium nitrides previously predominant in this steel. Remaining titanium nitrides, with the increased image contrast, now look very much darker than the surrounding matrix, with the niobium-rich precipitates now a blinding white.

These backscattered images were supported by repeated EDS analyses. The backscattered image of E3 in Fig. 4.67 shows two different precipitates as an example. The tiny, bright precipitate (1) is 63% iron, 24% chromium and 13% niobium. The larger, dark precipitate (2) is around 60% chromium, 25% iron and 15% nitrogen. The EDS interaction volume is probably greater than the precipitate. Nitrogen, a light element, is normally a weak signal in EDS, so its strong signal for the dark precipitate is striking. This suggests that the large precipitates are in fact chromium nitrides, while the smaller precipitates are Laves phase or niobium carbonitrides.

The specimens were aged at 850°C in a normal atmosphere, certainly not inert nitrogen, so there is no immediate reason why the matrix near the surface may have absorbed additional nitrogen. The surface of E3 was prepared and studied three times, which also lessens the likelihood that it was some form of surface contamination. One of the few remaining titanium nitrides (3) in E3 is shown in Fig. 4.68, surrounded by angular chromium nitrides. Its identity is supported by EDS, with titanium at 60% and nitrogen at 40%.

Specimen E1, with the smallest grains, had the least intergranular precipitation. It is probable that at 1050°C, more initial precipitation dissolved than at 950°C, freeing niobium to from Laves phase at grain boundaries in E2. It appears that the degree to which the precipitation has gone into solution during the prior ageing treatment is of greater importance in determining the nature of precipitation during ageing at 850°C than any grain size factor.

The real surprise is E3, with very different precipitation. The initial two hours at 1050°C were very significant. Even if more carbonitride precipitation occurred in two hours at 1050°C in E3 than in 10 minutes in E2, this still doesn't explain why some precipitates in E3 grew so large and so many more tiny grain boundary precipitates formed. It is also very interesting how the most prevalent large precipitates after 100 hours at 850°C are chromium nitrides, rather than titanium nitrides. This heat contains 0.022%N and 0.20%Ti, little different from the other 44101 heats studied. This was an unexpected result, with the titanium nitrides having been expected to be stable at 850°C. (see section 2.4.2)

Chapter 5 Conclusions

5.1 The Design of this Ferritic Stainless Steel, '44101'

This steel has been well formulated for high temperature applications in motor vehicle engines, as a cheaper alternative to an austenitic stainless steel. It is fully stabilised, and so is ferritic at all temperatures. Thus it is better suited to high temperature use than an AISI 430 steel which forms some austenite. Its dual stabilisation with titanium and niobium avoids the deleterious financial and property implications of heavy additions of only one element, especially with regard to the properties of welds. The additional niobium also improves the hot strength, with the formation of Laves phase improving the creep resistance. The Laves phase, including intragranular precipitates, inhibits the cross-slip of dislocations and hence recovery. It also obstructs the flow of vacancies down grain boundaries, a prerequisite of the Coble creep mechanism.

This steel's modern extra-low interstitial levels, with the carbon being precipitated out, means that remaining interstitial levels in the matrix are very low. The high temperature design features make very specific microstructural condition end requirements for this steel's manufacture mandatory. Therefore its production requires extra care and attention, especially if the production problems investigated here are not to recur.

5.2 Experimental Conclusions

An example of a production failure has been studied using electron microscopy. This revealed a brittle fracture surface. The failure appeared to have originated at clefts into the fracture surface, in the region initially under tension during bending. These lay between the grains. The embrittled steel was broken in tension and shown to be particularly vulnerable to constraint. A rolled sheet is subject to such constraint on its plastic deformation in the transverse direction. These tensile specimens exhibited similar cracks to those seen in the production specimen.

Modern theories of how these cracks could initiate and propagate were used to explain how precipitation at grain boundaries could lead to cracks being initiated at lower stresses. Then cracks could propagate more easily along grain boundaries, before cutting across grains transgranularly to cause a rapid coalescence and fast fracture.

With the fracture toughness of ferritic steels not being high, the steel could then shatter right across.

It does seem probable that grain boundary precipitation seen in the shattered steel may have promoted crack formation, especially if its avoidance allows the prevention of production failures. Yet other fundamental factors suggested or shown to play a role in intergranular crack formation could also have been present. These include the very low carbon levels in the matrix or titanium segregation to the grain boundaries. It seemed sensible to examine grain boundaries and test these hypotheses for this stainless steel. This attempt using Auger Electron Spectroscopy was not successful, because no part of the fracture surface ran purely along a grain boundary and therefore none could be analysed.

Time and temperature studies of the precipitation were done with optical microscopy. They showed that precipitation was rapid at 800°C and 900°C, appearing in less than an hour. It occurred far more slowly at 700°C, being only present after sixteen hours. Special emphasis was placed on looking at the grain boundaries and electron microscopy was also used to some good effect. Exposure to temperatures around 800°C for any length of time would be very detrimental for the steel's room temperature ductility, owing to grain boundary precipitation.

The precipitation after 100 hours at a simulated service temperature of 850°C was compared with the above results. The role of grain size with regard to the nature of the precipitation was investigated. The length of time at the annealing temperature of 1050°C prior to ageing at service temperatures was found to alter the nature of the precipitation substantially. Two hours rather than ten minutes of annealing caused chromium nitrides to form at the expense of carbonitrides during the 100 hours at 850°C.

5.3 Project Summation

This project was justified by the lack of information on this ferritic stainless steel relative to its commercial importance, especially the precipitation and its role in the toughness. A greater understanding should then allow for the alleviation of the production problems experienced by the manufacturer, Columbus Stainless. Changes in the production of 44101 (detailed in section 4.3.5) avoided further problems before the completion of this project. Yet these failures proved interesting, with an analysis of the metallurgical factors behind the failures providing a more theoretical understanding of the problem.

The optical and electron microscopy showed where the precipitation was forming, very quickly at 800°C and 900°C while far more slowly at 700°C. Intergranular precipitation was studied and then compared with the precipitation found after 100 hours at 850°C.

The hypotheses that low carbon levels or titanium grain boundary segregation were factors in the embrittlement could not be supported with Auger Electron Spectroscopy. This was because of difficulties in obtaining a distinct grain boundary, yet these possibilities remain plausible. Future work could find supporting evidence.

The degree to which the steel has been solution treated was found to have a major influence on the nature of precipitation under simulated service conditions. The predominance of chromium nitrides over carbonitrides after 100 hours at 850°C, contrary to expectations, does suggest that the precipitation in this steel may hold some more surprises.

References

[1] **Stainless Steels - ASM Speciality Handbook** edited by: J.R. Davis, International Handbook Committee, American Society for Metals

[2] **Stainless Steels** edited by P. Lacombe., B. Baroux. and G. Beranger, Les Editions de Physique Les Ulis, France, 1993

[3] PICKERING F.B. **Physical Metallurgical Development of Stainless Steels,** *The Metallurgical Evolution of Stainless Steels* edited by F.B. Pickering, American Society for Metals and The Metals Society, London, 1979

[4] **Steels - Microstructure and Properties** by R. Honeycombe and H.K.D.H. Bhadesia, Edward Arnold Publishers

[5] HEWITT J. **High-Chromium Controlled Hardenability Steels,** *Proceedings of the 1st International Chromium Steels and Alloys Congress,* Cape Town, Vol. 2, Johannesburg, SAIMM, 1992

[6] ANDREWS *J. Iron and Steel Institute* 184, 414, 1956 *(taken from reference 4)*

[7] STEIGERWALD R.F., DUNDAS H.J., REDMOND J.D. and DAVISON R.M. **The Physical Metallurgy of Fe-Cr-Mo Ferritic Stainless Steels,** *The Metallurgical Evolution of Stainless Steels* edited by: F.B. Pickering, American Society for Metals and The Metals Society, London, 1979

[8] GORDON W. and VAN BENNEKOM A. **Review of Stabilisation of Ferritic Stainless Steels,** *Materials Science and Technology,* Vol. 12, The Institute of Materials, February 1996

[9] V. ALBINO RODRIQUES, R. CLARET R. DA SILVA, J. NICACIO. DA SILVA, J. ANTONIO. N. DE CARVALHO, R. BARBOSA **Process for Production of Ferritic Stainless Steel,** *Innovation Stainless Steel,* Florence, Italy, 11-14 October 1993

[10] KUZUCU V., AKSOY M., KORKUT M.H. and YILDIRIM M.M. **The Effect of Niobium on the Microstructure of Ferritic Stainless Steel,** *Materials Science and Engineering,* A230, 1997, pp.75-80

[11] HUA M., GARCIA C.I., DEARDO A.J. and TITHER G. **Dual-Stabilised Ferritic Stainless Steels for Demanding Applications such as Automotive Exhaust Systems,** *I&SM*, April 1997, pp.41-44

[12] HISAMATSU S. **Current Status and Future Trends of Automotive Application of Stainless Steel,** *Proceedings of International Conference on Stainless Steels,* 1991, Chiba, Iron and Steel Institute of Japan, pp.1156-1165

[13] **'Stainless Steels Exports Net R3,5bn in Foreign Earnings'** by John Fraser, in the Business Report, Cape Times Newspaper, Cape Town, 6 April 2000, p. 7

[14] LAGIER J., ROMBEAUX P., RAGOT J. and VAUGEOIS P. **Ferritic Stainless Steels in Exhaust Systems,** *Innovation Stainless Steel,* Florence, Italy, 11-14 October 1993, Section 1, pp.159-164

[15] **Heat-Resistant and Refractory Metals** by K.L. Lanskaya, Freund, Tel-Aviv, 1979

[16] FUJITA N.,OHMURA K., KIKUCHI M., SUZUKI T., FUNAKI S. and HIROSHIGE I. **Effect of Nb on High-Temperature Properties for Ferritic Stainless Steel,** *Scripta Materialia,* 1996, Vol.35, No. 6, pp.705-710 and *Innovation Stainless Steel,* Florence, Italy, 11-14 October, 1993

[17] **Metals and Materials – Science, Processes, Applications** by R.E. Smallman and R.J. Bishop, Butterworth-Heinemann Ltd, 1995

[18] DEVINE T., RITTER A. and DRUMMOND B. *Metallic Trans.,* 1981, 12A, pp. 2063-2069 *(cited in reference 9)*

[19] STEIGERWALD R.F.,BOND A.P., DUNDAS H.J. and LIZLOVS E.A. *Corrosion,* 1977, 33, pp.279-295 *(cited in reference 9)*

[20] FUJIMURA H. and TSUGE S. **Effect of C,Ti, Nb on Recrystallisation Behaviour after Hot Rolling Deformation in 16% Cr Ferritic Stainless Steel,** *The Fourth International Conference on Recrystallisation and Related Phenomena,* The Japan Institute of Metals, 1999

[21] POLLARD B. **Effect of Titanium on the Ductility of 26% Chromium, Low Interstitial Ferritic Stainless Steel,** *Metals Technology,* 1974,Vol. 1, pp. 31-36

[22] CAHN J.W. **On Spinodal Decomposition,** *Acta Metallurgica,* Vol. 9, September 1961, p. 795

[23] USTINOVSHIKOV Y., SHIREN C. and SHIROBOKOVA M. **Laves Phase Formation in Solids,** *Journal of Materials Science,* Vol. 29, 1994, pp. 1411-1416

[24] SPEICH G.R. **Precipitation of Laves Phases from Iron-Niobium (Columbium) and Iron-Titanium Solid Solutions,** *Transactions of the Metallurgical Society of AIME,* Vol. 224, August 1962, pp.850-858

[25] FORBES JONES R.M. and WEST D.R.F. **Precipitation of Fe_2Nb From Supersaturated Ferrite in an Iron-Based 1.8Nb Alloy,** *Journal of the Iron and Steel Institute,* March 1970, pp. 270-275

[26] FUKUDA T., SUENAGA H. and TANINO M. **Effect of Morphology of Carbide and Nitride Precipitates on the Ductility in Fe-30%Cr Alloys,** *Proceedings of International Conference on Stainless Steels,* Iron and Steel Institute of Japan, Chiba, 1991, pp.533-540

[27] SAWATANI T., MINAMINO S. and MORIKAWA H. **Effect of Laves Phase on the Properties of Ti and Nb Stabilised Low C, N-19%Cr-2%Mo Stainless Steel Sheets,** *Transactions ISIJ,* Vol. 22, 1982, pp.172-180

[28] GRUBB J.F.,WRIGHT R.N. and FARRAR P. Jr. **Micromechanisms of Brittle Fracture in Titanium-Stabilised and α'-Embrittled Ferritic Stainless Steels,** ***Toughness*** *of Ferritic Stainless Steels,* ASTM STP 706, edited by R. A. Lula, American Society for Testing and Materials, 1980, pp.56-76

[29] PLUMTREE A. and GULLBERG R. **Influence of Interstitial and Some Substitutional Alloying Elements,** *Toughness of Ferritic Stainless Steels,* ASTM STP 706, edited by R.A. Lula, American Society for Testing and Materials, 1980, pp.34-55

[30] SEMCHYSEN M., BOND A.P. and DUNDAS H.J. **Effects of Composition on Ductility and Toughness of Ferritic Stainless Steels,** *Proceedings of the Symposium "Towards Improved Ductility and Toughness of Ferritic Stainless Steels,"* Climax Molybdenum Company, 1972

[31] WOOD J.R. **Effect of Residual Elements and Molybdenum Additions on Annealed and Welded Mechanical Properties of 18Cr Ferritic Stainless Steels,** *Toughness of Ferritic Stainless Steels,* ASTM STP 706, edited by R.A. Lula, American Society for Testing and Materials, 1980, pp.145-160

[32] REDMOND J.D. **Toughness of 18Cr-2Mo Stainless Steel,** *Toughness of Ferritic Stainless Steels,* ASTM STP 706, edited by R.A. Lula, American Society for Testing and Materials, 1980, pp.123-144

[33] REES W.P., HOPKINS B.E. and TIPLER H.R. **Tensile and Impact Properties of Iron and Some Iron Alloys of High Purity,** *Journal of the Iron and Steel Institute,* October 1951, pp. 151-168

[34] REES W.P. and HOPKINS B.E., **Intergranular Brittleness in Iron-Oxygen Alloys,** *Journal of the Iron and Steel Institute,* December 1952, , pp.403-409

[35] HONDA R. and TAGA H. **Effect of Carbon and Oxygen on the Fracture of Iron,** *Metal Science Journal,* Vol. 2, 1968, p. 172

[36] POWELL B.D., WESTWOOD H.J., TAPLIN D.M.R. and MYKURA H. **A Study of Intergranular Fracture in Iron using Auger Spectroscopy,** *Metallurgical Transactions,* Vol.4, October 1973

[37] PICHARD C., RIEU J. and GOUX C. **The Influence of Oxygen and Sulphur on the Intergranular Brittleness of Iron,** *Metallurgical Transactions A,* Vol. 7A, December 1976, pp. 1811-1815

[38] MATSUI H. and KIMURA H. **Intergranular Fracture of a High Purity Iron due to Oxygen,** *Transactions of the Japan Institute of Metals,* Vol. 24, No. 8, 1983, pp. 539 – 547

[39] NIIKURA M., YAMAMOTO S., OUCHI C. and KOZASU I. **Effects of Heat Treatment and Chemical Composition on Intergranular Embrittlement Phenomena in Ultra-Low Carbon Steels,** *Iron and Steel Institute of Japan,* Vol. 70, 1984, pp. 2254-2261

[40] **Durferrit® Cyanide-free Annealing Baths,** Information Pamphlet from Degussa AG, Germany

[41] **Surface Preparation and Microscopy of Materials** by Brian Bousfield, John Wiley and Sons, 1992

[42] **Struers Metalog Guide,** published by Struers Tech A/S, Denmark, 1992

[43] ASTM Standard Test Methods for Microetching Metals and Alloys – E407 (70) (Reapproved 1989)

[44] **Physical Methods for Materials Characterisation** by P.E.J. Flewitt and R.K. Wild, Graduate Student Series in Materials Science and Engineering, Institute of Physics, Bristol, 1994

[45] **SEM: A User's Manual for Materials Sciences** by Barbara L. Gabriel, American Society for Metals, Metals Park, Ohio 44073,1985

[46] ASTM Standard Test Methods for Tension Testing of Metallic Materials, E8

[47] WILIAMS D.B. and KEAST V.J. **Can Analytical Electron Microscopy Tell Us Why Materials Break?** *Asia/Pacific Microscopy and Analysis,* September 1999

[48] **Electron Beam X-Ray Microanalysis** by Kurt F. J. Heinrich, Van Nostrand Reinhold Company, 1981

[49] **Auger Electron Spectroscopy** by C.L. Briant and R.P. Messmer, Treatise on Materials Science and Technology, Vol. 30, Academic Press Inc., 1988

[50] **Handbook of Auger Electron Spectroscopy** edited by Carol L. Hedberg, Physical Electronics Inc. Minnesota

[51] **An Atlas of Metal Damage** by Lothar Engel and Hermann Klingele, translated by Stewart Murray, Wolfe Science Books with Carl Hanser Verlag, Munich

[52] STEELE J.H., Jr. **Correlation of Fractographic and Microstructural Features,** *Fractography and Materials Science,* ASTM STP 733, edited by L.N. Gilbertson and R.D. Zipp, American Society for Testing and Materials, 1981, pp. 117 – 130

[53] **Understanding How Components Fail** by Donald J. Wulpi, American Society for Metals, 1985, Metals Park, Ohio

[54] CHUN C.H. and POLONIS D.H. **Metallurgical Stability and the Fracture Behaviour of Ferritic Stainless Steels,** *Journal of Materials Engineering and Performance*, June 1992, pp.371 –382

[55] TANINO M., LIU C.M., AKIYAMA K., ABIKO K. and TAKAKI S. **Preparation of Ultra-High Purity Fe-Cr Alloys and their Mechanical Properties,** *Innovation Stainless Steel,* Florence , Italy, 11-14 October 1993

[56] NAKAMURA T. and SAKAKI T. **Intergranular Brittle Fracture of Iron,** *Transactions of the Iron and Steel Institute of Japan,* Vol. 10, 1970, pp. 229-231,

[57] KINOSHITA N **Brittle Cracking in Extra Low Interstitial Ferritic Stainless Steels,** *Stainless Steels '84,* September 1984, Goteborg, Sweden, The Institute of Metals, London, 1985

[58] OHASHI N.,ONO Y.,KINOSHITA N. and YOSHIOKA K. **Effects of Metallurgical and Mechanical Factors on Charpy Impact Toughness of Extra-Low Interstitial Ferritic Stainless Steels,** *Toughness of Ferritic Stainless Steels,* ASTM STP 706, edited by R.A. Lula, American Society for Testing and Materials, 1980, pp.202-220

[59] WRIGHT R.N. **Toughness of Ferritic Stainless Steels**, *Toughness of Ferritic Stainless Steels,* ASTM STP 706, edited by R.A.Lula, American Society for Testing and Materials, 1980, pp.2-33

[60] Private Email Communications with Bruce Muller, Research and Development, Columbus Stainless, Middelburg, 1998-2000